Biophysical Investigations of the Specificity between Rab GTPases and their Effectors

Trinity College Dublin
Coláiste na Tríonóide, Baile Átha Cliath
The University of Dublin

This Thesis is Submitted to Trinity College, the University of Dublin as Candidature for the Degree of Doctor of Philosophy

By Aoife Mairéad Kearney

School of Biochemistry & Immunology,

Trinity College, University of Dublin,

Ireland

Submitted 2018

Declaration

I declare that this thesis has not been submitted as an exercise for a degree at this or any other university and it is entirely my own work. With the exception of the structure determination of FIP2 which was performed by Dr Khan. I agree to deposit this thesis in the University's open access institutional repository or allow the Library to do so on my behalf, subject to Irish Copyright Legislation and Trinity College Library conditions of use and acknowledgement.

Summary

The specificity of protein-protein interactions is a complex process that is poorly understood and difficult to predict. Understanding the molecular basis for specificity of a protein and its binding partner requires a structural analysis of the interactions in the complex. However, static X-ray structures still do not reveal the thermodynamic basis for molecular recognition, nor the key contacts that provide specificity in recognition. Rab proteins are an intriguing case study as the Rabs display a high level of structural similarity amongst members. Despite this, Rabs bind many structurally diverse effectors with exquisite specificity. The main topic of this thesis, the Rab11 subfamily which includes Rab25, binds to a class of effectors termed the Rab11 Family of Interacting Proteins (FIPs). These effectors have been shown to have variable affinities for Rab11/25. Interestingly, some of the FIPs also bind to Rab14, which is an evolutionarily more distant relative. Despite the known crystal structures of Rab11 and Rab14 with their cognate FIPs, the structural basis for the distinct affinities are not apparent. Moreover, Rab14 can recognise a sub-family of FIPs (Class I) but cannot bind to Class II FIPs, while the Rab11 proteins can effectively bind to all FIPs. The cellular functions of Rab11 and Rab14 are independent and our hypothesis is that our thermodynamic and structural analyses may provide insight into their different cellular functions. Through a series of mutagenesis and binding studies, we identify sites in Rab11 that are unrelated to interfacial residues that can influence the affinities of interactions with class I FIPs. Further, we examine the structure of a class I FIP, FIP2, independent of its cognate Rab. No crystal structure of an uncomplexed FIP effector is present in the literature. We hypothesise that structure of FIP2 in solution is different to that formed under the conditions of the complex and that Rab binding may capture a particular conformation of the FIP2 molecule. This thesis provides insight into the specificity of effectors for Rab GTPases and their cellular functions in cells. We show that small changes in sequence and structure of a Rab may dictate its affinity for a given effector and determine preferential formation of one complex over another.

Acknowledgements

First and foremost, I would like to express my gratitude to Dr Amir Khan. Dr Khan has supervised my work both during my undergraduate degree and on to PhD level. Thank you for affording me these opportunities, for pushing me to pursue a better level of understanding and for guiding the project over the last number of years.

Thank you to all the members of the Khan Lab past and present. To Nick, Patrick, Elizabeth and Dieter, thank you for being teachers, for being patient, for supporting and directing me as a scientist and for listening to my many questions (I'm looking at you Nick). To the current Khan lab, Emma, Peter and Dieter, thank you for helping and advising me throughout my work. Most importantly, thank you for filling this experience with so much fun. From the 'angry chicken' protecting the centrifuge, to our lab sing-alongs, you have made the lab a very happy place to work. Late nights and weekends don't seem so bad knowing you are doing it with friends like you.

A special word of thanks to the TBSI support staff, without whom our lab, and therefore, my project, would have come to a grinding halt. To Des, Brian and David in the delivery bay and to the TBSI Technical officers Liam and Noel – thank you for doing me so many favours. For fixing equipment that should have died years ago, for autoclaving media outside of hours, for believing me when I called about a funny noise for the fifth time and for pulling all sorts of miracles. Thank you so much.

To all my friends who have come and gone through the fifth floor reading rooms, thank you for putting up with so much chatter, and thank you even more for partaking in said chatter. To the reading room postdocs, particularly John, Olga, Nadine and Yongjing. Thank you for the support, wisdom and advice. It means a lot coming from those who have been through it and come out the other end. A special thanks to the fab foursome, Nadine, Emma, Peter, and Úna. I'll never forget how you kept me together, come good times and bad, including plenty of panic, frustration and disappointment. This experience will have been worthwhile if only for having allowed me to meet such amazing people. I know that I have made friends for life here. As I say,

we're bonded by trauma now; there's no getting away from me. I see many more cups of tea our future.

To my friends in the 'real world', thank you for being there for me. To all my HSD friends, my Clondalkin girls, my college friends, I am blessed with you all. You have been the best kind of reminder that life exists outside of the lab. Problems with experiments do not seem so insurmountable when you have good friends willing to hear all about them.

To my loving family, all my aunts, uncles and cousins, particularly Sinead, Eamon and my wonderful, wonderful sister, Orlagh, thank you for your never-ceasing care and kindness. Thank you for bringing so much love to my life. I am safe in the knowledge that between family and friends, I will never want for someone to turn to should I need advice, encouragement, or simply a friendly face.

Brian, thank you for supporting me through this. For listening to me rant when I didn't even know what I was trying to say. Thank you for letting me be sad when I needed to and for letting me chat away excitedly about the project even though no normal person wants to hear that much about x-ray crystallography on date night (seriously, what's wrong with you). Thank you for being understanding when I worked late and for letting me convert an evening get together into a 'lab date'. I will never forget your unwavering belief in me.

To Mam and Dad, this is your achievement as much as it is mine. You instilled a love of learning in me from the very beginning. Most importantly you taught me that everyone has their strengths and weaknesses, that just because something is difficult for us, it does not mean that we give up, but that we must work hard to overcome life's challenges. You taught me to never pit myself against others, but to strive to do the best I was capable of myself. That is a lesson I will take with me through life, that as long as I have tried my best, I can be proud. I could never have done this without you.

Contents

Abbreviations

Abbreviation	Definition
A. thaliana	Arabidopsis thaliana
BCA	Bicinchoninic acid Assay
BSA	Bovine Serum Albumin
C. trachomatis	Chlamydia trachomatis
C.elegans	Caenorhabditis elegans
Cdk	Cyclin-dependent kinase
CIM	C-terminal Interacting Motif
D. melanogaster	Drosophila melanogaster
DAG	Diacylglycerol
DLS	Dynamic Light Scattering
DTT	Dithiothreitol
EBs	Elementary Bodies
EDTA	Ethylenediaminetetraacetic acid
EE	Early Endosomes
EEA	Early Endosome Antigen 1
EGFR	Epidermal Growth Factor Receptor
ERC	Endosomal Recycling Compartment
ERCs	Endosomal Recycling Compartments
ERK	Extracellular Signal Regulated Kinase
FIP	Rab11 Family Interacting Protein
FPLC	Fast Protein Liquid Chromatography
GAP	GTPase Activating Protein
GDF	GDI Displacement Factors
GDI	GDP Dissociation Inhibitor
GDP	Guanosine Diphosphate
GEF	Guanine Nucleotide Exchange Factor
GLUT4	Facultative Glucose Transporter Isoform 4
GOLPH3	Golgi Phosphoprotein 3
G-protein	Guanine Nucleotide Binding Protein

GSVs	Glut4 Storage Vesicles
GTP	Guanosine Triphosphate
HPLC	High-Performance Liquid Chromatography
ICB	Intercellular Bridge
IPTG	Isopropyl-β-D-thioglactopyranosid
ITC	Isothermal Titration Calorimetry
Kap-β	Karyopherin-β
kDa	Kilo Daltons
LB Media	Luria-Bertani Media
LE	Late Endosomes
LIC	Ligase Independent Cloning
LROs	Lysosome Related Organelles
MEK	Mitogen-activated protein kinase
MW	Molecular Weight
NPC	Nuclear Pore Complex
NTF2	Nuclear Transport Factor 2
NTR	N-Terminal Regions
OD	Optical-Density
PI4P5	Phosphatidylinositol-4-phosphate 5-kinase
PCR	Polymerase Chain Reaction
PI4IIIβ	Phosphatidylinositol 4-kinase
PLC	Phospholipase C
PLD	Phospholipase D
P-loop	Phosphate Binding Loop
Rab11FIP	Rab11 Family Interacting Protein
RabF	Rab Family
RabGGT	Rab Geranylgeranyl Transferase
RabSF	Rab Subfamily
RBD	Rab Binding Domain
RBs	Reticulate Bodies

RCP	Rab Coupling Protein AKA FIP1
RE	Recycling Endosomes
REP	Rab Escort Protein
RIP11	Rab11-interacting protein AKA FIP5
Rmsd	Root Mean Square Deviation
ROCK	Rho-associated protein kinase
Rpm	Revolutions per minute
rTEV	Tobacco Etch Virus nuclear-inclusion-a endopeptidase
S. pombe	Schizosaccharomyces pombe
SDS PAGE	Sodium Dodecyl Sulfate Polyacrylamide Gel Electrophoresis
SH2	Src Homology 2
SNARE	Soluble N-ethylmaleimide-sensitive Factor Attachment Protein Receptor
SPR	Surface Plasmon Resonance
TBD	Tre-2/Bub/Cdc16
TfnR	Transferrin Receptor
TGN	Trans-Golgi Network
TOR	Target of Rapamycin

Chapter 1:

Introduction

1.1 The Superfamily of Small GTPases

1.1.1 Cellular Organisation and the Ras Superfamily

Proteins which hydrolyse nucleoside triphosphates have many vital and varied functions across the cell. These proteins exist in many different folds, notably; the dinucleotide binding Rossmann fold, the tubulin/FtsZ fold, the protein kinase fold, the histidine kinase/HSP90/Topo II fold, the HSP70/RNAse H Fold and the mononucleotide binding fold/P-loop NTPases [5-9]. The P-loop NTPases are particularly numerous. Their structure consists of an α/β fold consisting of a central β-sheet surrounded on either side by α-helices. Their sequence is characterised by an N-terminal Walker A motif consisting of a flexible loop between a strand and a helix [5, 7, 10]. The consensus sequence for the Walker motif is GxxxxGK[ST]. The motif functions to position the triphosphate [10]. The distal Walker B motif contains a conserved aspartate/glutamate residue which binds a magnesium ion [10]. The P-loop NTPases can be divided into two subgroups based on their structures. The first subgroup are the nucleotide kinases and GTPaes in which the strand leading to the P-loop and Walker B motif are neighbours. The second subgroup are the AAA+, ABC, SF1/2 helicases and RecA/F1 which have an additional strand inserted between the P-loop and the Walker B motif. The first GTPases to be discovered were those which aid initiation, elongation and termination of translation and the seven transmembrane receptors, followed by the Ras small GTPases [11, 12].

The Ras superfamily of small GTPases consists of five protein families related by their GTP binding functions and conserved G protein fold. The member families are; Ras, Ran, Rho, Arf and Rab. These families of enzymes are thought of as molecular switches. They cycle between GTP and GDP bound forms allowing their functions to alter accordingly. The families have varied and vital roles in cellular organisation and homeostasis. Ras was the first family member to be characterised structurally with the publication of the structure of H-Ras [13]. This structure shows the basic fold reflected in all the members of the small GTPase family [13-15].

1.1.2 Cellular Functions of the Ras Superfamily

Through diversification, the Ras superfamily has evolved five protein families with distinct functional roles within the cell. The Ras family has vital roles in controlling cell proliferation, differentiation and regulation of apoptosis. Thus, it has become implicated in various forms of cancer when these regulations go awry [16]. Rho proteins regulate actin dynamics within the cell and therefore play a role in cell division and migration, as well as vesicle transport [17]. Rab and Arf proteins control vesicle trafficking [18, 19]. Finally, the Ran family is responsible for nuclear transport. In humans, only one member of the Ran family is expressed but due to its vital role it is one of the most abundant small GTPases in the cell.

(i) Cellular Functions of Ras

Ras is a key member of various signal transduction pathways. Extracellular signals lead to the activation of Ras which stimulates cytoplasmic signalling leading to altered gene expression and cellular response. Ras functions downstream of membrane associated kinases and upstream of cytoplasmic kinases (reviewed [20]).

The classical Ras signalling pathway is the EGF receptor tyrosine kinase pathway first delineated in 1993. Activated EGFR dimerises and auto-phosphorylates at the membrane and recruits Grb2. The adaptor protein Grb2 has a central Src homology 2 domain (SH2) which associates with the phosphorylated tyrosine peptide sequence of the EGFR. It also has two SH3 domains which recognise proline rich sequences. The Grb2 recruits cytosolic protein Sos1, a Ras GEF protein (Guanine nucleotide Exchange Factor), to the membrane which activates Ras [21-28]. Downstream, Ras activates Raf, followed by MEK and ERK. Finally, the cascade leads to a change in gene expression leading to cell growth and development [29-32]. Diverse stimuli converge on Ras activation. Other Ras GEFs are regulated by distinct signalling mechanisms. For example, Ras GRPs, another class of Ras GEF, are recruited to DAG via their C1 domains. PLC-catalysed production of DAG by receptors such as PLCγ, PLCβ, and PLCϵ recruit Ras GRPs to the plasma membrane, converging on the activation of Ras [33]. Ras is not only

a member of diverse signalling pathways in humans, but also, homologous Ras family members are signal transducers in pathways across species. This high level of evolutionary conservation shows the importance of Ras as one of the basic building blocks of signal transduction [34].

Ras has long been known to play a role in various cancers. In the case of cancer, Ras has preference for the GTP active state. Trahey and McCormik identified GAP proteins as being responsible for a 300x acceleration in GTP hydrolysis and also identified that mutant Ras is insensitive to GAP activity, leading to increased activation and the formation of cancer [35].

(ii) Cellular Functions of Rho

Rho GTPases play a vital regulatory role in mitosis and cytokinesis in mammalian cells. This is a tightly regulated mechanism in which the sequence of events is vitally important. A number of Rho GTPase family members play a role at discrete points in the process, all tightly regulated by their associated guanine nucleotide exchange factors (GEFs) and GTPase activating proteins (GAPs). For example, active GTP-Cdc42 peaks at metaphase concurrent with chromosomal alignment, whereas GTP-RhoA increases through anaphase to a maximum at telophase at the time of cytokinesis [36]. Depletion of active GEFs and GAPs cause catastrophic losses in regulation leading to multinucleated cells [37-39].

Rho proteins have important roles in the regulation of the cell cycle. The role of Rho proteins begins with the very first stages of mitosis. RhoA has been implicated in cell rounding and cortical stiffening at mitotic onset. RhoA activity is elevated and concentrated to the cortex and functions as the primary driver of actin remodelling resulting in mitotic cell rounding and cortical stiffening [40, 41]. This process is mediated through downstream effectors of RhoA which activates Rho kinase (ROCK) which subsequently phosphorylates myosin II [41, 42]. The cell rounding process is also associated with an increase in Cdk1 activity. Cdk1/cyclin B1 mediated phosphorylation is thought to play a role in the timing of these events. Upon mitotic onset, Cdk1/cyclin B1 mediates the phosphorylation of RhoA GEF Ect2 and GAP p190RhoGAP resulting in a global increase in RhoA activity.

Metaphase, which is associated with spindle formation and chromosome alignment, is also regulated by Rho GTPases; primarily Cdc42. Cdc42 plays a role in spindle orientation in polarised epithelial cells, centrosome integrity and chromosomal attachment [43, 44].

In cytokinesis, the recruitment of RhoA determines the site of cell division [45-49]. RhoA undergoes a spatially controlled activation pattern along a narrow zone at the equatorial cell cortex. This is controlled by the localisation of RhoA activator proteins to the central spindle. A wider zone of activation of RhoA leads to ingression failure and ultimately a failure in membrane abscission [50-53].

(iii) Cellular Functions of Arf

Arf GTPases function to control membrane trafficking and organelle structure. They regulate cytoskeletal factors, recruit coat proteins to membranes and recruit and activate enzymes to regulate the lipid composition of the membranes themselves [54]. As an example of Arf cellular function, we will discuss Arf6. Arf6 is important for mammalian development. Knock-out mice die mid-gestation or shortly after birth displaying impaired liver development [55]. Arf6 is known to have roles at the plasma membrane, regulating the cortical actin cytoskeleton and endosomal membrane recycling [56]. Arf6 activates 1-phosphatidylinositol-4-phosphate 5-kinase (PI4P5) and phospholipase D (PLD) which alter the lipid composition of the membrane. Arf6 may enter cells via clathrin-coated vesicles or in some cells in a clathrin independent mechanism [57, 58].

Arf6 facilitates polarised delivery of Cdc2, Rac and Par6 to the leading edge of polarised cells [59]. Arf plays a role in cell adhesion and both the assembly and disassembly of adherent junctions. In the formation of an adherent junction, Par3 recruits the scaffold protein FRMD4A which in turn recruits cytohesin GEFs which activates Arf6 [60]. Interestingly, and perhaps counterintuitively, Arf6 is also activated in the disassembly of adherent junctions. Hepatocyte growth factors cause activation of Arf6 by ArfGEF GEP100/BRAG2. GTP Arf6 then activates Rac and mediates disassembly at the adherent junction [61].

Arf proteins are thought to have an extra dimension in their signalling. Some inactive Arfs bind a different subset of effectors to those bound in their activated state. In the case of Arf6-GDP it binds TBC domain containing proteins (Tre-2/Bub/Cdc16) which often have Rab GAP activity, opening up the interesting possibility for regulation of small GTPases by inactive Arf [62]. Arf6-GDP also binds to the Kalirin family of Rho GEFs and recruits it to the membrane where it serves to activate Rac and RhoG to regulate actin dynamics [63].

(iv) Cellular Functions of Ran

The small GTPase Ran has dual functions; it regulates nucleocytoplasmic transport during interphase, and later in the cell cycle, it functions in mitotic spindle formation. It is thought that these two different functions are regulated largely through a similar mechanism of Ran action.

In eukaryotes active transport between the nucleus and the cytoplasm is achieved by a class of transfer cargo macromolecules dubbed nuclear transport receptors (NTRs) [64]. These receptors interact with the permeability barrier surrounding the nucleus dubbed the nuclear pore complex (NPC). These receptor molecules recognise FG repeats on the nuclear pore complex components (nucleoporins) which allows them to penetrate the permeability barrier with their cargo [65, 66]. The NTR proteins consist of the Karyopherin Kap-β family, including importins (for import), exportins (for export) and kap-β (bidirectional) proteins. These proteins all display a similar architecture [67].

Transport receptors recognise their cargo via import and export signals on these molecules. The vectorial movement of cargo-receptor complexes is aided through interactions with Ran. RanGTP binds all importin family members in a GTP dependent manner. In the case of cargo import, RanGTP interacts with importin inside the nuclear envelope and causes it to release its cargo. In the case of nuclear export, RanGTP increases the affinity of the exporting receptor for its cargo inside the nuclear envelope. The influence of the Ran on receptor-cargo binding is nucleotide dependent and is regulated by differential localisation of Ran GAP and GEF proteins. Ran GAP protein

RanGAP1 is enriched at cytoplasmic filaments of nuclear pore complexes during interphase, whereas the Ran GEF RCC1 is concentrated on chromatin throughout the cell cycle [68-72]. RanGDP enters the nuclear envelope mediated by nuclear transport factor 2 (NTF2) [73, 74]. In the nucleus RCC1 mediates nucleotide exchange to RanGTP. Meanwhile NLS-containing proteins are associated with importin β in the cytoplasm and translocated to the nucleus. Here, active RanGTP associates with importin β causing importin β to release its cargo. The Ran importin complex may then translocate to the cytoplasm where RanGAP1 mediates GTP hydrolysis. RanGDP disassociates from importin allowing it to bind other cargo in the cytoplasm for nuclear translocation. RanGDP may then re-enter the nucleus for activation and the cycle begins again [75-77]. This process allows for the accumulation of cargo against the concentration gradient.

Ran has also been implicated in spindle formation during mitotic cell division. In most eukaryotic cells, with the exemption of yeast, the nuclear envelope breaks down at prometaphase. This breakdown allows for RanGAP1 to diffuse throughout the cytoplasm, disrupting the localisation of Ran GEFs and GAPs which is associated with nucleocytoplasmic transport [78, 79]. GEF activated Ran may bind importin β in the cytoplasm, freeing factors that would usually be bound to importin [80-82]. For example, it frees NuMA and TPX2, both aster promoting factors. It also frees cyclinB-Cdc1 which is an important factor in progression through the cell cycle [80].

(v) Cellular Functions of Rab Proteins

Rab proteins function as regulators of vesicle trafficking. The Rab protein family is the most numerous family of Ras like small GTPases. It has 11 identified member genes in yeast and at least 60 in humans [1]. Rab function is influenced by GEFs, GAPs, and effector proteins (which will each be discussed in detail later in this work) [83-85]. In their active GTP bound state, Rabs are membrane associated via a C-terminal anchor. This anchor is therefore essential to their function [86]. Upon hydrolysis Rabs become soluble and associate with GDP dissociation inhibitor (GDI) in the cytoplasm. This cycling between active membrane bound and inactive

cytosolic states allow Rabs to transfer between membranes [85, 87, 88]. Membranes are organised into overlapping Rab specific domains with distinct functional properties [18]. Rab effectors are numerous and they are an extremely structurally diverse group [89]. Effectors include sorting complexes, motor proteins, tethering factors and lipid metabolic enzymes [90]. A degree of effector promiscuity exists. Some Rabs bind multiple different effectors and equally some effectors bind multiple different Rabs.

The Rab family can be organised into eight phylogenetic groups. Separate groups have more distinct functions, but within the groups there may be many subfamily members and homologues which have similar, overlapping or even functionally redundant roles and overlapping subcellular distributions [1, 91].

Rab Proteins and the Endosomal System

Eukaryotic cells feature a level of compartmentalisation and cellular organisation not found in prokaryotic cells. Therefore, intracellular transport between compartments is of vital importance to eukarya. Members of the Rab family are localised to distinct subcellular compartments and they play pivotal roles in intracellular membrane trafficking events, including; cargo sorting, vesicle budding, vesicle formation, vesicle transport, docking, tethering and fusion with target membranes [92]. An example of the wide range of transport roles carried out by Rabs is illustrated if figure 1.1.1. Rabs are promiscuous towards their effectors and this allows their functions to be coupled. In fact, the activation and recruitment of Rabs to particular membranes may be influenced by other family members. One Rab may recruit a GEF of another Rab to the membrane which will in turn activate its Rab and allow it to be inserted in the membrane. In this way the Rab profile of an organelle may be altered over time. An example of this may be seen in the case of Rab5 recruiting and being replaced by Rab7 during endosome maturation [93].

Proteins internalised from the plasma membrane are transported to early endosomes. After this a number of pathways may be undertaken by the cargo. The proteins may be transported to the lysosome via late endosomes to be degraded. A classic example of this is the degradation of EGF receptor.

Alternatively, the material may be recycled to the plasma membrane via recycling endosomes. A typical example for study is the recycling of the transferrin receptor [94]. The Retromer-mediated pathway allows cargo to be sorted from the endosome to the TGN (retrograde transport) [95]. Alternatively, the cargo can be sorted from early endosomes to LROs (Lysosome Related Organelles), for example, the sorting of Tyrp1 from early/recycling endosomes to melanosomes [96, 97].

The initial step in vesicle trafficking involves formation of the vesicle at the donor membrane. During formation the vesicle must not only be loaded with the required cargo, but it must also contain all of the targeting machinery that it will require for its journey. The mechanisms for this process are still emerging. The best studied example of Rab-mediated cargo sorting is the rhodopsin photoreceptor and the polycystins. In this case, a C-terminal signal in the cargo (VxPx) binds to Arf4 which then recruits a cohort of Rabs (Rab6/ Rab8/ Rab11) and associated regulators (ASAP1/Rabin8) initiating a cascade to promote ciliary targeting [98, 99]. The Rab-mediated cargo selection and vesicle budding processes involve signal dependent cargo binding and cooperativity between Arfs, Rabs and regulators.

The translocation of vesicles may be achieved in either a microtubule dependent or actin dependent fashion. Both processes are mediated by Rabs. Microtubule dependent transport controls the long range motility of endosomes. This is a bi-directional process and functions in a ‘stop-and-go’ fashion due to the alternating activities of plus end directed kinesin motors and minus end directed dynein-dynactin motors. The microtubule dependent motility of endosomes is regulated by different Rabs at different stages of the endosomal cycle. Rab5 regulates the motility of early endosomes [100]. Rab4 also regulates early endosomes and also recycling endosomes [101]. Rab9 regulates motility of late endosomes and Rab7 regulates the activity for late endosomes and lysosomes [102-105]. Actin dependent translocation of endocytic compartments such as lysosomes, melanosomes and phagosomes accomplish motility over shorter distances. Their movement is frequently coordinated by Rab-regulated handoffs between motor proteins that control microtubule based motility, those that control actin based motility and

proteins that mediate membrane docking [106]. Rab11a was the first Rab found to interact with myosin Vb, an interaction required for recycling of cargo to the plasma membrane [107]. Since then, multiple Rabs have been shown to associate with myosin motors, including; Rab3a,b,c,d, Rab6a,b, Rab8a, Rab10, Rab11a,b, Rab27a, Rab14, Rab25 and Rab39b indicating that multiple Rabs can use the same motor protein to regulate vesicle motility [108].

When vesicles reach their destination Rabs form part of large molecular complexes that orchestrate the controlled recruitment and activity of docking and tethering factors onto the membrane [18, 84, 109]. In yeast and metazoans, a modular assembly of tethering complexes has been discovered. This process is thought to be conserved in mammals. The equivalent structures in mammals are, as yet, incompletely characterised [110]. Membrane docking and fusion are driven by the formation of trans-SNARE complexes which bring different membranes into close proximity for fusion [111-115]. Rab proteins act upstream of SNARE complex and provide the first layer of specificity in the recognition of two membranes for fusion. In the case of Rab5, Rab5 and PI3P recruit an effector complex of Rabenosyn-5 and Vps45 to the early endosome membrane. These effectors regulate the formation of SNAREs and cooperate to stimulate membrane fusion [116-118].

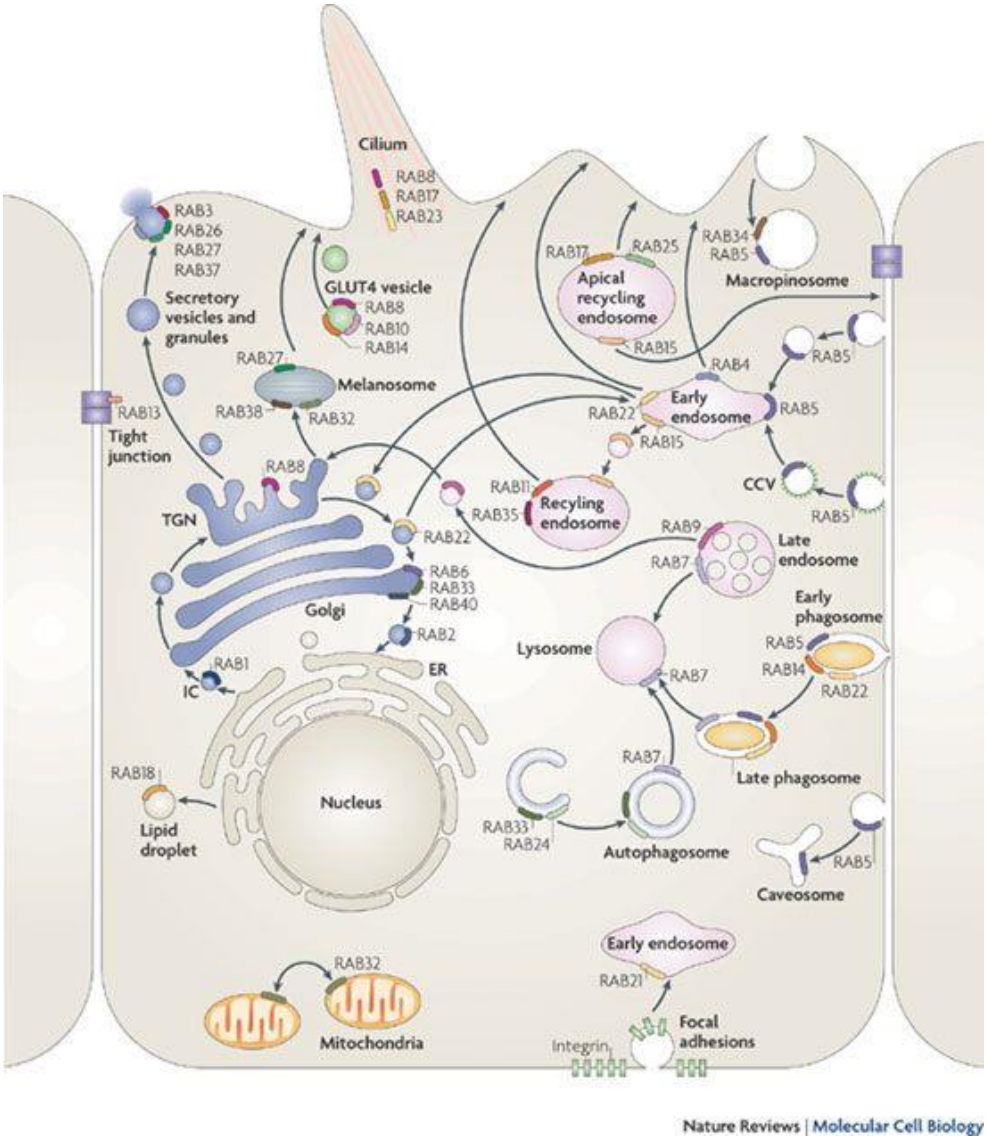

Figure 1.1.1 Rab Proteins Play a Vital Role in Vesicle Trafficking. Cellular compartmentalisation is a hallmark of eukaryotic cells. Therefore, intracellular transport between compartments is of vital importance to eukaryote. This transport is mediated by the Rab family of small GTPases. Each member of the Rab family are localised to distinct subcellular compartments and they play pivotal roles in intracellular membrane trafficking events. The figure above represents the localisations and functions of some of the Rab proteins in human cells. Figure taken from [3].

Rabs and Cell Signalling

Rab proteins have been implicated in cell signalling by regulating endocytic/exocytic trafficking of receptors and ligands through their vesicle trafficking functions [119, 120]. However, an alternative mechanism of regulation of cell signalling by Rab proteins can be seen though their regulation of molecular interactions. This shows a role for Rab proteins in the downstream events of cell signalling. Ultimately, Rabs have an impact on gene expression and growth control via their roles in cell signalling [92].

An example of the influence of Rab proteins on cell signalling can be seen in the target of rapamycin (TOR) pathway. This pathway regulates cell growth processes and is conserved between yeast and metazoan cells highlighting its biological importance [121]. Two homologues of the TOR receptor exist; TORC1 and TORC2. TORC1 is resident on vacuoles. It is activated by nutrient abundance in the cell. In the absence of nutrients TOR1 can trigger autophagy [122]. TORC2 is localised at the plasma membrane and is activated by growth factors [123]. Both homologues converge on a pathway to activate cell growth and proliferation.

TORC1 is recruited to lysosomes by the Ragulator complex indicating possible roles for Rab5 and Rab7 proteins resident on these organelles [121]. The Ragulator complex is a heteropentameric complex containing compent domains: p18, p14, MP1, p10 and HBXIP. The p18 domain represents the minimum region required for assembly, in the structure the p18 domain wraps around heterodimers of p14:MP1 and P10:HBXIP [124]. In *Drosophila*, it was found that depletion of Rab5 led to reduced TORC1 activity [125]. Further studies in mammalian cells showed that overexpression of Rab5 wild-type, or the constitutively active mutant, resulted in an altered localisation of mTORC1 and the inhibition of its activation by insulin [126]. These results show a direct effect on cell signalling through the modulation of Rabs.

1.1.3 Evolution of the Small GTPases

(i) Evolution of the Ras Superfamily

Examples of the five major Ras subfamilies exist across eukarya. It is believed that their diversification is an ancient event that predates the evolution of the last eukaryotic common ancestor. A 2012 study by Rojas *et al.* suggests that the root of the protein superfamily lies in the Arf family and not the Ras family as previously thought. This evidence suggests that the function of the ancestral root was membrane trafficking and quick diversification of protein families and functions soon followed [127]. Perhaps one could speculate that the diversification of the Ras superfamily has aided in the development of increased cell complexity required for the development of eukarya. Indeed, further research in the area will be intriguing in this respect.

Functional diversification may be assumed to be related to the evolutionary diversification of the protein family. For example, the Ran protein family appears to be a sub-functionalisation of the Rab family in order to accommodate the evolutionary niche of transport to and from the nuclear envelope [127]. During both functional diversification and speciation a number of gene loss and gene duplication events have occurred. For example the Ras family is completely absent from the *A. thaliana* species. In contrast, in humans the Rab11 family has undergone multiple gene duplication events to create a subfamily of closely related proteins [128].

(ii) Evolution of the Rab Family

The Rab subfamily members can be identified by a number of features. They each contain a GTP binding motif, like the other members of the small GTPases. They also contain two cysteine prenylation motifs (apart from a few notable exceptions) [129]. The family also have specific sequence elements which have been conserved across their evolution. These Rab family (RabF) motifs are conserved across species and have been useful in identifying and classifying Rab genes in various species [91]. The RabF motifs are clustered around the switch regions. Aside from the RabF motifs,

there exist a set of Rab subfamily (RabSF) motifs which aid in determining the specificity of Rab interacting proteins for their specific Rab. These motifs support a conserved mechanism of recognition between Rabs and their regulators and effectors. It is likely that a conserved mechanism of effector and regulator recognition was present at the point of divergence from other small GTPases [1, 91].

Upon examination of the segregation of Rab proteins in various species it may be speculated that Rabs do not follow a phylogeny of species, but rather a phylogeny of function. The Rab proteins show a pattern of co-segregation of Rabs with similar functions, localisations and sequence. The patterns of co-segregation and RabSF motif conservation across species may together be used to assign orthologues [1, 130].

Orthologues across species allow for the classification of Rabs into families. In *S.pombe*, only seven Rabs have been identified, the lowest number of any species examined [131]. Each of these Rabs can be associated with a particular function and an obvious phenotype associated with their absence/loss of function. In contrast, humans have the largest number of Rabs, many of which are homologous and form subfamilies with each subfamily corresponding to a function.

The conservation of RabSF motifs within Rab families indicates a conserved mechanism of recognition between Rabs and their regulators and effectors. It is likely that a conserved mechanism of effector and regulator recognition was present at the point of divergence from other small GTPases and that these interacting mechanisms impose an evolutionary constraint upon the divergence of Rab proteins. This also implies an element of effector conservation supported by the fact that Rabs from different organisms show functional complementation [1].

Taking into account the segregation of Rabs according to their functions, the Rabs have been classified into eight functional groups containing Rabs from different species which have similar functions and always co-segregate. An example form of segregation is given in figure 1.1.2. Some Rab proteins, for example, Rab1 and Rab35, co-segregate even if they are not isoforms. The

proteins in each functional group are more similar to each other at the amino acid level than any two random Rabs. This phylogeny of function is thought to represent an evolutionary relatedness. This hypothesis is supported by the conservation of discrete regions, the RabF motifs, genomic structure, and intron-exon boundaries [1, 91].

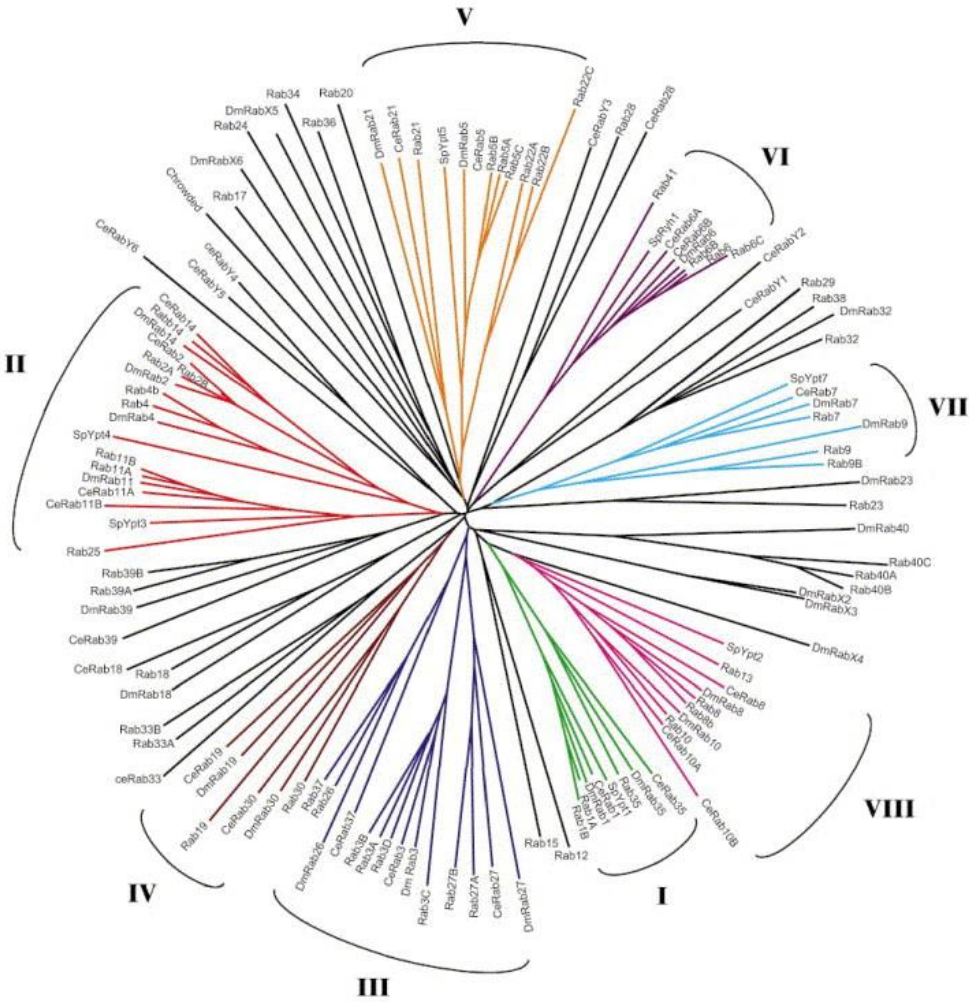

Figure 1.1.2 Rab Proteins across Species Segregate into Eight Functional Groups. The figure above, taken from Pereira-Leal et al [1], shows Rab proteins from diverse species, human (no prefix), nematode (prefix-Ce), fly (prefix-Dm) and fission yeast (prefix-Sp) arranged in a neighbour-joining diagram. The Rabs are arranged into groups, marked by roman numerals, based on their evolutionary segregation according to their functions.

1.1.4 Family Members and their Structures

The Ras superfamily of small GTPases contains five member families; Ras, Rho, Ran, Rab and Arf. Divided based on sequence and functional differences, these proteins are joined into a superfamily by their ability to bind GTP/GDP nucleotides using a conserved G protein fold [12]. Though a diverse family, they each maintain the sequence features required for nucleotide binding and intrinsic GTP hydrolysis [127].

(i) The G Protein Fold

The G protein fold was first elucidated in H-Ras in 1989. In fact, it was the first atomic description of any proto-oncogene product. The fold consists of a six stranded β-sheet containing five parallel strands and one antiparallel strand. The β-sheet is flanked by five α-helices and the fold contains nine connecting loops [13]. The protein binds both a GTP/GDP molecule and a magnesium ion. Four of the loops interact with the nucleotide. The magnesium ion has a catalytic role and interacts with a non-bridging oxygen of the GTP nucleotide.

The regions of the fold whose conformations are sensitive to the nucleotide state of the protein are dubbed the 'switch' regions; switch I and switch II. Indeed, the proteins may be thought of as molecular switches with active GTP bound conformations and inactive GDP bound conformations. In the GTP bound state the two switch regions form new, more rigid conformations. In Ras, two invariant residues, Thr35 in switch I and Gly60 in switch II, form hydrogen bonds between the NH groups of their main chain and the γ-phosphate of GTP. This mechanism has come to be known as the 'loaded spring' mechanism [132]. The conservation of these essential G protein fold elements across the Ras superfamily is delineated in the sequence alignment in figure 1.1.3. The protein structure is further illustrated in figure 1.1.4 which shows the conserved fold as well as highlighting the switch regions and the P-loop.

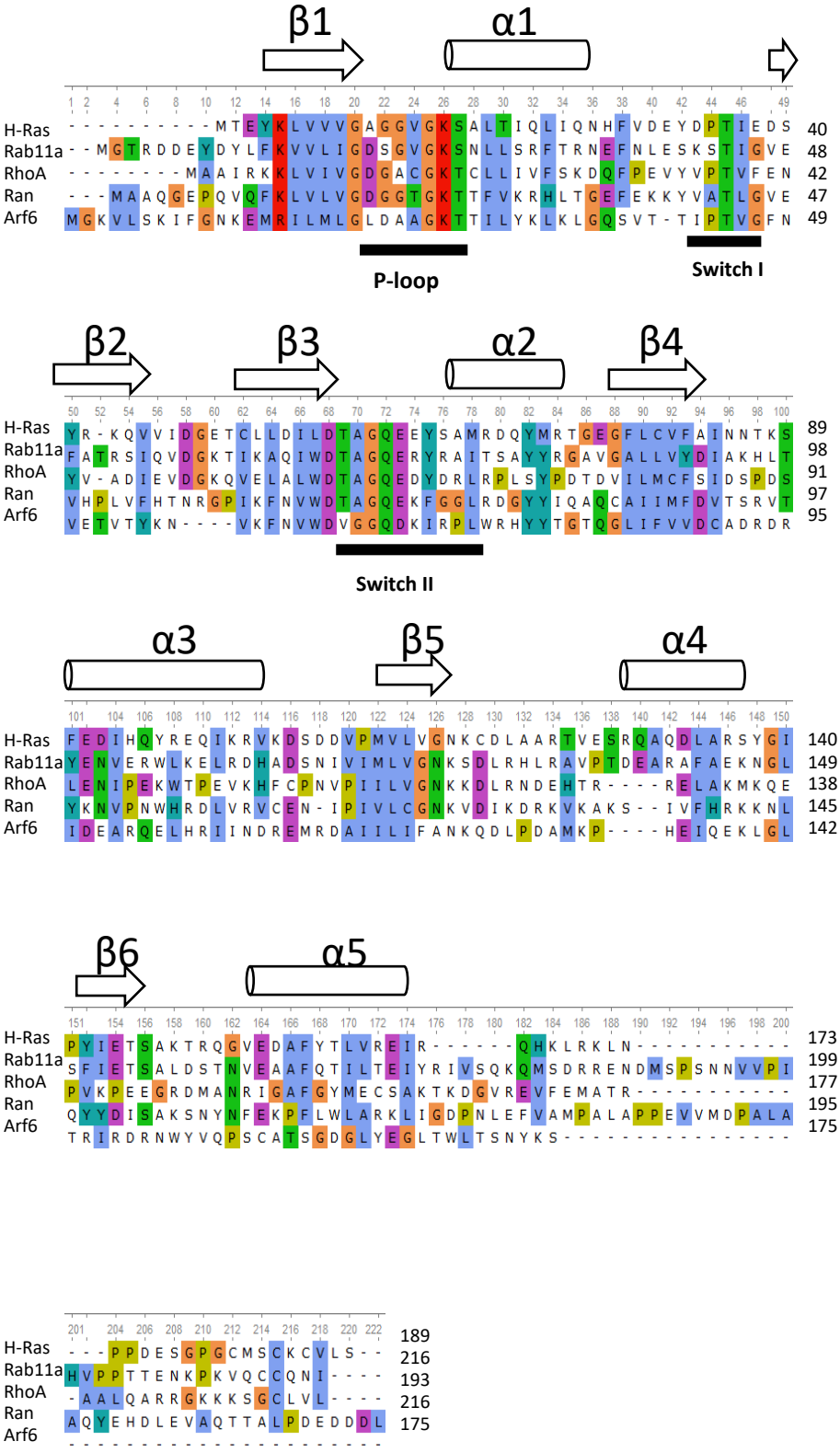

Figure 1.1.3 Multiple Sequence Alignment of Members of the Ras Superfamily. Shown above is a multiple sequence alignment of H-Ras, Rab11a, RhoA, Ran and Arf6. The secondary structure of the conserved G protein fold is shown above the sequences with an arrow indicating β-sheet and a cylinder indicating α-helix. The P-loop and the switch regions are underlined.

(ii) Ras Proteins are Enzymes

In general, the intrinsic GTPase activity of the Ras superfamily of proteins is very low. Regulatory proteins cycle the GTPases through their active and inactive state by increasing the rate of GTP hydrolysis (GAPs) and then encouraging the exchange of GDP for GTP (GEFs) [133]. The mechanism of GTP hydrolysis by GTPases remains an active and ongoing debate. It is theoretically possible for phosphate hydrolysis to occur via a range of mechanistic pathways; the associative pathway, or the dissociative pathway. In the associative pathway, nucleophilic attack occurs prior to leaving group departure. In the dissociative pathway, the leaving group departs before nucleophilic attack resulting in the formation of a metaphosphate intermediate. Another dissociative possibility is that bond formation and bond cleavage can occur simultaneously in a single transition state [134, 135]. A second question posed by the mechanism is how does nucleophile activation take place? Multiple options exist. Perhaps, the nucleophile is activated by general-base catalysis by the bulk solvent, or by direct proton transfer to the basic non-bridging oxygens or by proton transfer to the phosphate by an intervening water molecule. Another option is that a conserved glutamine (Gln61 in H-Ras) activates a nucleophilic water by itself acting as a base and removing a proton from the water molecule [136]. This model appears to be supported by the crystal structure of the Ras-RasGAP complex [137]. However, questions remain about the nature of the activation of the nucleophile and multiple arguments against this hypothesis have been presented [138-141]. Computationally, the energy barrier for this proton transfer, as examined by Langen and Co and subsequent studies [139], is thought to be very large. The structures of active Ras and Ras-RasGAP shed some light on the question. In H-Ras, Thr35 in the switch I region interacts with the magnesium ion and a non-bridging oxygen of GTP. In the Ras-GAP complex we see that in switch II a conserved glutamate (Gln61) interacts with a water molecule in a perfect position for nucleophilic attack on the gamma phosphate [13, 14, 137, 142]. The conformations of these two important residues are highlighted in figure 1.1.4. GAP proteins accelerate hydrolysis by up to five orders of magnitude [143]. The GAP protein contributes an

arginine finger (Arg789) which stabilises the transition state during GTP hydrolysis [137].

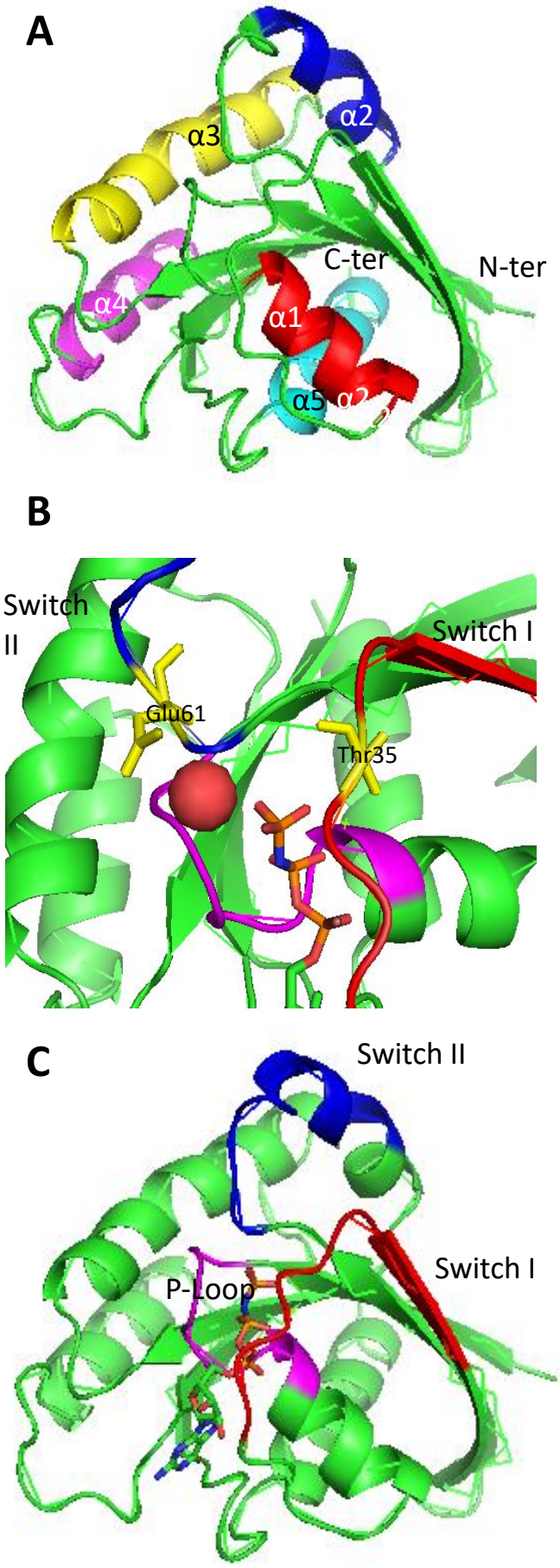
A
α3
α2
C-ter
N-ter
α4
α1
α5
α2
B
Switch
II
Switch I
Glu61
Thr35
C
Switch II
Switch I
P-Loop

Figure1.1.4. The G Protein Fold.

A. The G protein fold is here shown in H-Ras, the fold consists of a 6 stranded β sheet surrounded by 5 α helices. Helix1-red, helix2-blue, helix3-yellow, helix4-magenta and helix5-cyan.
B. Here important residues Glu61 and Thr35, shown here in yellow, interact with the γ phosphate. Glu61 is hypothesised to align a catalytic water molecule during GTP hydrolysis. The water molecule is shown here in red.
C. The structure of active H-Ras is shown here, bound to a non-hydrolysable GTP analogue. Switch I is shown in Red, switch II in blue and the P-loop is shown in magenta.

Figure made using Pymol [2]

The debate on the nature of the transition state also continues. An alternate substrate-as-base mechanism supported by multiple studies is currently the most accepted mechanism [139, 140, 144-149]. In support of this mechanism Klahn et al produced studies showing that the transition state has an associative character and calculated a theoretical energy barrier of 14 kcal/mol which is in good agreement with the experimental result of 16 kcal/mol [138]. Although Gln61 mutation studies have shown an important effect on oncogene activity, it has now been suggested that this activity is due to mutation induced conformational change to the switch II region thereby disrupting GAP activity and not due to the activation of the nucleophile by the glutamine residue [150, 151].

(iii) Insertions and Extensions to the G Fold

Each member of the Ras family contains the basic G fold. However, various individual auxiliary features and modifications exist within families. The Ras family itself is modified at its C-terminus by palmitoylation of a cysteine residue [152]. Rho family proteins contain an extra helix between β5 and α4 known as the 'insert region'. The region forms a single turn helix followed by an α-helix [90]. Rho proteins are prenylated at their C-terminus by geranylgeranyl groups at one site [153]. The Arf protein family have an N-terminal extension which forms an amphiphatic α-helix. In the GTP form this aids in membrane association and allows the protein to sit closer to the membrane than other G proteins such as Rabs which have some 30 amino acids as a linker between the membrane and the globular domain [154]. Some Arfs are myristolated at an N-terminal Glycine also aiding in membrane association [155, 156]. Diverging from the traditional G protein fold Arf proteins have four nucleotide sensitive regions. They contain the two conserved switch regions found in all small GTPases, an N-terminal helix and an 'interswitch toggle'. The conformations of these extra regions alter depending on the nucleotide bound. The 'interswitch toggle' involves two central antiparallel β-strands of the β-sheet. On the GDP form these strands are retracted towards the nucleotide pocket. Upon nucleotide exchange the strands move by a distance corresponding to two amino acids. This, in turn, displaces the N-terminal helix making it available for interaction with the

membrane [157-159]. Ran proteins have a C-terminal extension which forms an extra α-helix. The Ran GTPases are not subject to any lipid modification [90]. Rab proteins follow the canonical G protein fold. They are prenylated at their C-terminus by two geranylgeranyl groups [153]. Structural variations between families allow for various cellular localisations and specialised functional roles.

1.2 Rab Proteins; Life cycle and Effector Interactions

1.2.1 Rab Synthesis, Post Translational Modification and Delivery to the Membrane

The function of Rabs is under spatiotemporal control connected to their switching between GTP and GDP bound forms. In their GTP bound state, Rab proteins are membrane associated and localised to particular organelles where they recruit effector proteins and preform various functions. The amount of time they spend in their active, effector binding state is restricted by GTP hydrolysis after which Rab effector affinity is altered. The localisation of Rabs is also controlled by their nucleotide state. Upon GTP hydrolysis Rabs are extracted from the membrane and become cytosolic until their subsequent re-activation. This cyclical process is controlled by a number of Rab interacting proteins; Rab Escort Protein (REP), GDP Dissociation Inhibitor (GDI), Guanine nucleotide Exchange Factors (GEF) and GTPase Activating Proteins (GAP).

After synthesis, the majority of Rab proteins undergo prenylation at two cysteine residues at their C-termini. The prenylation of all Rabs uses shared machinery. Rab geranylgeranyl transferase (RabGGT) is responsible for the prenylation of all Rab proteins despite the fact that a number of different prenylation motifs exist [160]. In fact, RabGGT is not responsible for the recognition of the Rab C-terminal region. Instead, an adaptor protein is required for Rab prenylation [161, 162]. Rab Escort Protein (REP) associates with Rab proteins and with RabGGT and facilitates prenylation. The crystal structures of a Rab-REP complex and REP-RabGGT complex have allowed for a model of the tripartite complex to be formed [163-165]. Newly synthesised, unmodified Rabs in the GDP associated state bind to domain I of REP via their conserved RabF1-F4 motifs and their C-terminal Interacting motif (CIM) [164, 165]. Domain II of REP then interacts with the α subunit of RabGGT and orients the C-terminus of the Rab towards the active site of RabGGT which will then prenylate the Rab recognising a range of C-terminal motifs. After modification, the C-terminus of the Rab protein binds to a

pocket on domain II of REP and is subsequently chaperoned to the membrane [163].

GDP dissociation inhibitor (GDI) is a paralogue of REP and also functions to chaperone prenylated Rab-GDP in the cytosol. The proteins are structurally related and display a similar binding mode with Rabs through conserved residues in the G-domain and CIM. In contrast, GDI cannot support Rab prenylation and has a higher affinity for Rabs which are already prenylated [166-168]. GDI functions later in the Rab cycle to extract Rabs from the membrane after hydrolysis and, in this way, play a role in Rab recycling [169]. The localisation of Rabs to a particular membrane is still under study. It is thought to be aided by a number of factors. The C-terminal region is thought to play a role in membrane association in some Rabs [88, 170, 171]. There is also evidence for a role of GEFs in recruitment of Rabs to a specific membrane [172-174]. It is further thought that GDI displacement factors (GDFs) promote GDI dissociation and membrane incorporation [88].

1.2.2 Rabs and their Regulators

(i) Guanine Nucleotide Exchange Factors

An interesting property of Rab proteins is that although they use a common mechanism for prenylation and share cytosolic chaperones, they display specificity for a particular subset of a range of diverse effectors and regulators (GEFs and GAPs). In order to perform their effector binding functions Rabs must be in their active, GTP bound state. GEFs allow for the activation of Rabs by promoting the exchange of nucleotide. The human GEFs show low homology. Two major families exist, the VPS9-domaining GEFs of which there are at least 9 in humans [175-177], and the DENN domain containing GEFs of which there are at least 18 in humans [178]. Apart from these two families, there are others which display low homology with the two major families. Many GEFs are yet to be identified. This task is made more difficult by their variable structures [179]. Several GEFs are controlled by auto-inhibition and subsequent release by regulatory proteins. For example, the Vps9 domain containing GEF Rabex-5 is activated in a feedback loop upon

interaction with the Rab5 effector Rabaptin-5 [180]. Furthermore, GEFs play a role in Rab cascades where a GEF for a subsequent Rab may be recruited by a Rab already present at the membrane. In this way GEFs may play a role in the recruitment and localisation of Rabs [171, 174, 181].

GEFs function by stabilising the intermediate nucleotide-free state during nucleotide exchange. GEFs bind nucleotide-free Rabs with high affinity. In most GEF-Rab structures solved, the Rab is in the nucleotide free state. The GEF proteins bind switch I, switch II and the interswitch region of Rab proteins and induce conformational rearrangements incompatible with nucleotide binding. The most dramatic of these rearrangements occur within the switch I region where the switch forms a disordered conformation. In fact, the residues in the switch I region undergo a 10-30 Å shift and often can't be defined in the electron density of a crystal structure, indicating that their conformation is flexible and not rigidly defined. In switch II, less dramatic conformational change occurs and the structure of the switch region is more like that found in the GTP-bound state. It has been suggested that the initial recognition of the GEF for its Rab is different depending on the nucleotide bound. In the GDP form the GEF recognises switch I first but in the GTP from the GEF recognises switch II first. The conformation of the P-loop is also changed although less dramatically [182, 183]. In the structures of Rab21-Rabex5 and Ypt1-TRAPP, negatively charged residues from the GEF project into the vicinity of the P-loop lysine in order to substitute for the negative charge lost with the phosphate dissociation and stabilise the nucleotide-free state [184]. In many structures, electrostatic repulsion between acidic residues of the GEF and/or Rab point towards the phosphate groups and encourage their dissociation by lowering nucleotide affinity [183, 185].

(ii) GTPase Activating Proteins

Left unregulated, Rabs remain in their GTP associated state for a considerable length of time. Intrinsic hydrolysis rates are slow, the half-life of the active state ranges between 30 mins and several hours [186-188]. In order to regulate the 'switching off' of their functions a range of regulators (GAPs)

exist. GAPs allow for Rabs to be turned off in a meaningful timeframe. Whereas GEFs have diverse structures, there is only one major GAP family. The TBC domain GAPS (Tre-2/Bub2/Cdc16) have at least 40 members in humans with many yet to be identified [189]. Only one non TBC GAP has been identified in humans; the Rab3GAP complex [190]. GAPs display a promiscuous activity towards Rabs, one GAP may bind to multiple different Rabs [189]. Like GEFs, GAPs are involved in Rab cascades and help establish transitions between Rab localisations at a given organelle [181, 191, 192].

TBC domain GAPs are interesting in that they use a slightly different mechanism to GAPs of other small GTPases. In most cases, GAPs provide an arginine finger to assist hydrolysis along with Gln from the G3 motif of the GTPase [193]. However, in the majority of TBC GAPs, a dual finger mechanism exists. Both an Arg and a Gln finger are provided and the GAP Gln substitutes for the Gln of the Rab protein. The Arginine finger neutralises the developing negative charge during hydrolysis and the Glutamine is thought to align the water molecule for nucleophilic attack on the γ-phosphate [133]. An important consequence of this dual finger mechanism is that it is still active on Rabs which have been mutated to remain active (QL/QA mutations of the catalytic glutamine). This has implications for *in vivo* experiments containing these mutant Rabs [193, 194]. After hydrolysis aided by GAPs, the Rab-GDP may be extracted from the membrane by GDI and held in the cytosol ready for a new cycle to begin. GDI displacement factor (GDF) facilitates the disassociation of the Rab from GDI, thus facilitating the re-insertion into the membrane [195]. The lifecycle of a typical Rab protein is further illustrated in figure 1.2.1.

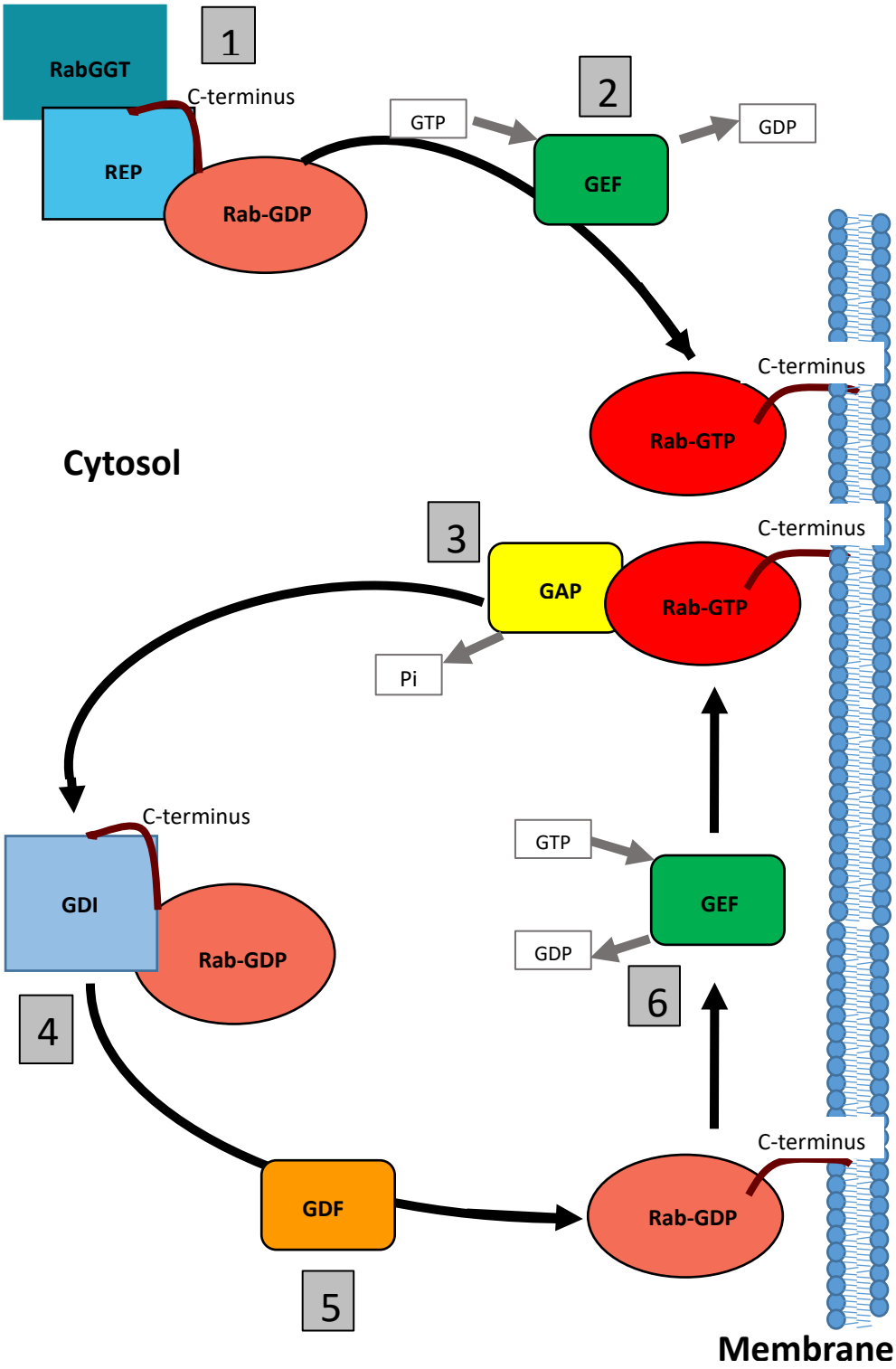

Figure 1.2.1 The Cycle of Active and Inactive Rab Proteins.

Upon production, REP protein facilitates the prenylation of Rab by RabGGT (1). Rab GEFs allow for the exchange of nucleotide, usually from the GDP form to the GTP form (2). GTP Rab is membrane associated and may bind effectors. Rabs are inactivated by GAP proteins which aid GTP hydrolysis (3). GDP Rabs are extracted from the membrane by GDI proteins and held in the cytoplasm (4). GDF facilitates the displacement of GDI allowing Rabs to be re-inserted into the membrane (5) where they are available for re-activation by GEF (6).

1.2.3 Rab Effector Specificity

(i) Rab Effector Interactions

Active Rabs are localised to the membrane. In this form they can be recognised by a range of effector proteins which modulate their downstream functions. Due to the large number of Rab proteins, Rab-effector interactions must encode specificity for their particular Rab. Rab effectors primarily recognise the switch I-interswitch-switch II region of the Rab protein. This region is relatively conserved amongst Rab proteins and so the mechanism by which effectors recognise their specific Rab partners poses an interesting question. Rab effectors are highly divergent in sequence and structure. The majority are multidomain proteins which contain a Rab binding domain (RBD) and other domains which modulate their functions [85]. Rab effector interactions display a degree of promiscuity, one effector may be recruited by a range of different Rabs either through shared or adjacent Rab binding domains [3, 84, 85]. Conversely, a single Rab may bind many different effectors. The specificity of a Rab for its effector, or subset of effectors, is a multifactorial process including the orientation of the aromatic triad, the hydrophobic surface at the switch junction and sequence variability at the edges of the switch regions [196].

(ii) Rab-Effector Binding and Conformational Change

For most Rabs, their active conformations are very similar to the conformations which they adopt in their Rab-Effector complexes. For these RBDs the recognised epitope is restricted to the Switch I-interswitch- Switch II region [197-200]. In these cases, selectivity is thought to come from non-conserved residues within this region including critical recognition determinants in the RabF1 and switch II regions [200]. For example, two Rab5 subgroup Rabs; Rab5 and Rab22 show minimal changes in their structures when binding various effectors, including; EEA1, Rabaptin5 and Rabenosyn5. In an attempt to determine whether the specificity of these effectors for these Rabs is determined by specific sequence elements, Mishra et al mutated specific residues in Rab4 to match those in Rab5 which are involved in effector interactions. However, it was found that these mutations were not sufficient to allow the Rab4 to bind the Rab5 effectors. It was

necessary to mutate further core residues to produce binding [200]. This indicates that although specific sequence elements aid in binding in these cases of low plasticity, the system is still by no means straightforward. It seems that the whole binding surface, and in particular, the hydrophobic triad is influenced by non-conserved core residues which determine the epitopes recognised by RBDs [201]

In contrast, Rab11 does not follow this trend. In the case of the Rab11-FIPs (Rab11 Family Interacting Proteins) switch II of Rab11 undergoes large conformational change in comparison to the active Rab11 structure [202-204]. Furthermore, in the case of the Rab11-MyoV interaction, both switches are extensively remodelled [205, 206]. These interactions involve rearrangement of the switch regions and the hydrophobic triad leading to adaptation of the Rab binding epitope. It is thought that the ability of Rab11 to remodel depending on the effector with which it is interacting may lead to an element of promiscuity amongst these interactions [207].

(iii) Some Rabs have Multiple Effector Binding Sites

An interesting, and relatively new development in the study of Rab-effector interactions has been the discovery of a second effector binding site on some Rabs. These Rabs are capable of binding two effectors simultaneously thereby coordinating the functions of both effectors and allowing for cooperation between them. Two examples of dual effector binding exist for Rab11. A second binding site adjacent to the primary binding site at the switch I-interswitch-switch II region exists and can be re-organised by the structurally diverse effectors Rabin8 and phosphatidylinositol 4-kinase (PI4kIIIβ) [208, 209].

Rab11 may form a tertiary complex with PI4KIIIβ and Rab11FIP3 wherein Rab11FIP3 associates with the Rab at the canonical binding site and PI4KIIIβ bind the secondary binding site. This complex functions to coordinate Rab11 and FIP3 on PI(4)P enriched membranes [209]. PI4KIIIβ is localised to the Golgi either by Arf1 or ACBD3. Its presence there is required for Rab11 recruitment [210]. Therefore, the secondary binding site for Rab11 may be considered to act in a localisation/targeting capacity. The tertiary complex

also plays a role in cytokinesis. PI4KIIIβ is involved in the localisation of secretory organelles at the cleavage site and Rab11FIP3 is important in the targeting of Rab11 vesicles to the cleavage furrow [211]. PI(4)P enriched membranes define the localisation of the Rab11 effector Golgi phosphoprotein 3 (GOLPH3) which is required for cleavage furrow ingression [212]. Simultaneous binding to Rab11 allows for the coordination of effector functions with vital roles in cytokinesis. The importance of this pathway is highlighted by consequences of its dysregulation. Overexpressed PI4KIIIβ and Rab11a lead to the activation of Akt which regulates cell survival, proliferation and growth, a mechanism which is activated in an unregulated fashion in breast cancer [213].

Rab11 may also form a tertiary complex with Rabin8 and Rab11FIP3. In this complex multiple weak interactions collaborate to form the tertiary complex. Rabin8 binds the secondary binding site of Rab11 and Rab11FIP3 binds at the canonical site. Some weak interactions exist between the RBDs of the effectors [208]. Rabin8 is a GEF for Rab8 and its recruitment to Rab11-Rab11FIP3 positive membranes is part of a Rab11-Rabin8-Rab8 functional cascade which allows for the spatially controlled activation of Rab8 and conversion to a Rab8 positive compartment [214, 215]. This process is important for maturation of the compartment and endosomal trafficking during primary ciliogenesis and epithelial polarisation.

(iv) Rab Effectors Display Promiscuity

Some Rab effectors bind a wide range of Rab proteins. A model example of this is the OCRL1 effector. This promiscuous effector binds Rabs from different functional groups such as Rab1, Rab5, Rab6, Rab8, Rab14 and Rab35 [216-218]. Rabs localised to the Golgi and endosomal membrane compartments bind to OCRL1 which functions to change to phosphoinositide composition of the membrane via its 5-phosphatase domain activity. The protein achieves its binding promiscuity by forming tight contacts with conserved Rab residues alongside contacts with the main chain atoms which reduces the dependence on sequence for the protein interaction [219, 220].

It is also possible for effectors to bind more than one Rab at the same time through adjacent Rab binding sites with distinct specificities. These effectors provide ways to couple GTPase activities and enable crosstalk between compartments. They may link the functional processes of Rabs or link Rabs of different membranes and aid in membrane tethering. For example, Ranenosyn5 is a bifunctional effector of Rab5 and Rab4 implicated in early endosome trafficking which binds both Rabs via two structurally similar RBDs [221, 222]. It is required for early endosome fusion both homotypically and of clathrin coated vesicles and endosomes. The effector is critical to the processing of transferrin receptors internalised by clathrin mediated endocytosis [221-223].

(v) Rab-Effector Interactions Follow a Range of Binding Modes

Rab binding domains follow various structural motifs. They often involve two helices that form the centre of the interface. However, the helices are not positioned with strict or predictable orientations [90, 196].

Rab effector interactions may be classified into a number of binding modes. The most common of these binding modes are; all α-helical, mixed α-helical, β-β zipping and a bivalent mode of binding [196].

In the all α-helical mode of binding the effector binds the Rab with 2 α-helices placed alongside the switch regions. These helices may come from a monomer or one from each of a dimer of proteins. Examples of this binding mode include; Rab6-DENND5 where the C-terminus of DENND5 consists of two RUN domains separated by a PLAT domain. The first and last helices of the RUN1 domain stack parallel to each other and interact with the switch regions of Rab6 [224]. In the case of Rab11-FIP2 the conserved Rab binding domain of the FIP (RBD) binds to the switch region of Rabs. In this interaction, a heterotetramer is formed where the RBDs of two FIP2 molecules form a coiled coil with two Rab binding sites, one on either side [204].

In the case of the mixed α-helical mode of binding, a single α-helical segment interacts with the switch region, with a second interaction occurring outside of the switch/interswitch region. Both the interaction within the switch region

and this second interaction are important for the correct binding affinity to be achieved. An example of this mode of binding can be found in the interaction of the Rab27 family of effectors (Slac2-a, Slp2-a and Rabphilin-3/Exophilin-1) binding to Rab27 or Rab3. A single helix packs alongside the switch/interswitch region but, in addition to this, the RBD has a globular zinc stabilised subdomain which interacts with a hydrophobic patch outside of the switch region of the Rab [225].

An alternative mode of Rab binding is the β-β zipping model. This involves a β-β zipping interaction between the effector and the β2 strand of the interswitch. An example of this binding is the interaction between Rab8 and OCRL1. Here, the Rab binds to the ASH domain of OCRL1. The RBD fold is an N-terminal α-helix followed by a β sandwich. Binding occurs between β9 of the ASH domain and a preceding α-helix linker and the switch1/interswitch regions [219].

Finally, the bivalent mode of binding must be considered. Here, complexes assemble as heterotetramer with the Rab binding domains forming a central symmetric homodimer. This mode of binding can be present in the other modes, as is the case for the Rab11FIPs. All known Rabs are monomeric, so this mode of binding may be important for assembling complexes that may be biologically relevant as this mechanism would increase effector residence time at the membrane. This mode of binding also imposes orientation restrictions on the effector complex relative to the membrane[196].

1.3 The Rab11 Subfamily

1.3.1 Rab11 Isoforms and their Effectors

The Rab11 subfamily members are closely related small GTPases. In Drosophila there is only a single Rab11 gene, but in vertebrates the family consists of three isoforms, Rab11a, Rab11b and Rab25, which is sometimes referred to as Rab11c [1]. Rab11a and Rab11b are ubiquitously expressed [226, 227] but Rab25 is only found in epithelial cell types [228]. These proteins interact with a group of effectors termed the Rab11 family of interacting proteins (FIPs) [229-232]. The Rab 11 subfamily interact with both class I and class II FIPs. Rab14, which is more distantly related, also binds class I FIPs and will be part of our discussion here [233-235]. The most extensively studied subfamily member is Rab11a, which is often referred to in the literature simply as Rab11. For the purposes of our study, all Rab11 constructs used were Rab11a derivatives.

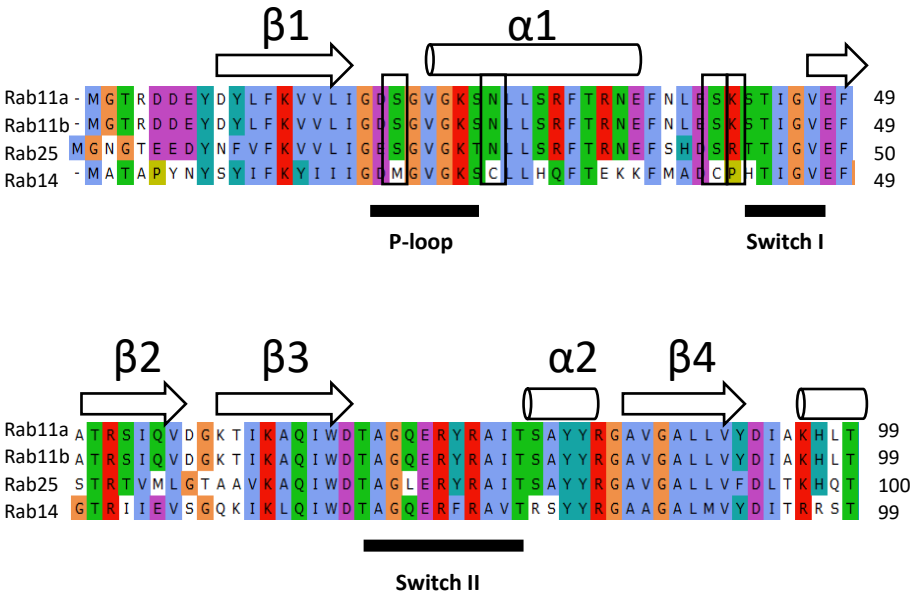

Figure 1.3.1 Multiple Sequence Alignment of the Rab11 Subfamily. The alignment shows sequences for Rab11a, Rab11b, Rab25 and Rab14. The P-loop and the switch regions are underlined and the secondary structure is shown by the cartoons above the sequence. The boxed residues represent significant differences between Rab11/Rab25 and Rab14; S20M, K41P and the two residues which form a disulphide bond C26C40 (Rab14).

(i) FIP Classification

The FIPs are an evolutionarily conserved family of effectors for a subset of Rabs and Arfs. Although diverse in sequence and length, they are characterised into the family by their ability to bind members of the Rab11 subfamily through a 20aa C-terminal RBD. The FIPs are encoded by five genes although alternative splice variants have been reported. The FIPs can be divided into two groups. The class I FIPs all contain C2 domains and they include RCP (FIP1), FIP2 and Rip11 (FIP5). These FIPs are mostly localised to the endocytic recycling compartment and their C2 domains participate in this localisation through interaction with the lipid bilayer [232]. The class II FIPs; FIP3 and FIP4, are known to interact with Arfs and contain ERM domains, EF hands and a proline-rich region [236]. The FIPs form dimeric α-helical coiled coils, providing two symmetrical Rab binding sites at their C-termini and domains which can modulate other functions at their N-termini.

(ii) The Rab11 Subfamily and their Effectors Modulate Various Functions

The Rab11 family are associated with recycling endosomes (REs) and regulate the pathway from early endosomes to the endocytic recycling compartment [237]. Function and dysfunction of the Rab11 family members have been associated with various disease states, including Alzheimer's disease [238], Huntington's disease [238-240], Type 2 diabetes [241] and multiple forms of cancer [242].

The existence of multiple FIP effectors indicates that they have evolved to regulate several distinct subcellular events. In fact, the FIPs modulate three main classes of functions; the recycling of cargo to the cell surface, delivery of membrane to the cleavage furrow during cytokinesis and acting as linkers between Rab11 and motor proteins.

The Rab11 family and their effectors are essential regulators of endosomal recycling [237, 243]. The Rab11FIPs define discrete subdomains within the endosomal recycling pathway [244]. The FIPs were first implicated in the recycling of cargo to the plasma membrane when it was discovered that N-terminal truncations of class I FIPs impede the recycling of endocytosed

transferrin receptor (TfnR) to the cell surface in BHK and HeLa cells. The C2 domains of class I FIPs can function to target the FIP containing complex along with its associated cargo to docking sites on the plasma membrane enriched in Phosphatidylinositol (PtdIns) and P_3phosphatidic acid. It has since become obvious that FIPs function to regulate endocytic recycling at multiple points via their Rab binding and functional activities. N-terminally truncated FIP2 (129-512) inhibits trafficking through the recycling system and results in the accumulation of Rab11a in a collapsed membrane cisterna [230, 232, 245]. Similarly, mutant FIP2 also caused inhibition of the recycling system, although its effect appears later in the pathway [245]. Similar effects are seen for other FIPs. FIP1C and RIP11 N-terminal truncations which remove their C2 domains, inhibit recycling and cause the accumulation of Rab11a [229, 246]. Further studies have revealed that individual FIPs may traffic specific cargo to the cell surface. For example, RIP11 functions to inhibit insulin-stimulated uptake of 2-deoxyglucose and insertion of the facultative glucose transporter isoform 4 (Glut4) containing vesicles to the plasma membrane [247].

Another group II Rab, Rab14, is divergent from the Rab11 family, but retains the ability to bind class I FIPs [233]. More recent studies have implicated Rab14 in insulin dependent Glut4 trafficking. Insulin regulates the amount of Glut4 receptor on the cell surface by regulating the ratios of endocytosis and exocytosis taking place and stimulating the release of insulin receptors from Glut4 storage vesicles (GSVs). Glut4 is endocytosed via the endocytic pathway into early endosomes and subsequently recycled through the slow constitutive recycling pathway through endosomal recycling intermediate compartments (ERCs) [248-252]. In adipocytes Glut4 may also be trafficked through an insulin sensitive sequestration pathway into GSVs. The insulin sensitive protein Akt substrate of 160 kDa (AS160) has been shown to effect sorting of endocytosed material into GSVs and subsequent exocytosis from these compartments. The AS160 protein is a GAP for both Rab14 and Rab10, which have both been implicated in Glut4 trafficking in adipocytes and in muscle cells [250, 253]. In fact, the knockdown of Rabs 8, 10 or 14 effects the prevalence of cell surface Glut4 [254-257]. In muscle cells

overexpression of Rab8 or Rab14 is sufficient to overcome the decrease in the cell surface concentration of Glut4 caused by constitutively active mutant 4P-AS160 [258]. Interestingly, in adipocytes overexpression of wild type constitutively active mutant Rab14 causes a decrease in Glut4 receptors at the cell surface and results in their accumulation at enlarged early endosomes, indicating that Rab14 limits the fusion of ERC derived vesicles with the cell surface [259]. Rab14 has been found to limit the trafficking of endosomes into the GSV sequestration pathway whereas Rab10 limits exocytosis from GSVs. Rab14 also limits trafficking through the Rab10 independent ERC pathway indicating that Rab14 functions at a shared step between the pathways [260].

Recycling endosomes are important in mediating abscission during cytokinesis [211, 261, 262]. Changes to endocytic recycling occur during mitosis and are required for successful completion of cytokinesis. Although it was postulated that the re-direction of REs initiated abscission by fusing with the plasma membrane and building a new membrane between the two daughter cells, it has more recently been shown that fusion of REs mediates the formation of a secondary ingression thereby initiating recruitment of vital factors such as ESCRT-III to the abscission site [263-265]. Rab11 is a key regulator of RE transport to the intracellular bridge (ICB) during abscission modulated by FIP3 [211, 262]. Rab11-FIP3 complex accumulates at the IBC during mitosis. siRNA depletion of FIP3 causes cells to arrest in late telophase [266]. It has been shown that FIP3 positive endosomes deliver p50RhoGAP to the ingression furrow during late telophase where it mediates nested depolymerisation of the actin cytoskeleton leading to the formation of the secondary ingression and abscission [264].

The motor protein MyosinVa binds multiple Rabs. It has been shown to bind Rab14 through its central coiled-coil RBD, and Rab11 and Rab25 through the RBD on its globular tail domain [108]. It also binds Rab effector FIP2 [267]. It is possible that crosstalk occurs between these binding sites but that is, as yet, unclear. MyosinVa is largely found on Rab11 and Rab10 positive intracellular membranes. It is also required for maintaining a peripheral distribution of Rab14-positive endosomes [108]. The interaction between

Rab11a and MyoVa mediates apical recycling in epithelial cells. FIP2 acts to couple this motor protein (MyoVb) to Rab11 recycling endosomes [267]. This coupling is critical for the recycling of plasma membrane and receptor trafficking.

(iii) Rab14 and its Implication in Chlamydial Infection

Chlamydia trachomatis is a gram negative, obligate intracellular pathogen which lives in host compartments referred to as inclusion bodies [268]. The bacterium is the leading cause of bacterial sexually transmitted disease worldwide and also the leading cause of preventable blindness [269].

The infectious form of the bacterium enters the cell as elementary bodies (EBs). The EBs take up residence within a modified membrane bound vacuole termed an inclusion. The bacteria then differentiate into reticulate bodies (RBs) which are metabolically active, but non-infectious. After rounds of replication the RBs may differentiate back into EBs and spread to surrounding cells [268].

Having subverted the phagocytic system, *C. trachomatis* hijacks vesicular transport pathways for its growth and replication. Chlamydial infected vesicles dissociate from their normal pathway and intercept TGN derived vesicles. These nutrient rich vesicles traffic to the peri-Golgi region and fuse to form a single vacuole, an inclusion [270].

The chlamydia bacterium influences the protein composition of the inclusion with the aim of subverting the host defence system and gaining nutrients. Rab1, Rab4 and Rab11 have been found to be recruited to inclusion membranes in all species whereas Rab6 and Rab10 are species specific [271-273]. In contrast, Rab5 and Rab7, components of the phagocytic pathway, are excluded from the inclusion membrane [274, 275]. There is evidence for the importance of these Rabs in bacterial life cycle. For example, siRNA silencing of Rab6 and Rab11 impaired lipid acquisition and bacterial replication in *C. trachomatis* [272]. Especially relevant to our study, both FIP2 and Rab14 have been independently implicated in chlamydial development.

Rab14 controls vesicular transport from the Golgi to endosomes. This function ties in with the chlamydia bacterium's close relationship with the Golgi apparatus [234]. In the case of *C trachomatis*, recruitment of Rab14 has been shown to be bacterial protein dependent and independent of both microtubule and Golgi integrity. Rab14 has been shown to associate with bacterial inclusions from ten hours post infection. This association is increased throughout the bacterium's development cycle. Mid-stage inclusions at 24 hours post infection show a Rab14-positive rim surrounding the inclusion. In late stage inclusions Rab14 can be seen to be associated with structures resembling intrainclusion vesicles inside the lumen. Rab14 is required for chlamydial inclusion growth and development. The expression of the negative cytosolic mutant delays inclusion enlargement and impairs bacterial replication. Further, siRNA silencing of Rab14 leads to impaired bacterial replication and impaired infectivity [276].

FIP2 has also been shown to be recruited to chlamydial inclusions. FIP2 functions in regulating transcytosis [245], apical targeting [277] and recycling systems [231]. The protein and its Rab interacting proteins have been implicated in chlamydial infection. However, no other member of the FIPs have been shown to be localised to these structures [230, 278]. The association of FIP2 is RBD dependent and FIP2 is required for efficient bacterial replication and infectivity. FIP2 silencing decreases the amount of bacterial progeny demonstrating its importance for bacterial replication. FIP2 binds to Rab11 at the inclusion membrane. The bound FIP2 then favours the recruitment of Rab14. It is likely that the bacteria recruits FIP2 to hijack host intracellular trafficking in order to redirect vesicles full of nutrients to the inclusion [279].

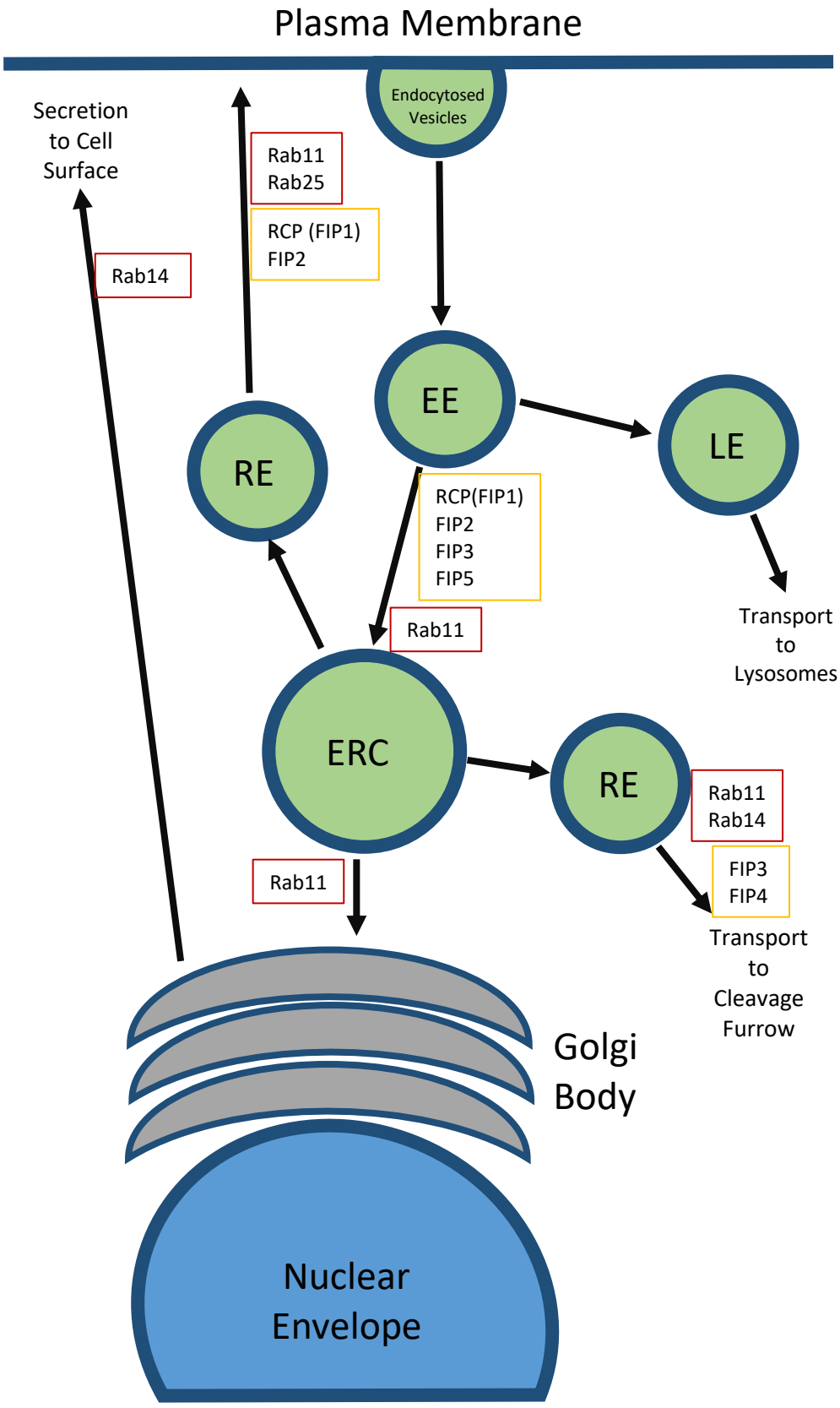

Figure 1.3.2 The Endosomal Recycling System. The diagram above depicts a simplified cartoon of the endosomal recycling system. The localisations of the Rab11 family and Rab14 are shown in red, and the FIPs are shown in yellow. Rab11a and Rab11b have overlapping localisations and are not differentiated

(iv) Rab11 Subfamily and their FIP Effectors; Binding Specificity

The Rab11 subfamily of proteins bind to class I and class II IFIPS. The more distantly related Rab14 has also been shown to bind class I FIPs in a GTP dependent manner and will be part of our discussion here [233]. By virtue of the fact that Rab14 is selective for Class II FIPs, and that the Rab-effector interactions display variable affinities, it follows that there must be significant differences between the interactions of the subspecies of effectors with their Rabs to allow for this discrimination. The factors which determine the specificity of FIP binding and also those which determine the affinities of said binding pose interesting questions. The functional significance of the sharing of effectors among the Rab11 subfamily and also Rab14 is another question which remains unanswered. It has been postulated that the sharing of effectors may aid in the coupling of different Rab functions or, perhaps, the Rabs may be part of a cascade [233]. The Rab11 family and their interaction proteins display similar binding interfaces. Here, we take three structures as examples and discuss the similarities between Rab11-FIP3, Rab11-FIP2, and Rab14-RCP. We may begin to understand the elements of these interactions which determine specificity and affinity, particularly in the case of the more discriminatory Rab14, through careful examination of their structures.

In the case of Rab11 binding a class II FIP, FIP3, the complex formed is a quaternary complex with the FIP forming a central symmetric coiled coil with two symmetrical Rab binding sites on either side [202]. This is reminiscent of other Rab11-FIP complexes. The complex buries 771 Å and 736 Å surface areas on the two Rab11 binding sites. The binding site involves both switch regions and the interswitch. However, the RabSF motifs are not found to contribute [91]. The amphiphilic RBD of the FIP3 form a coiled coil with the homodimerisation occurring on the hydrophobic side. The same region is involved in a hydrophobic interaction with switch I of the Rab molecule with a Tyr737 side chain of the RBD packed against an Ile44 side chain and Gly44 of the Rab11. Switch II of Rab11 forms a unique conformation relative to other Rabs and contributes to the specificity of the interaction without the RabSF motifs contributing. The aromatic triad member Try80 is in an unusual

side chain conformation in the complex. It points inward to form a large hydrophobic pocket with switch I to accommodate the RBD whereas, in most Rab-effector complexes, it is found to face the solvent [199]. Another individuality is that although in other Rab-effector complexes an effector residue close to the conserved Rab glycine helps to recognise the switches, in the case of Rab11-FIP3 the equivalent Ile742 has limited interaction with switch II and Gly45, rather, Asp739 and Met746 participate in the interaction [280].

The complex formed between Rab11 and the class I FIP, FIP2, shares some similarities with Rab11-FIP3. The complex forms a central symmetric coiled coil consisting of a dimer of FIP2 with Rab11 binding sites on either side. Both helices of the coiled coil interact with the Rab. The interactions are formed between the C-terminal RBD of FIP2 and the switch regions of the Rab11. There are also interactions between the FIP and the β2 strand of the Rab. Like the Rab11-FIP3 complex, switch I of Rab11 is embedded between the FIP dimer and forms hydrophobic interactions while the switch II of the Rab11 molecule is in a more flexible conformation than switch I which is unique to Rab11 [281].

In the complex the FIP2 dimer forms a gently curving α-helix followed by a 3_{10} helix, a short β strand and a loop. A conserved Glu455 forms a hydrogen bond with the backbone NH of Thr452 capping the first α-helix. At the C-terminus, Pro499, conserved in class I FIPs and FIP1, is in a cis configuration and reverses the polypeptide direction to orient the C-terminus towards the second protomer. This serves to reinforce the dimer interaction between the two FIP2 molecules. The side chain of Tyr500, a residue unique to FIP2, bonds to Glu491 via its hydroxyl group further reinforcing the dimerisation. Furthermore, the phenyl ring of the Tyr500 lies below the guanidino group of Arg487 and forms cation π interactions.

In the complex, switch I of Rab11 is buried between the two helices of the FIP2 dimer packed against Leu447 and Try80 and Ile481. Tyr480 hydrogen bonds with Val46 of the Rab and Ile481 is capable of forming a Van der Waals interaction with Gly45 of the Rab switch I. C-terminal to these

interactions, further interactions occur between the Rab11 and only one of the FIP2 molecules. The side chain of Met489, conserved in all FIPs bar FIP4, rests in a hydrophobic pocket formed by Val46 from switch 1, Trp65 and Ile76 and Ala79 of switch II. A 3_{10} helix at the C-terminus orients the polypeptide perpendicularly to the central β sheet of Rab11 (β2) and hydrogen bonding occurs between the β strands. This β sheet interaction is found to be essential to Rab11-FIP2 complex formation as truncation of the FIP2 molecule below Met489 results in the loss of complex formation despite the α-helical conformation of the FIP being retained [282].

A number of elements combine to determine the specificity of this interaction. The unusual conformation of switch II in the Rab11 active form is a contributing factor. In Rab11 the switch is displaced away from switch I towards the α3 helix leaving switch I free to contact both FIP2 protomers. In most Rabs the conformation of switch II would encounter steric repulsion with FIP2 regions 475-482. The guanidino group of a conserved Arg (Arg74 in Rab11) would be in steric conflict with the effector. However, in Rab11 the orientation of switch II is such that Arg74 is capable of forming a salt bridge with the Asp482 of FIP2. Lys41 of switch II and Thr50 also impart specificity by forming a salt bridge and a hydrogen bond with the effector. Rab11 and Rab7 are the only Rabs to have both of these residues; Rab7 is precluded from the interaction by a 90° rotation in the side chain of Lys [281].

As discussed previously, a single effector may bind multiple Rabs. Rab14, a more distantly related Rab, binds to class I FIPs and appears to regulate overlapping endocytic pathways [233-235]. It also binds RUFY1/Rabip4 effector, a shared Rab4/Rab14 effector and regulates endosomal trafficking [283]. In association with RCP it has been shown to function in neuritogenesis [284].

Rab14 binds to RCP with reduced affinity compared to the conventional Rab11-FIP/ Rab25-FIP complexes. It also differs in stoichiometry. In dilute solutions it associates in an unconventional 1:2 assembly. However, it still interacts with the canonical, conserved, FIP RBD. The basis for variable affinities between Rab-FIP complexes and the physiological relevance of

these differences pose interesting questions. Careful interpretation of a combination of structural, thermodynamic and biological properties of these complexes must be considered to understand the interplay between Rabs and their effectors and how they combine to organise vesicle trafficking.

The Rab14-RCP structure reveals an interface topologically identical to the Rab11/Rab25 interactions with FIPs. The biological assembly in solution forms a 2:1 complex. However, in the highly concentrated environment of the crystallisation condition, a second Rab14 is loaded onto the symmetric binding site of RCP (see Figure 1.3.2). Several distinct features of the structure exist. In switch I of Rab14 Cys40 forms an intramolecular disulphide bond with Cys26 in a GTP dependent manner (see Figure 1.3.2). Another distinct feature is the lack of electrostatic parity compared to Rab11/Rab25 FIP interactions. A positively charged residue in Rab11 (Lys41) and Rab25 (Arg41) is replaced by a Pro residue in Rab14. This disrupts a salt bridge formed between the former two Rabs with their FIP effectors as a conserved Glu (Glu616) in the effector has no partner. Distinct features are also seen in switch II. A P-loop Met20 protrudes into space usually occupied by the catalytic glutamine and causes residues 70-73 to form an alternative backbone conformation compared to the switch II conformation observed in the interaction of Rab11/Rab25 with FIPs. As a result, although the switch I conformation closely resembles the structures of Rab11/Rab25 FIPs, switch II differs significantly. It is possible that the reduced affinity of Rab14-RCP is a result of these conformational differences and lack of electrostatic parity. Further studies are required. In this work, we will address this question with biophysical analysis in an attempt to determine the factors influencing effector affinity and specificity.

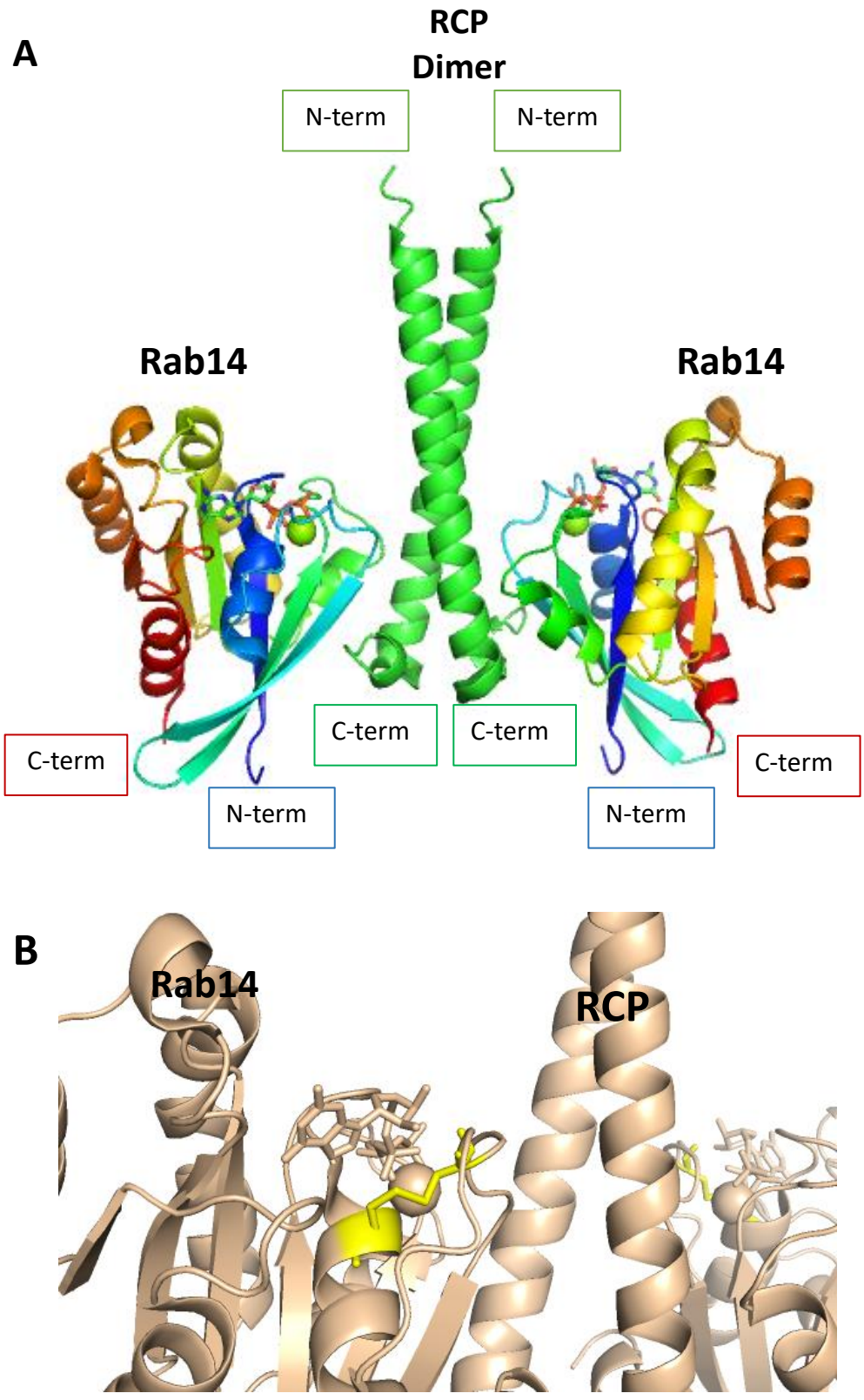

Figure 1.3.3 Structure of Rab14-RCP. In the figure overleaf, Panel A shows the crystal structure of Rab14-RCP which resembles the structure of Rab11 subfamily members in complex with their FIP effectors. The effector forms a centrosymmetric coiled coil with Rab binding sites on either side. Panel B highlights a unique feature of Rab14. A GTP dependent intramolecular disulphide bond (shown in yellow) exists between residue 26 and and residue 40 in switch I. Figure made using Pymol [2]

1.4 Discussion of Scientific Techniques

The biophysical analysis carried out in this work largely relies on the technique of isothermal titration calorimetry (ITC). ITC allows for measurements of the K_d of protein-protein interactions to be made by relying on the exothermic/endothermic properties of these interactions. ITC has a distinct advantage over other methods as it allows for the molecules being examined to be measured in solution, where the molecules are free to rotate, and therefore all the possible binding surfaces are exposed. In contrast, alternative techniques for measuring binding affinity, such as surface plasmon resonance (SPR), require that the ligand be bonded to the surface of a chip before the analysis takes place. It follows that, by using this fixed orientation technique not all of the possible surfaces of the ligand will be exposed to the binding partner.

These different techniques, ITC and SPR, have different ways of measuring affinity. As illustrated in figure 1.4.1, ITC allows for the direct measurement of the association constant (K_a), stoichiometry (N) and enthalpy (ΔH) of the reaction. From these values, the dissociation constant (K_d), the entropy (ΔS) and the Gibbs free energy (ΔG) values may be calculated. In contrast, SPR allows for the calculation of the K_d by measurement of the on rates and off rates of the binding at multiple analyte concentrations [4].

However, it should be noted that limitations of the usefulness of ITC exist. Importantly, not every protein-protein interaction is suitable for analysis by ITC. Some interactions do not evolve or absorb sufficient heat to allow the affinity to be measured. Practical limitations exist. Most importantly, the proteins in question must be available in sufficient quantity and concentration to perform the experiments. For weaker protein-protein interactions, a higher protein concentration is required. The proteins under examination must be stable at sufficient concentrations in order for the experiment to be carried out. The heat evolved in dilution of the sample or buffer mismatch may cause noise and cloud the result of the experiment. In the case of particularly viscous samples, the heat generated from stirring the sample may also become significant. Therefore, the protein samples must be stable in an appropriate buffer. Ideally, the buffer should be identical for all samples.

Although, like all techniques, ITC has limitations, it proved to be a powerful technique in generating the results shown later in the work.

The crystallographic techniques presented in this work are reflective of standard practice used worldwide. Initial crystallisation trials were performed using high-throughput robotic pipetting techniques and commercially available sparse matrix screens from Hampton Research. Once a crystallisation hit was identified, focused screening and crystal replication were performed by hand in a 24 well format. Various methods were employed during attempts at structure determination, including attempts at gaining phase information using selenomethionine derivatisation and, in a more novel strategy, using cobalt atoms present in the crystallisation condition. Structure determination was finally achieved using *ab initio* methods. This method has traditionally only been useful for small proteins with a minimum resolution requirement of 1.2Å. However, this method was successful in refining our dataset (>2Å) by using the programme Arcimboldo, which has become available within the CCP4 suite since January 2016.

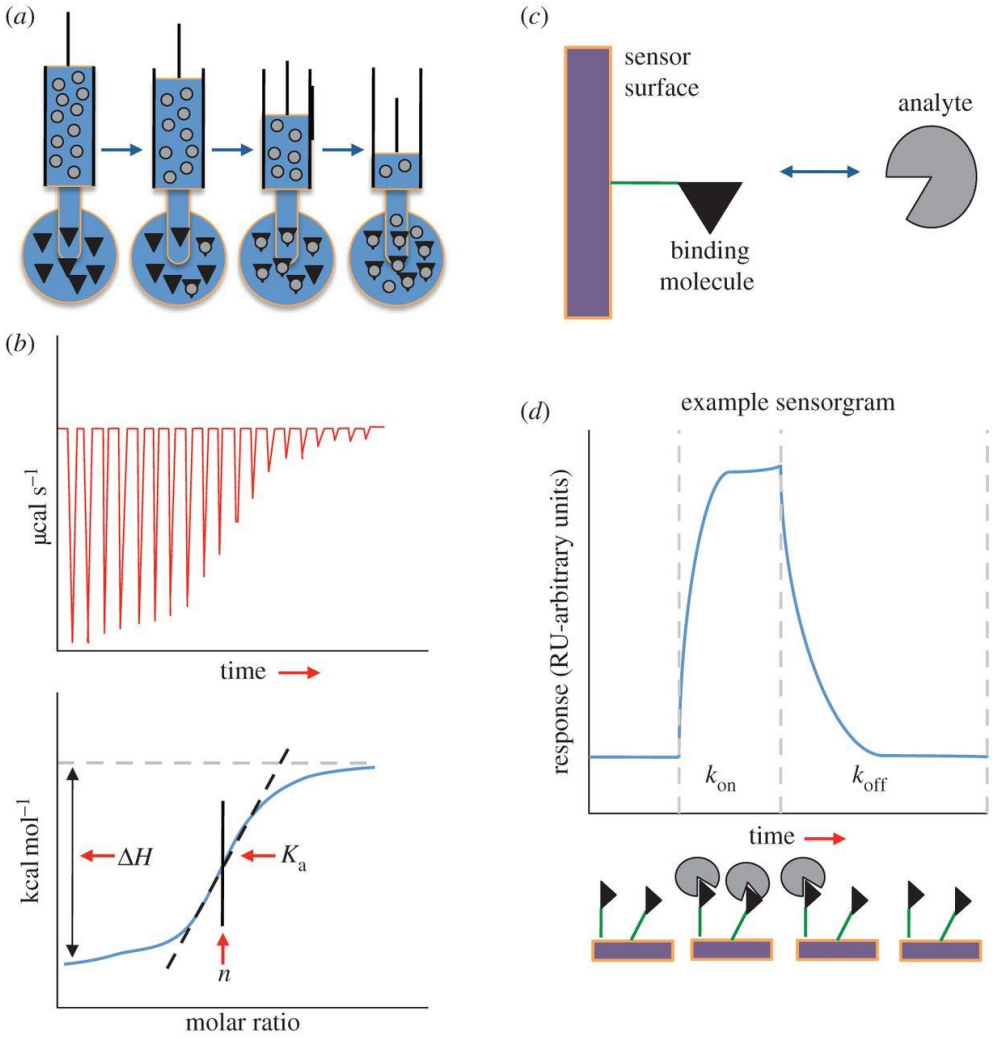

Figure 1.4.1 Experimental Techniques: ITC in Comparison with SPR. Panels A and B are an example of the measurements carried out in a standard ITC experiment. In panel A, the protein held in the syringe (grey circles) is injected iteratively into the protein held in the experimental cell (black triangles) until all the binding sites are saturated and an equilibrium is reached. In panel B, the energy of the binding events associated with each injection is measured directly in µcals^{-1} and depicted as a red peak. These peaks are integrated to form a sigmodal binding curve (shown in blue), from which the enthalpy (ΔH), association constant (K_a) and stoichiometry (N) can be measured directly. Panels C and D depict an example of the measurements carried out in a standard SPR experiment. The ligand protein (black triangles) is fused to a sensor surface and the analyte protein (grey circles) is passed over the surface (see panel A). The on rates and off rates of the interaction are measured directly by taking advantage of the difference in refractive index associated with binding (see panel B). Figure taken from [4] .

1.5 Scientific Objectives

Rab proteins regulate a complex network of vesicle trafficking through their highly conserved Ras superfamily fold. However, despite this, they bind to many diverse effectors with exquisite specificity. The molecular determinants of Rab specificity and the mechanisms by which they may bind shared effectors are of interest to us here.

- Rab14 and Rab11 are divergent Rabs with independent cellular functions. These Rabs share interacting partners; the class I FIPs. Here, we will examine the interactions between Rab11 and Rab14 with their shared partner, FIP2. We hypothesise that our thermodynamic and structural analyses are linked to the distinct cellular functions of Rab11 and Rab14. We will also identify residues and regions of Rabs that can influence the affinities of interactions with class I FIPs. Overall, we hypothesise that small changes in sequence and structure of a Rab may dictate its affinity for a given effector and determine preferential formation of one complex over another.

- We will investigate the structural basis for effector specificity by X-ray crystallography. The unbound state of the effector, FIP2, has not yet been determined. Our aim is to determine the pre-binding state of an effector to understand any conformational changes that are involved in effector recruitment by Rab GTPases.

Chapter 2:

Materials and Methods

2.1 Materials

2.1.1 Chemicals

Chemicals used were of analytical grade and, where possible, generally obtained from Sigma-Aldrich.

Table 2.1.2 List of Protein Constructs

Name	Protein	Length	Vector	Mutations
Rab11QL AJ	Rab11a	1-173	pET28b	Q70L
Rab11CC	Rab11a	1-173	pET28b	N26C, S40C, Q70L
Rab11N26C	Rab11a	1-173	pET28b	N26C, Q70L
Rab11SMKP	Rab11a	1-173	pET15b	S20M, K14P, Q70L
FIP2	FIP2	441-498	pNIC BSA4	Wildtype
Rab14QL	Rab14	7-175	pNIC BSA4	Q70L

Table 2.1.2 List of Protein Constructs. Protein constructs used were tested for solubility and stability during recombinant expression and subsequent purification. All constructs in this work utilised a six histidine tag system for ease of purification. Maps of the plasmids used can be viewed in the appendix.

2.2 Methods

DNA Manipulation Techniques

2.2.1 Mutagenesis

PCR primers for site directed mutagenesis were designed and ordered from Eurofins Genomics. PCR was performed using fusion polymerase (New England Biolabs), standard reaction times, for 25cycles. The resulting PCR products were digested by incubation with *Dpn*1 enzyme (New England Biolabs) for 1 hr at 37°C. The subsequent product was then transformed into DH5α. DNA was extracted from the DH5α by miniprep and individual clones were further analysed by DNA sequencing.

2.2.2 Transformation of Cells

Agar plates were placed in a 37^{o}C incubator to warm/dry in preparation for the transformation. A competent cell stock (CC) of the appropriate strain was thawed on ice. 50 µl of cells were added per 1 µl of DNA used. The cells were gently added to a cooled Eppendorf tube, followed by the DNA. The solution was mixed by tapping. The tubes were incubated on ice for 30 min followed by heat shock at 37^{o}C for 3 min. The cells were returned to ice for 2 min. 1 ml of sterile LB medium was added to the cells. The cells were then incubated at 37^{o}C, 800 rpm for 45 min. The cells were centrifuged for 10-15 s at full speed and the pellet re-suspended in 150 µl of supernatant. Of this supernatant, 50-60 µl was spread onto the warmed plates under sterile conditions. The plates were incubated at 37^{o}C overnight in an inverted orientation. Individual colonies from the plates were then used to set up overnight cultures to produce glycerol stocks.

2.2.3 DNA Electrophoresis

DNA was analysed by electrophoresis through a 1% agarose gel containing 8% nancy 520 DNA stain. Samples were prepared with loading dye (0.4% orange G 0.03% bromophenol blue, 0.03% xylene cyanol, 15% Ficoll, 0.62% DSD, 50mM EDTA, 10 mM Tris-HCl pH8) and the gel was run at 100 V for 50-60 min.

2.2.4 Plasmid Extraction and Sequencing

An overnight culture was set up containing 5 ml LB medium and a 1 in 1000 dilution of appropriate antibiotic. To this, a single colony from a transformed colony of *E.coli* cells containing the plasmid was added (see section 2.2.2 Transformation of Cells). The culture was grown overnight at 37˚C, shaking at 180 rpm. Cells were harvested by centrifuging at 4000 rpm in a benchtop centrifuge. Plasmids were purified from the cell pellet using QIAprep Spin Miniprep Kit. To sequence the DNA, a minimum of 15 µl of 50 ng/µl DNA was sent for sequence analysis at Eurofins Genomics.

Protein Expression and Purification

2.2.5 Small Scale Expression and Extraction of His Tagged Protein

Initial expression tests were carried out to determine protein solubility and optimum expression conditions. Overnight cultures were set up by adding a suitable antibiotic to 2 ml of sterile LB medium in a 1 in 1000 dilution. Solutions were inoculated with a single colony of bacteria and incubated overnight at 37°C, 150 rpm. 5 ml of sterile LB medium were added to a conical tube along with a 1:1000 dilution of suitable antibiotic. Solutions were inoculated with 100 µl of the overnight culture in a 1:50 ratio. The solutions were incubated at 37°C, 150 rpm until an optical density (OD) equivalent to an A_{600} reading of between 0.6 and 0.8 was reached.

Glycerol stocks were made by pipetting 200 µl of autoclaved sterile glycerol into a clean labelled 1.5 ml Eppendorf tube. To this, 400 µl of overnight culture was added and mixed thoroughly. The resulting stocks were snap frozen in liquid nitrogen and stored at -80^{o}C.

At this point expression was induced in the culture. Expression was tested at 37°C for 3 hours induced with 0.5 µM of IPTG and at 18°C for 18 hours induced with 0.5 µM IPTG.

At the end of the allotted incubation time, the cultures were spun at 4,000 rpm for 10 min in a benchtop centrifuge set to 4°C. The supernatant was decanted into waste and the remaining cell pellet was stored at -20°C.

Protein Isolation;

Cell pellets were thawed on ice. Cell pellets were re-suspended in 1 ml of extraction buffer (300 mM NaCl, 10 mM Tris, 10 mM imidazole, 5 mM 2-mercaptoethanol) and transferred to a 1.5 ml Eppendorf tube. The samples were sonicated in a cold room (20 pulses each, output 5, duty cycle 30%). Each sample underwent two rounds of sonication. Samples were spun in a micro centrifuge in the cold room at maximum speed 15000 rpm for 20 min. The supernatant, containing the soluble fraction, was then removed into a clean Eppendorf tube. To each soluble fraction, 30 µl of nickel resin was added. Samples were spun on a spiral rotor for 2 min at 20 rpm and then centrifuged at 2000 rpm for 1 min. The supernatant was removed from the nickel bed and the beads were washed with 1 ml of extraction buffer. The spinning and centrifugation steps were then repeated and the supernatant removed again. Sample buffer was then added to the remaining volume of nickel. The insoluble pellets were re-suspended in 1 ml of milliQ H_2O and 24 µl of the cell suspension was combined with sample buffer. The samples were analysed by SDS PAGE.

2.2.6 Large Scale Expression and Extraction of His Tagged Protein

20 ml of sterile LB medium was pipetted into a labelled 50 ml conical tube. To this, 20 µl of the appropriate antibiotic was added to a final dilution of 1 in 1000. The solution was inoculated with *E.coli* containing the appropriate plasmid and incubated overnight, 37^{o}C, 150 rpm.

Protein expression;

The 20 ml overnight culture was added to a conical flask containing 1 l sterile 2XYT broth medium (1 in 50 dilution) along with a 1 in 1000 dilution of antibiotic. The culture was incubated at 37^{o}C, 180 rpm until an OD (A_{600}) reading between 0.6-0.8 was reached. At this point, protein expression was induced with 0.5 mM IPTG and the temperature of the shaking incubator was adjusted to the optimum temperature for expression of the protein. At 18°C, the culture was left to incubate overnight or approximately 18 hr. At 37 °C, the culture was left to incubate for 3hr.

Extraction from 1 l Culture;

The culture was spun down in a floor centrifuge, 4^{o}C, 3000 rpm for 15 min. The supernatant was discarded. The pellet was re-suspended in 1x PBS and transferred to a 50 ml tube. The solution was spun down at 4000 rpm, 4^{o}C, 10 min. The supernatant was discarded and pellets were stored at -20 ^{o}C.

To isolate protein, 20 µl of extraction buffer (300 mM NaCl, 10 mM Tris, 10 mM imidazole, 5 mM 2-mercaptoethanol) were added to each 1 l pellet and the pellet was re-suspended. The cell lysate was homogenised and the solution was sonicated in a series of 2 min pulses (duty cycle 30%, output 5). Each sample was subjected to sonication three times, resting on ice in between rounds of sonication. The lysate was spun in a floor centrifuge, 18000 rpm 4^{o}C, 30 min. The resulting supernatant was applied to a nickel agarose gravity flow chromatography column. The column was then washed thoroughly with extraction buffer (300 mM NaCl, 10 mM Tris, 10 mM imidazole, 5 mM 2-mercaptoethanol). For some proteins, a higher stringency wash was applied (300 mM NaCl, 10 mM Tris, 40 mM imidazole, 5 mM 2-mercaptoethanol). The protein was eluted from the column with elution buffer (300 mM NaCl, 10 mM Tris, 200 mM imidazole, 5 mM 2-mercaptoethanol). The progress of the elution was followed with Bradford assay to judge when the protein elution was completed. This extraction process is delineated in the flow chart shown in figure 2.2.1. Following extraction the protein was cleaved with the suitable enzyme overnight in the cold room, under dialysis with extraction buffer. After cleavage, the protein solution was reapplied to a nickel agarose gravity flow chromatography column. The flow through from the column, containing the cleaved protein, was collected.

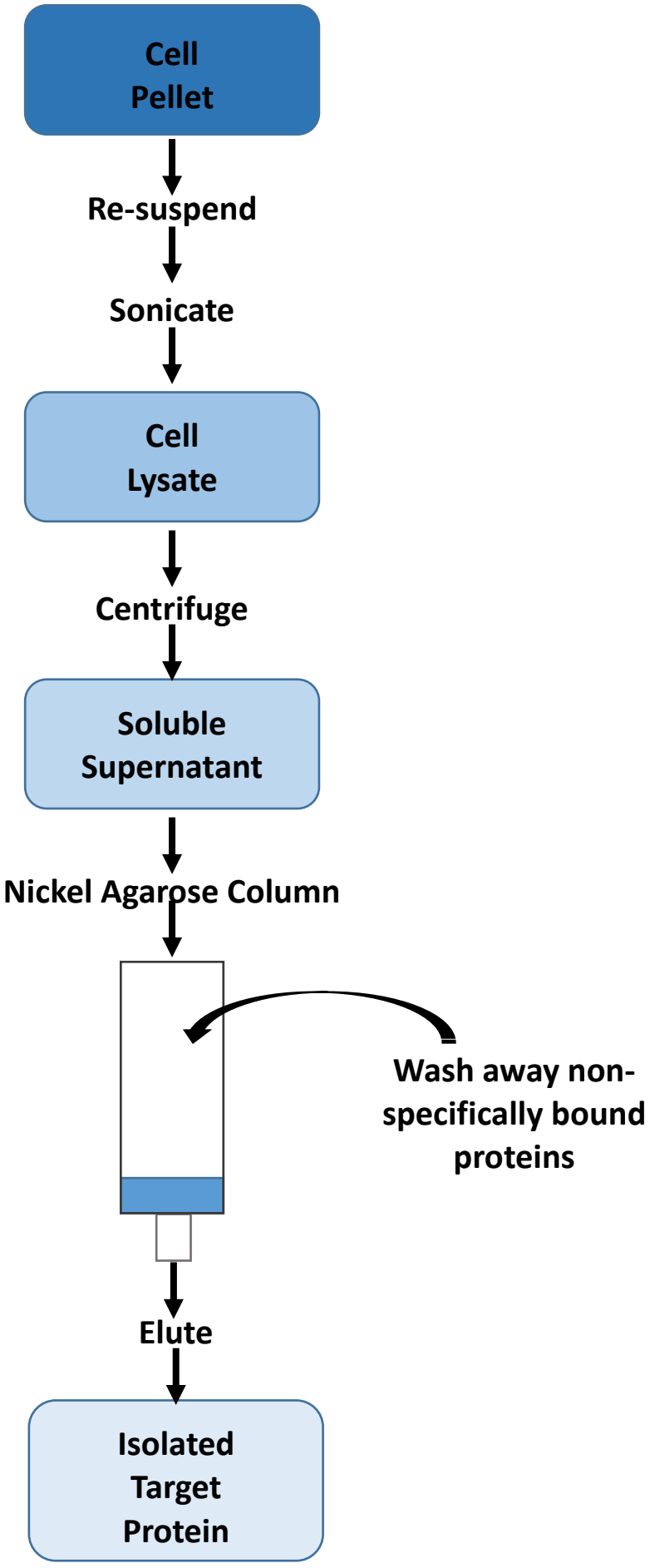
Cell Pellet
Re-suspend
Sonicate
Cell Lysate
Centrifuge
Soluble Supernatant
Nickel Agarose Column
Wash away non-specifically bound proteins
Elute
Isolated Target Protein

Figure 2.2.1 Flowchart of Protein Extraction and Nickel Affinity Purification. The figure shows the workflow for extracting and isolating a His tagged protein from an *E.coli* cell pellet. The pellet is first re-suspended to form a smooth homogeneous liquid and then sonicated to break open the cells resulting in a whole cell lysate. The soluble portion of the cell lysate is then isolated by centrifugation. The resulting supernatant is applied to a nickel affinity column. The column is subsequently washed of all non-specifically bound proteins. The target protein is then eluted from the column with a high imidazole buffer and the isolated target protein is collected.

2.2.7 Expression of Selenomethionine Derivatised FIP2

FIP2 was transformed from a DNA stock into BL21 DE3 *E.coli* cells and grown on a kanamycin containing agar plate overnight. 10 ml of LB medium was inoculated with a single *E.coli* colony from the agar plate. The following morning this culture was used to inoculate a 1 l culture of M9 minimal medium (2 mM $MgSO_4$, 0.4 % glucose, antibiotic(s) (1:1000), 1% BME vitamins 100x (Sigma-Aldrich), 1% trace elements 100x (13.4 mM EDTA, 3.1 mM $FeCl_3$, 0.62 mM $ZnCl_2$, 76 µM $CuCl_2$, 42 µM $CoCl_2$ 162µM H_3BO_3 8.1 µM $MnCl_2$, pH to 7.0, sterile filtered)).

The culture was let grow to an OD (A_{600}) of between 0.8 and 1. At this point the following amino acids were added as solids:

0.1g of lysine, threonine, phenylalanine,

0.05g of leucine, isoleucine, valine

0.05g of L (+) selenomethionine (ACROS Organics 259960025)

Expression was induced 15 min later and the culture was grown overnight at 18°C. The following morning the cells were spun down at 3500 rpm in a floor centrifuge. The cell pellets were purified as described in section 2.2.6.

2.2.8 Purification of Proteins for Isothermal Titration Calorimetry

Proteins produced for ITC analysis were expressed in *E.coli* culture. All Rab11 mutants and FIP2 were expressed at 18°C as described in section 2.2.6. The cells were then harvested in a floor centrifuge by spinning at 3500 rpm for 10 min. Cells were either washed in PBS and then stored at -20 °C or purified immediately. When purified immediately, the cells were re-suspended in extraction buffer (300 mM NaCl, 10 mM Tris, 10 mM imidazole, 5 mM 2-mercaptoethanol, 5 mM $MgCl_2$) and passed through a dounce homogeniser until the suspension was smooth. The cells were then lysed by sonication as described in section 2.2.6. The cell lysate was centrifuged at 18000 rpm for 45 min. The resulting supernatant was applied to a gravity column containing nickel agarose resin. The resin was washed thoroughly with extraction buffer (300 mM NaCl, 10 mM Tris, 10 mM

imidazole, 5 mM 2-mercaptoethanol, 5 mM $MgCl_2$) until it was demonstrated by Bradford assay that the buffer was no longer removing protein from the column. Following this, the resin was washed with approximately 20 ml of wash buffer (300 mM NaCl, 10 mM Tris, 40 mM imidazole, 5 mM 2-mercaptoethanol, 5 mM $MgCl_2$). The protein was then eluted from the column using elution buffer (300 mM NaCl, 10 mM Tris, 200 mM imidazole, 5 mM 2-mercaptoethanol, 5 mM $MgCl_2$). The elution was tested with Bradford assay and halted after the drops stopped showing the presence of protein.

Eluted protein was concentrated to a volume of 5 ml or less and subjected to gel filtration chromatography using a superdex 75 16/60 gel filtration column (GE Lifesciences) (150 mM NaCl, 10 mM Tris, 1mM DTT, 5 mM $MgCl_2$). In the case of the effector FIP2, the protein was first subjected to ion exchange purification. The resulting peak was then pooled and the purity assessed by SDS PAGE. The proteins were co-dialysed overnight to ensure homogeneity of buffer solutions before the ITC experiment was performed.

2.2.9 Purification of FIP2 for Crystallisation

FIP2 was expressed in culture overnight at 18°C and purified from *E.coli* as described in section 2.2.6.

The isolated FIP2 protein was cleaved overnight with Tobacco Etch Virus nuclear-inclusion-a endopeptidase (rTEV) protease in dialysis with low salt buffer (5 mM NaCl, 10 mM Tris, 5 mM 2-mercaptoethanol). The uncleaved protein was separated from the cleaved protein using the batch method of nickel affinity chromatography. 2.5 ml of nickel resin was added per 5 ml of protein solution and rotated slowly for 45 min. Following this, the protein resin solution was passed through a gravity flow column to remove the beads from the protein solution. The remaining cleaved protein was washed from the beads with a few millilitres of dialysis buffer. The protein was then dialysed further into low salt buffer (5 mM NaCl, 10 mM Tris, 5 mM 2-mercaptoethanol) for up to 3 hrs.

The protein was applied to a Mono Q anion exchange column (GE Lifesciences) and a salt gradient was applied from low salt (5 mM NaCl, 10

mM Tris, 1 mM DTT) to high salt (1 M NaCl, 10 mM Tris, 1 mM DTT). The left side of the resulting peak contained pure, cleaved FIP2 as demonstrated by SDS PAGE. The purified FIP was then run on a gel filtration column superdex 75 16/60 (150 mM NaCl, 10 mM Tris, 1 mM DTT). The resulting peak was taken and concentrated to >6 mg/ml for crystallisation.

Biophysical Techniques

2.2.10 Isothermal Titration Calorimetry

Proteins were purified as described in section 2.2.8. Following purification, Rab proteins were concentrated to a minimum concentration of 500 µM, and the effector protein, FIP2, was concentrated to a minimum concentration of 50 µM. The proteins were then co-dialysed into ITC buffer (150 mM NaCl, 10 mM Tris, 1 mM DTT) in order to prevent buffer mismatch during the titration experiment. The calorimetric measurements were taken using an ITC-200 instrument (MicroCal Inc.). Titrations were performed at 293.15K. In each case, the effector protein FIP2 was in the calorimetric cell and the Rab protein was injected into the FIP2 in 2.5 µl injections. Data analysis was performed using Origin 7.0 software. Curves were fitted to a single site binding model.

2.2.11 HPLC Analysis of Rab Nucleotide Composition

After completion of the ITC titrations, samples of Rab proteins were frozen for analysis by HPLC. Having been thawed, Rab proteins were subjected to boiling for 3 min to denature the proteins and release the nucleotide. Samples were then cooled on ice for a few minutes before being centrifuged in a minifuge in the cold room for 30 mins.

To prepare samples for HPLC analysis, 100 µl of supernatant was taken and combined with 50 µl of buffer (100mM potassium phosphate, 8mM TBA, pH6.5), the pH of the solution was confirmed by pH strip and the solution was passed through a syringe top filter.

Standards were prepared by creating a solution of 100 µl of 100 µM GTP/GDP. This solution was then supplemented with 50 µl buffer A and filtered.

Samples were analysed using a Zorbax 300SB-C18 (solvent saver plus 3.0x150mm 3.5micron)(P.N. 863974-302) 20-25 µl of sample was injected and eluted via an isocratic gradient of buffer (100mM potassium phosphate, 8mM TBA, pH6.5). The column temperature was set at 40°C.

Protein Analysis

2.2.12 Bradford Protein Assay

To assess the presence of protein in a solution during a purification scheme, a rudimentary Bradford protein assay was performed. On a piece of parafilm 30 µl drops of Bradford solution were aliquoted. To these, 3 µl drops of the solution to be assessed were added. The resulting colour change from brown to blue was judged by eye and used to confirm the presence or absence of protein in a qualitative fashion.

For a more accurate assessment of protein concentration, a standard curve was set up using bovine serum albumin (BSA). Various concentrations of BSA, ranging from 0.1 mg/ml to 1 mg/ml were added to a Bradford solution (10 µl BSA into 590 µl Bradford solution). These solutions were assessed in a spectrophotometer at 280 nm and a standard curve constructed. Following this the protein sample of unknown concentration was assessed with the Bradford solution in the same way and the standard curve was used to determine its concentration.

2.2.13 Determining Concentration by Nanodrop Spectrophotometry

The nanodrop spectrophotometer was used as the primary method of determining protein or DNA concentration during this study. The instrument pedestal was first cleaned thoroughly using water and a lint free wipe. The appropriate mode for measuring nucleic acid or protein solution was selected on the computer interface. The instrument was initialised using milliQ H_2O. Following this, a 2 µl drop of buffer was applied to the pedestal and the instrument was normalised to the appropriate buffer. The sample was then applied to the pedestal and the absorbance measurement taken twice. An average of the two results was used as the measure of absorbance. For protein,

the Beer-Lambert law was then employed to work out the concentration of the protein from the absorbance.

2.2.14 Bicinchoninic Acid Assay

The BCA assay was employed as an alternative measure of protein concentration. A QuantiPro BCA assay kit (Sigma) was used and the standard protocol was followed.

Crystallisation Techniques

2.2.15 Crystal Screening

Protein targets were purified and concentrated to between 5-10 mg/ml before being screened for crystallisation hits. Screens were set up in a 1:1 ratio using 96 well plates using a Mosquito robot (TTP Labtech). Sparse matrix screens were employed to set up vapour diffusion sitting drops containing 100 nl of protein solution and 100 nl of reservoir. The reservoir volume used was 70 µl. Sparse matrix screens were obtained from Jena Bioscience, Molecular Dimension, and Qiagen.

2.2.16 Crystal Optimisation

Hit conditions were optimised in 24 well grid screens. The vapour diffusion method was employed as in the initial screening process; however, during optimisation, hanging drops were set up using larger volumes- 2 µl of reservoir and 2 µl of protein.

2.2.17 Circular Dichroism analysis

Protein structure of FIP2 was analysed by CD analysis using a Jasco815 instrument. Pure, uncleaved FIP2 was dialysed into 100mM phosphate buffer at a range of pH values: pH 8, 7, 6.5 and 5.8. Proteins were analysed at a concentration of 0.1mg/ml in a 0.02 cm path length cell using Jasco-815 spectrapolarimeter (Jasco Inc.). Elipticity was recorded between 190 nm and 250 nm wavelengths with 4 accumulations being made per sample.

2.2.18 Dynamic Light Scattering

Protein structure of FIP2 was analysed by DLS. After purification, uncleaved protein, at a concentration of 0.6mg/ml in gel filtration buffer

(100mM NaCl, 10mM Tris, 1mM DTT) was diluted 1:1 into either gel filtration buffer, or sodium acetate pH4.8. Samples were spun down to remove insoluble aggregates and filtered before being analysed.

Chapter 3:

Thermodynamics of Rab11/Rab14 Association with FIP2

3.1 Introduction

The Rab11 family members are associated with recycling endosomes (REs) and have functions in the recycling of early endosomes (EEs) to the TGN [237]. Rab11 family members interact with a class of effectors termed the Rab11FIPs. The FIPs are divided into two subclasses, class I and class II. Rab11 family members interact with both classes of FIPs. Rab14 is another group II Rab. Although it is not part of the Rab11 subfamily, Rab14 has the ability to binds class I FIPs [233-235]. FIP2, a class I FIP, is a shared effector for Rab11 and Rab14. Previous work has shown that Rab14 has a reduced affinity for FIPs in comparison to Rab11 and is tenfold weaker in its affinity to FIP2 [284, 285]. For the purposes of our study, all Rab11 constructs used were Rab11a derivatives. By comparing the structures of Rab11-FIP2 and Rab14-RCP (another class I FIP), we may speculate about the structural differences determining the affinities of the complexes [281, 284].

Although the complexes are topologically identical, distinct features of sequence and structure exist between them. The starkest of these differences occurs in Switch I of Rab14, which has an unusual intramolecular disulphide bond between C26 and C40 which is not present in Rab11. This GTP dependent disulphide is a distinct and unique feature of Rab14 and the effect it may have on effector binding is an intriguing question. Furthermore, other less obvious differences between the Rabs exist. In Rab14 a lack of electrostatic parity is observed in comparison to Rab11-FIP complexes. A positively charged residue in Rab11 (Lys41) is replaced by a proline residue in Rab14. This disrupts a salt bridge formed between Rab11 and FIP. Significant differences are apparent in switch II of Rab14 when compared with Rab11. In Rab14 a P-loop methionine at position 20 protrudes into space usually occupied by the catalytic glutamine and causes residues 70-73 to form an alternative backbone conformation [281, 284] (see Figure 1.3.1).

In this work, we will examine these three differences: the existence of the disulphide bond, the lack of electrostatic parity between Rab14 and FIP effectors and the methionine residue causing alterations to the switch II

conformation by mutation analysis. We will determine whether mutating Rab11 at specific points to match the equivalent residues in Rab14 will have an effect on the affinity of the Rab for FIP2. Thereby we will establish which elements are important in determining the affinity of the Rabs for their shared effector.

3.1.2 Scientific Objectives

- To determine the factors which influence the reduced affinity of Rab14 to class I FIPs in comparison to Rab11.

3.2 Results

3.2.1 Generation of Rab11 Mutants

In order to fulfil our goal of establishing those factors which influence the affinity of Rab11/Rab14 for FIP2, we first chose key sequence elements which we postulated may influence the differential affinities between the Rab-effector complexes. We then mutated specific Rab11a residues to make the protein more 'Rab14-like' in character.

The most obvious of these differences is the intramolecular disulphide bond found in the Rab14-RCP structure [284]. Rab11a constructs were generated containing a single cysteine mutation (N26C) and a double cysteine mutation (N26C, S40C) as found in Rab14. A parent construct containing these mutations was already extant in the lab. However, the construct was tested for the presence of nucleotide by HPLC analysis and found to be in the GDP locked state. Therefore, further mutations were produced in order to produce constitutively active Rab11 constructs (Q70L) containing the mutations in question. All Rab11 and Rab14 constructs discussed here are in the constitutively active (Q70L) form unless expressly labelled wt (wild type). The Q70L mutation locks the protein in the GTP bound form by substituting a catalytic glutamine, which is necessary for hydrolysis, with a leucine residue. This method ensures that the proportion of Rab in the GTP bound state is comparable between samples. When using wild type Rabs a number of problems arise. Different wild type Rabs hydrolyse GTP at different rates and, therefore, it is difficult to guarantee that equivalent proportions of two different Rabs are in the active form. The use of GppNHp may help to combat this problem. However, the efficiency of nucleotide exchange also varies between Rab proteins and this process may be prohibitively expensive.

Another Rab11 mutant was produced which contained two other mutations which appear to be significantly different between Rab11 and Rab14, S20M and K41P.This construct was also in the constitutively active form (Q70L) (see list of constructs Table 2.1.1).

The cysteine mutations were analysed by SDS PAGE (see Figure 3.2.1). The mutants were run on an SDS PAGE along with Rab11.The samples were run

in a loading dye containing reducing agent DTT and then in a loading dye containing no reducing agent. Differences in the mobility of the proteins containing the cysteine mutations under non-reducing conditions are clearly observable. The Rab11 double cysteine mutant (Rab11CC) runs faster than Rab11. This may indicate that the protein is more compact due to the presence of a disulphide bridge. Interestingly, the Rab11 single cysteine mutant (Rab11NC) runs as a double band under non-reducing conditions. This suggests that the protein exists as two species, one similar to the double cysteine state and one similar to the Rab11 state. This may indicate that the difference in mobility is not due to the formation of a disulphide. Perhaps the cysteine residues are contributing to the mobility of the Rabs in another way, possibly due to the oxidisation state of the cysteine side chain sulphur residue.

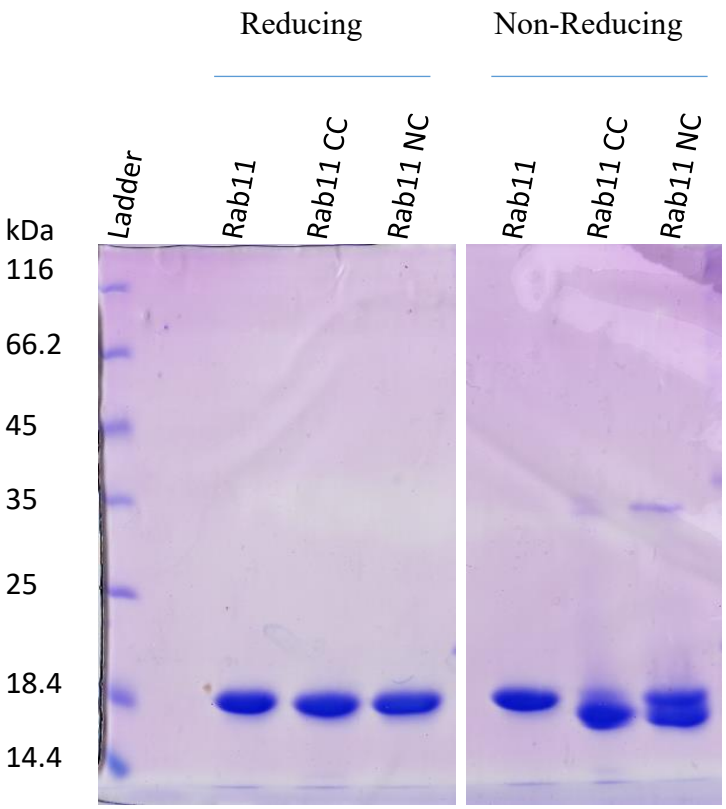

Figure 3.2.1 Reducing/Non-Reducing Analysis of Rab11 Cysteine Mutants. Differences in the mobility of the proteins containing the cysteine mutations under non-reducing conditions are observable. The Rab11CC sample runs faster than Rab11. The Rab11NC mutant runs as a double band under non-reducing conditions suggesting that the protein exists as two species, partially similar to the double cysteine and partially similar to Rab11.

3.2.2 Biophysical Analysis of Rab11 Mutants and Rab11 by Isothermal Titration Calorimetry

The Rab11 mutants and Rab11 were analysed by Isothermal Titration Calorimetry (ITC) to examine their binding to FIP2. All proteins were expressed in *E.coli* and purified by nickel affinity chromatography, followed by gel filtration chromatography (see Figures 3.2.2 – 3.2.6). In the case of FIP2, an additional ion exchange chromatography step was included in the purification scheme (not shown).

A series of titrations were then performed between the Rabs and FIP2. Interestingly, the most distinct feature of Rab14, the intramolecular disulphide, does not appear to have an effect on the affinity of Rab11 for FIP2. Rather, it appears that the less dramatic sequence mutations (K41P and S20M) cause reduced affinity to FIP2 (See Table 3.2.7/ Figures 3.2.8-3.2.14).

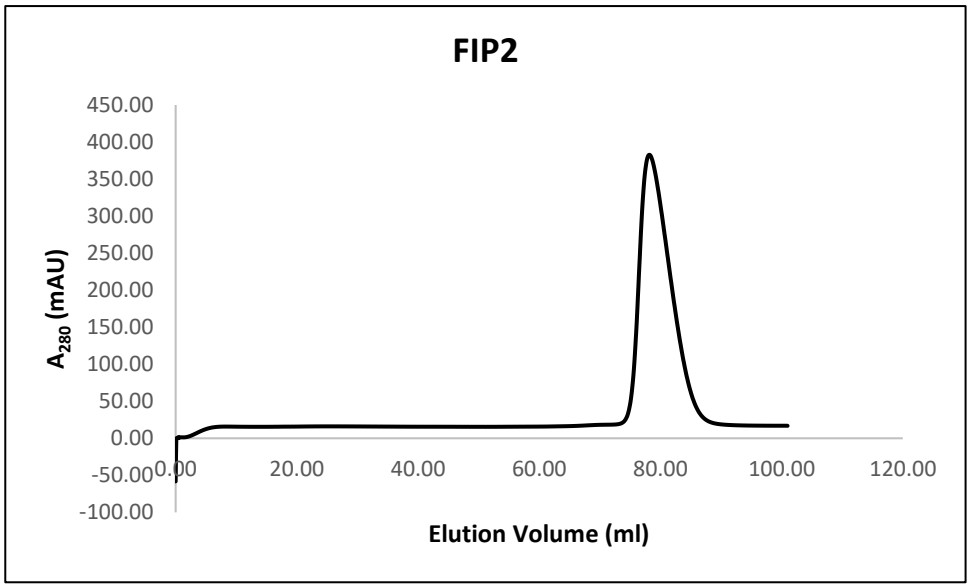

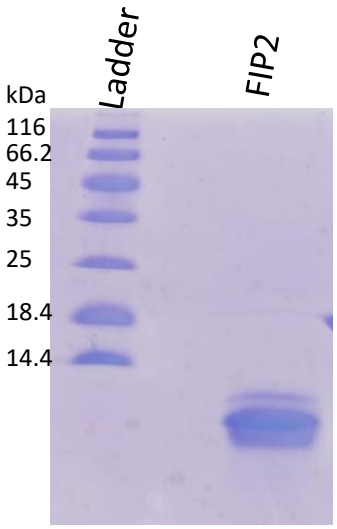

Figure 3.2.2 Purification of FIP2 for ITC. FIP2 was expressed and extracted from *E.coli* cell culture as described in Chapter 2. The protein was not cleaved. A small impurity exists running close to the bulk FIP2 as seen by SDS PAGE analysis (bottom panel). This may be a contaminating bacterial protein or, alternatively, may represent a cleavage event in the FIP2. In order to minimise this impurity, the FIP2 was first subjected to ion exchange chromatography followed by gel filtration chromatography (top panel).

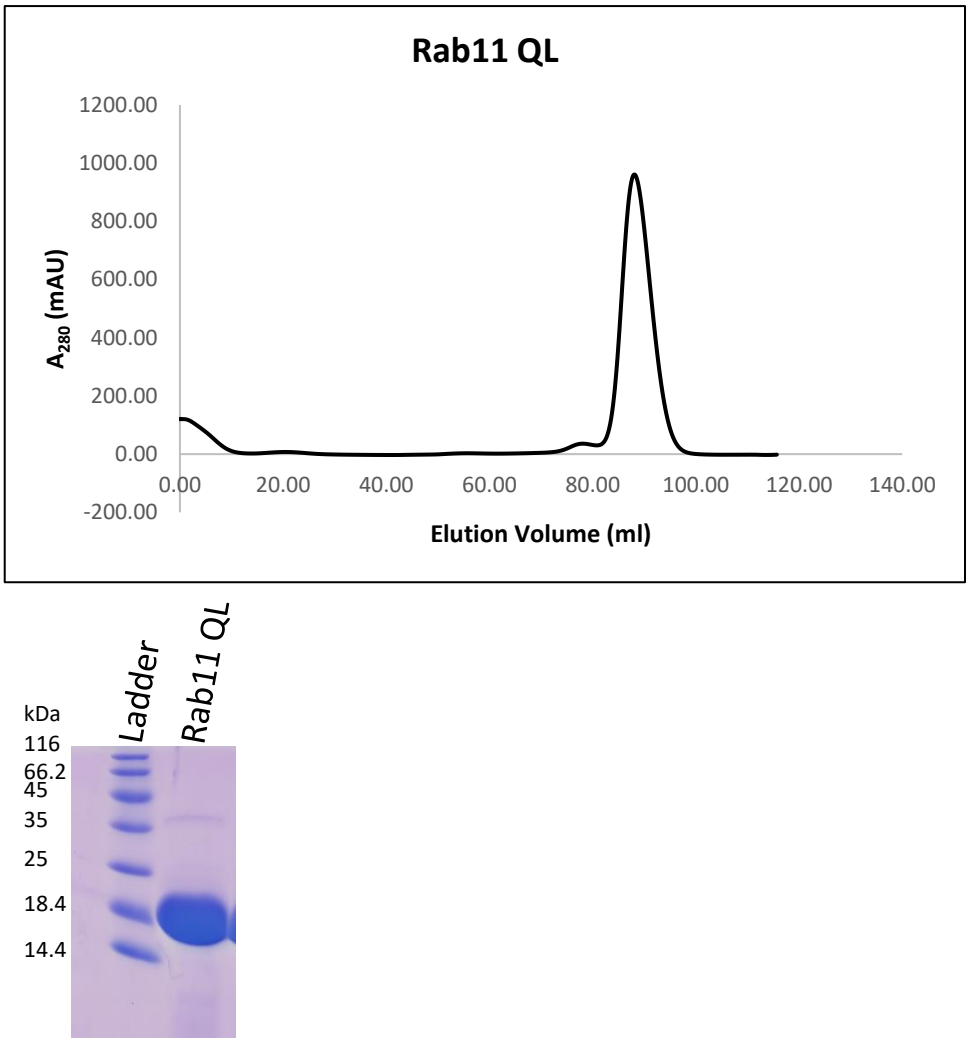

Figure 3.2.3 Purification of Rab11 for ITC. Constitutively active Rab11 (Q70L) was expressed and purified from *E.coli* culture as described in Chapter 2. The protein was further purified by gel filtration chromatography and elutes as one major peak (see upper panel). The Rab11QL is of reasonable purity as shown by SDS PAGE analysis (bottom panel). This figure represents an example of a Rab11 Purification. Many replicates of Rab11QL titrations were repeated over the course of the experiment (n=7).

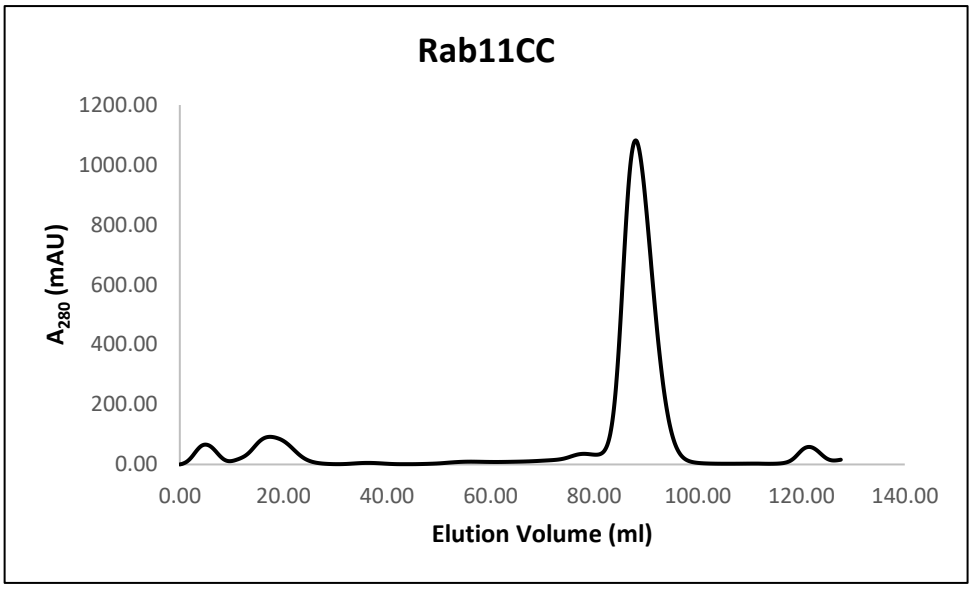

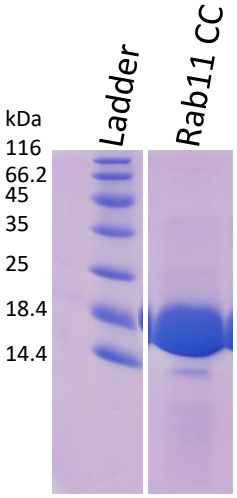

Figure 3.2.4 Purification of Rab11CC for ITC. Constitutively active Rab11 double cysteine mutant (Q70L, N26C, S40C) was expressed and purified from *E.coli* culture as described in Chapter 2. The protein was further purified by gel filtration chromatography and elutes as one major peak with some high and low molecular weight impurities (see upper panel). The Rab11CC is of reasonable purity as shown by SDS PAGE analysis (bottom panel) with a lower molecular weight impurity representing a very small fraction of the solution.

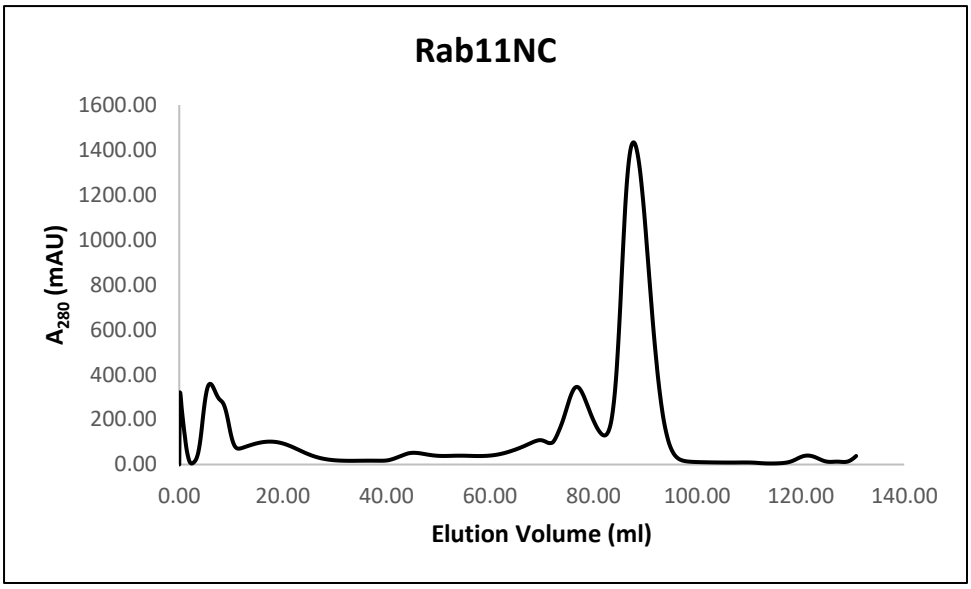

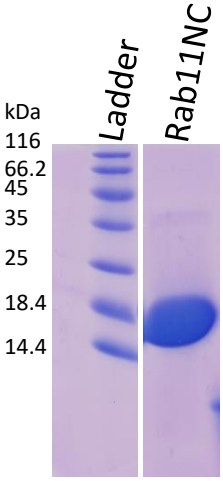

Figure 3.2.5 Purification of Rab11NC for ITC. Constitutively active Rab11 single cysteine mutant (Q70L, N26C) was expressed and purified from *E.coli* cell culture as described in Chapter 2. The protein was further purified by gel filtration chromatography and elutes as one major peak with a number of minor peaks (see upper panel). The Rab11NC is of good purity as shown by SDS PAGE analysis (bottom panel).

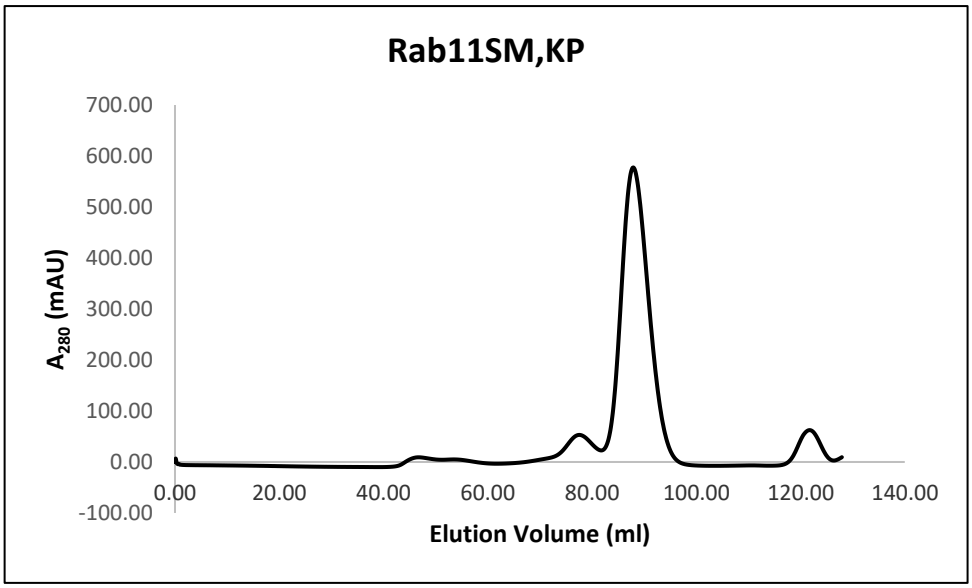

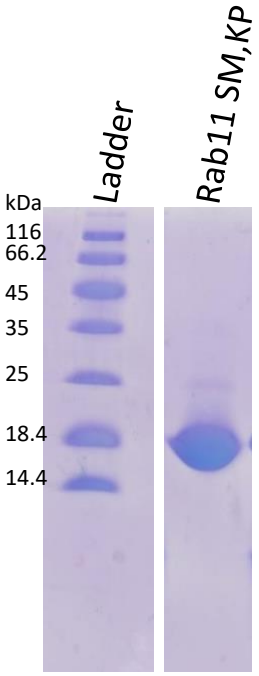

Figure 3.2.6 Purification of Rab11SM,KP for ITC. Constitutively active Rab11 containing two mutants (Q70L, S20M, K41P) was expressed and purified from *E.coli* culture as described in Chapter 2. The protein was further purified by gel filtration chromatography and elutes as one major peak with some minor peaks (see upper panel). The Rab11SM,KP is of good purity as shown by SDS PAGE analysis (bottom panel).

Rab	*Effe-ctor*	K_d *(nM)*	*N*	*ΔG (kcal/K/mol)*	*ΔH (kcal/mol)*	*ΔS (cal/mol/deg)*
Rab11 QL	FIP2	223±35%	0.9	-7.9	-10	-7
Rab11 wt (GDP)	FIP2	1831	0.7	-7.7	-10.1	-8.2
Rab11CC	FIP2	243±10%	0.9	-8.9	-12.5	-12.3
Rab11NC	FIP2	252±10%	0.8	-8.8	-11.8	-10.2
Rab11SM, KP	FIP2	704±25%	0.9	-8.3	-11.5	-10.8

Table 3.2.7 Biophysical Analysis of Rab11 and Rab11 Mutants. In each titration, Rab protein was injected into a calorimeter cell containing FIP2 at approximately 10X lower concentration. All experiments were performed at least twice, except for the titration of Rab11wt into FIP2 which was performed only once. No significant difference in affinity (K_d) is measurable between Rab11QL and Rab11 double/single cysteine mutant. Nor is there a significant difference in the entropy (ΔS), enthalpy (ΔH) or Gibbs free energy (ΔG) values of the interaction. However, the Rab11SM,KP mutant shows approximately 3X weaker affinity for FIP2. The stoichiometry (N) for all reactions is similar and close to a 1:1 interaction.

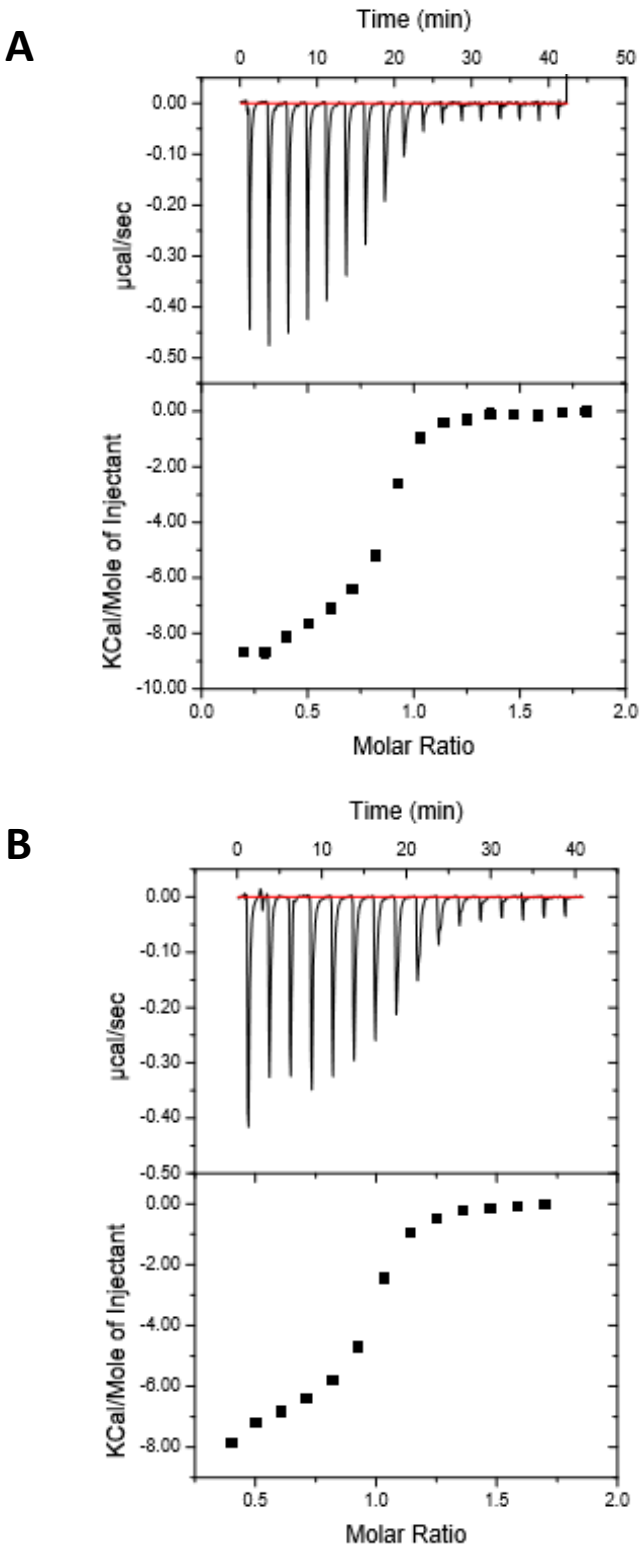

Figure 3.2.8 Titrations of Rab11QL into FIP2. Figure A and B overleaf show the raw data (top panel) and integrated heats (bottom panel) for two titrations of Rab11QL into FIP2. For each titration approximately 400 µM Rab11QL was injected into a cell containing approximately 40 µM FIP2. Data was processed using Origin software provided by Microcal, LLC. The Binding model was assumed to be 1:1. Data were fit to a quadratic binding curve using the isothermal titration calorimetry plugin for Origin (version 7.0). Multiple replicates were performed (n=7).

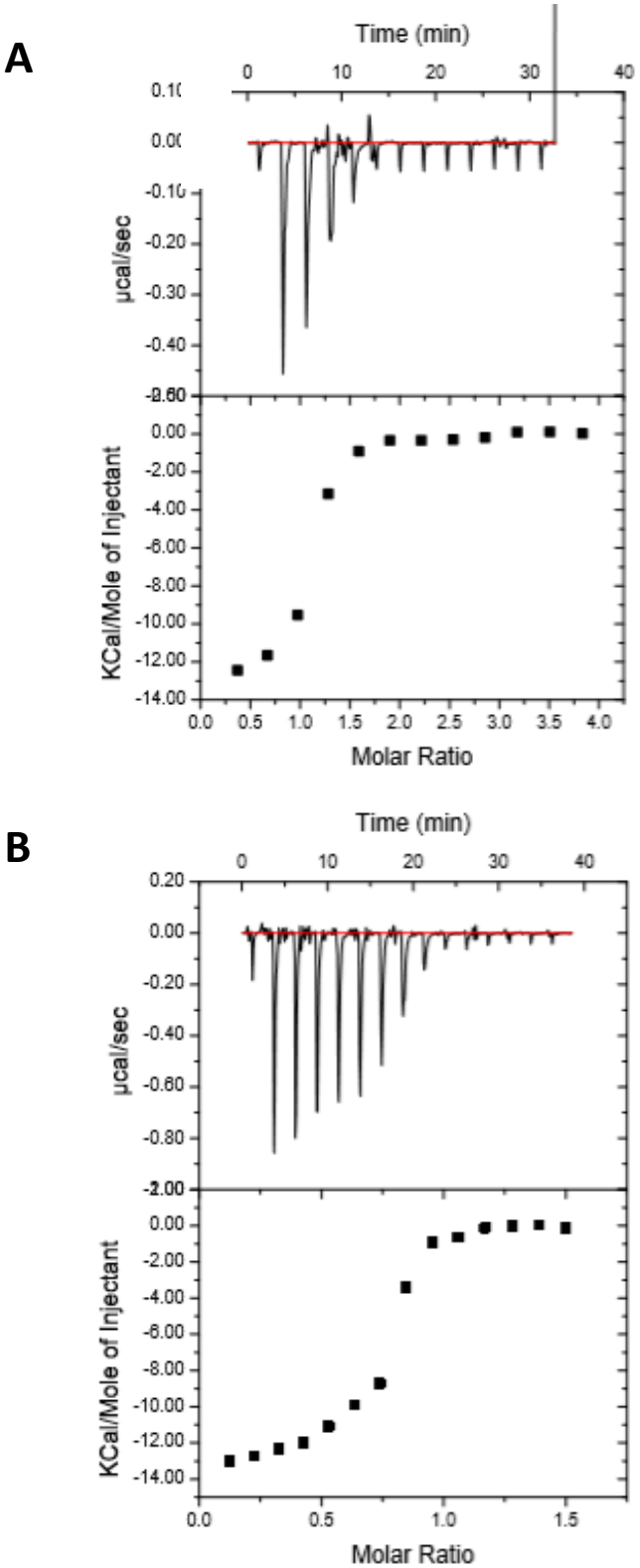

Figure 3.2.10 Titrations of Rab11CC into FIP2. Figure A and B overleaf show the raw data (top panel) and integrated heats (bottom panel) for two titrations of Rab11CC into FIP2. For the titration shown in panel A 500 µM Rab11QL was injected into a cell containing 50 µM FIP2. For the titration shown in panel B 300 µM Rab11QL was injected into a cell containing 30 µM FIP2. Data was processed using Origin software provided by Microcal, LLC. The Binding model was assumed to be 1:1. Data were fit to a quadratic binding curve using the isothermal titration calorimetry plugin for Origin (version 7.0).

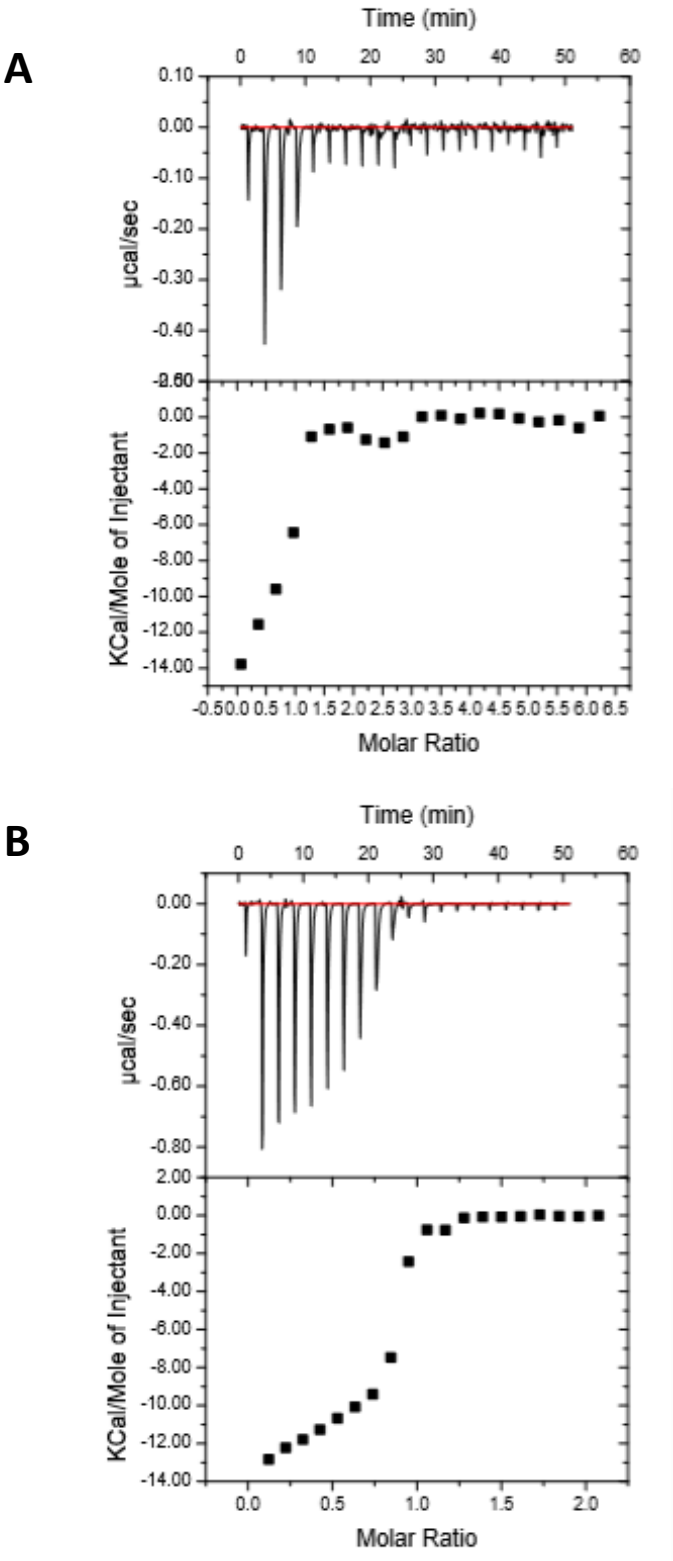

Figure 3.2.11 Titrations of Rab11NC into FIP2. Figure A and B overleaf show the raw data (top panel) and integrated heats (bottom panel) for two titrations of Rab11NC into FIP2. For the titration shown in panel A, 500 µM Rab11NC was injected into a cell containing 50 µM FIP2. For the titration shown in panel B 300 µM Rab11QL was injected into a cell containing 30 µM FIP2. Data was processed using Origin software provided by Microcal, LLC. The Binding model was assumed to be 1:1. Data were fit to a quadratic binding curve using the isothermal titration calorimetry plugin for Origin (version 7.0).

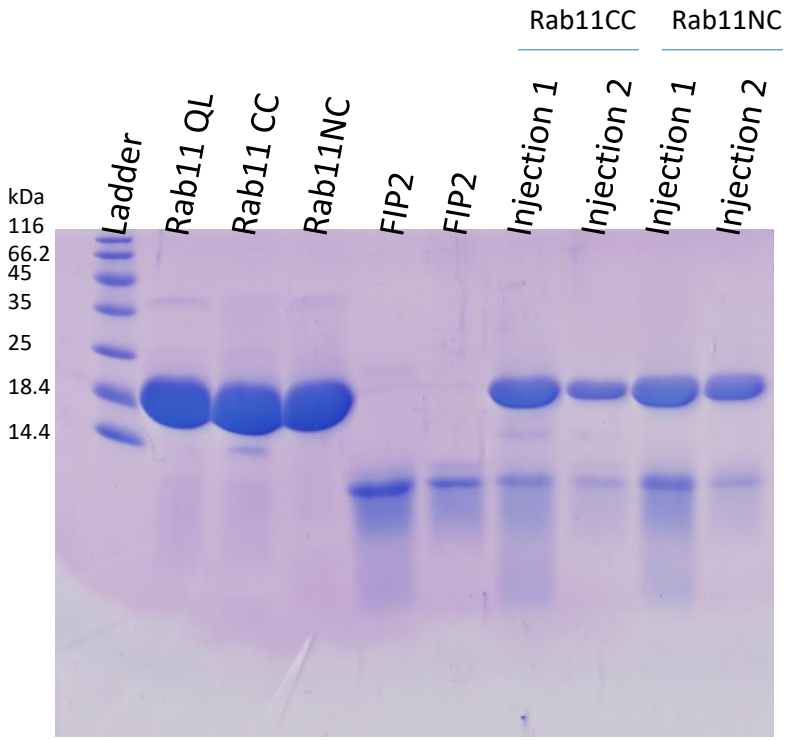

Figure 3.2.12 SDS PAGE Analysis of Titrations of Rab11CC and Rab11NC into FIP2. The quality of protein used for the titrations shown in figure 3.2.10 and 3.2.11 was analysed by SDS PAGE. Rab11CC, Rab11NC and FIP2 are shown above. The protein recovered from the experimental cell at the end point of the titrations is also shown for each titration.

Injection 1- 500 µM Rab11CC into 50 µM FIP2.

Injection 2- 300 µM Rab11CC into 30µM FIP2.

Injection 1-500 µM Rab11NC into 50 µM FIP2.

Injection 2- 300 µM Rab11NC into 30 µM FIP2

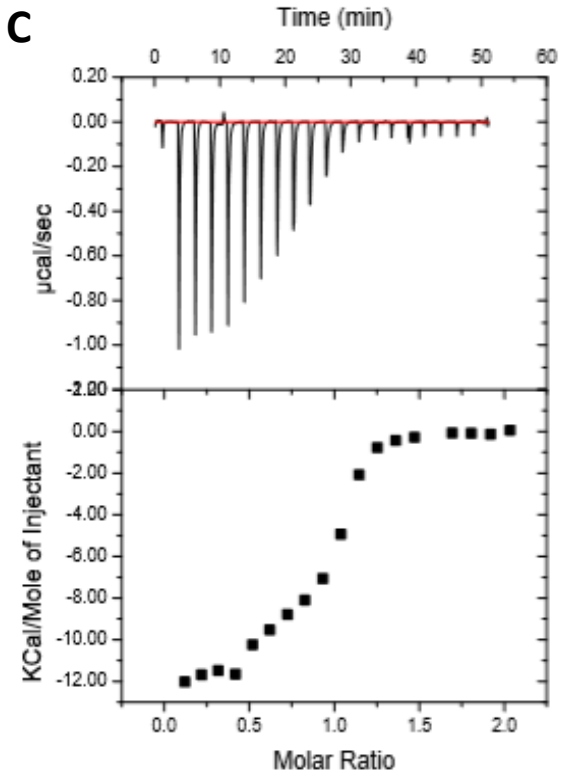

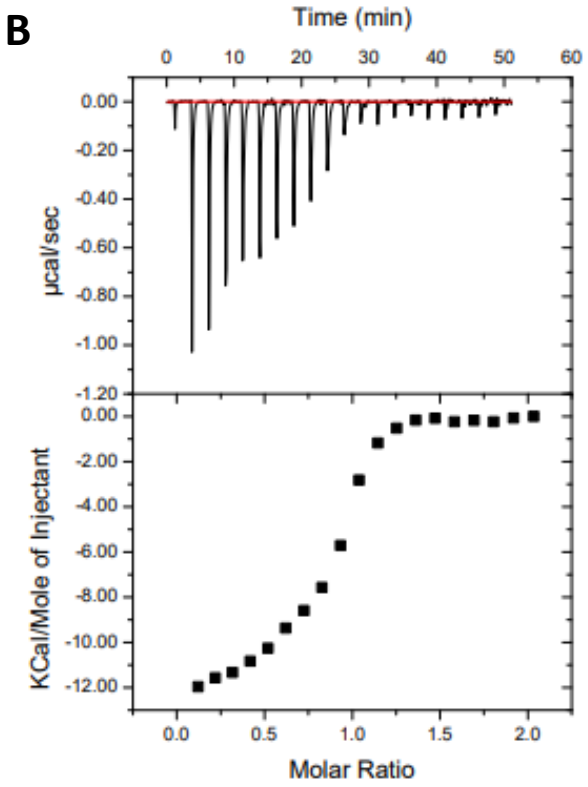

Figure 3.2.13 Titrations of Rab11SMKP into FIP2. Figures A and B (overleaf) and C (above) show the raw data (top panel) and integrated heats (bottom panel) for three titrations of Rab11SMKP into FIP2. For all the titrations 490 µM Rab11NC was injected into a cell containing 50 µM FIP2. Data was processed using Origin software provided by Microcal, LLC. The Binding model was assumed to be 1:1. Data were fit to a quadratic binding curve using the isothermal titration calorimetry plugin for Origin (version 7.0).

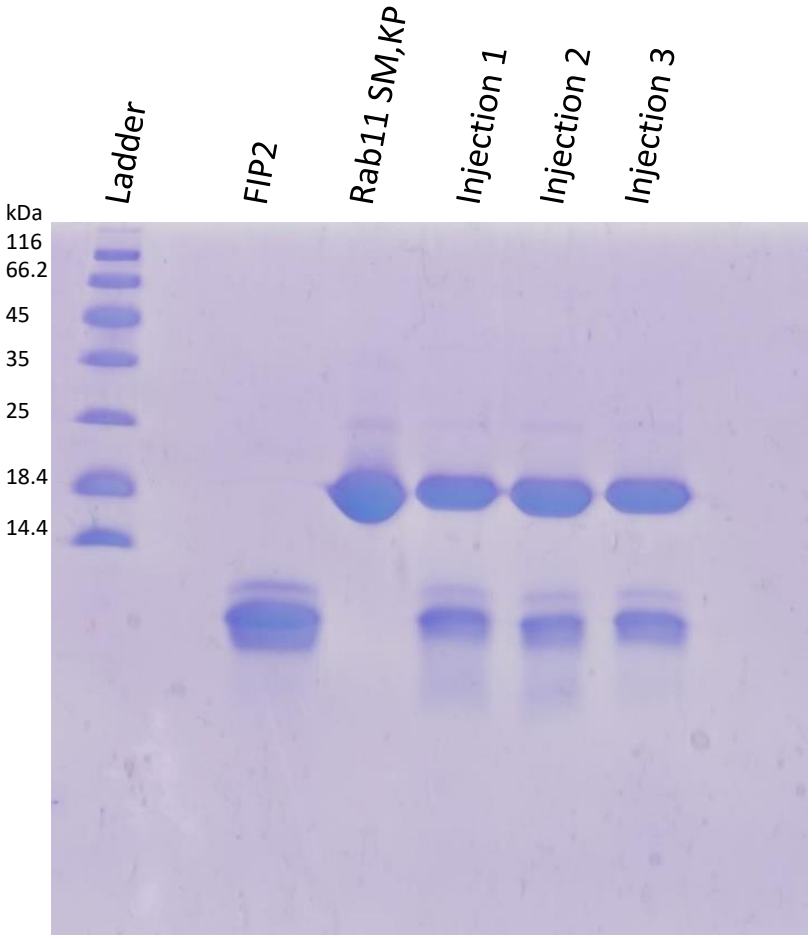

Figure 3.2.14 SDS PAGE Analysis of Titrations of Rab11SM,KP into FIP2. The quality of protein used for the titrations shown in figure 3.2.12 was analysed by SDS PAGE. Rab11SM,KP and FIP2 are shown above. The protein recovered from the experimental cell at the end point of each of the titrations is also shown.

3.2.3 Nucleotide analysis by HPLC

In order to perform biophysical analysis on the Rabs in the active GTP bound state, a series of constitutively active Rab mutants were generated (Q70L). It was confirmed that wild type Rab11 is largely in the GDP bound form after purification. Therefore, we sought to confirm that the Q70L mutation was successful in 'locking' the Rab in the GTP bound state. This analysis was done using reverse phase HPLC. All Rabs and mutants were shown to contain a majority of GTP nucleotide bound, with a minor fraction of GDP (see Figures 3.2.15 and 3.2.16). The proportion of nucleotide was similar for all Rab mutants tested, ensuring that differences in affinity could not be contributed to the Rab activity state.

A

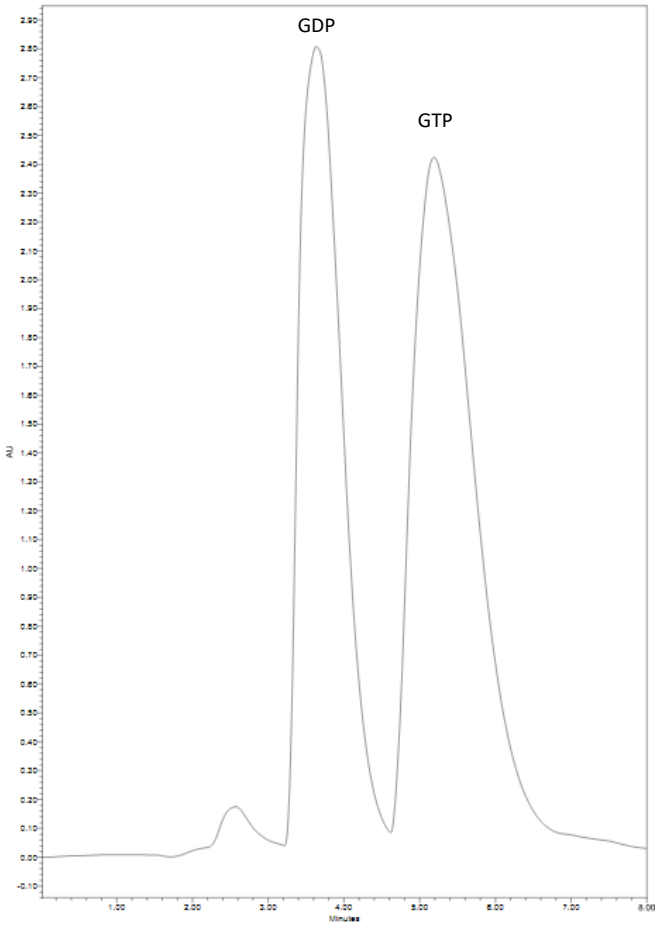

B

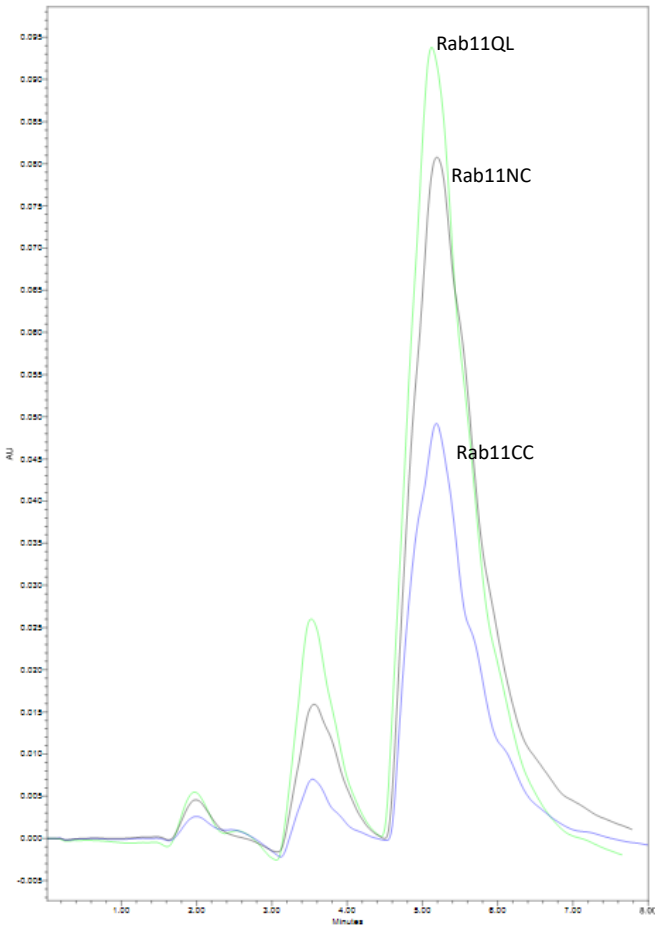

Figure 3.2.15 HPLC Analysis of Rab11CC, Rab11NC and Rab11QL. Panel A (overleaf) shows GDP/GTP standards analysed by reverse phase HPLC. Panel B shows nucleotide extracted from Rab11CC, Rab11NC and Rab11QL analysed in a similar fashion. The X-axis shows the time in minutes and the Y-axis shows the absorbance in AU. Protein samples were taken from those Rabs which were prepared for ITC analysis. Rab proteins for HPLC analysis were of slightly different concentration owning to constraints in the amount of protein available for analysis. This is reflected in the variable quantities of nucleotide eluted from the column. However, in each case a similar proportion of GDP:GTP is seen for each Rab. The percentage area under the GTP peak is similar to or slightly higher than that of the constitutively active (QL) sample in the case of each of the mutants.

Rab11QL: GDP- 16.2%, GTP- 81.8%

Rab11NC: GDP- 11.6%, GTP- 86.5%

Rab11CC: GDP- 10.6%, GTP- 87.8%

It follows that all Rabs analysed are, for the major part, in the active GTP bound state, with the lowest percentage active Rab being the Rab11QL sample.

A

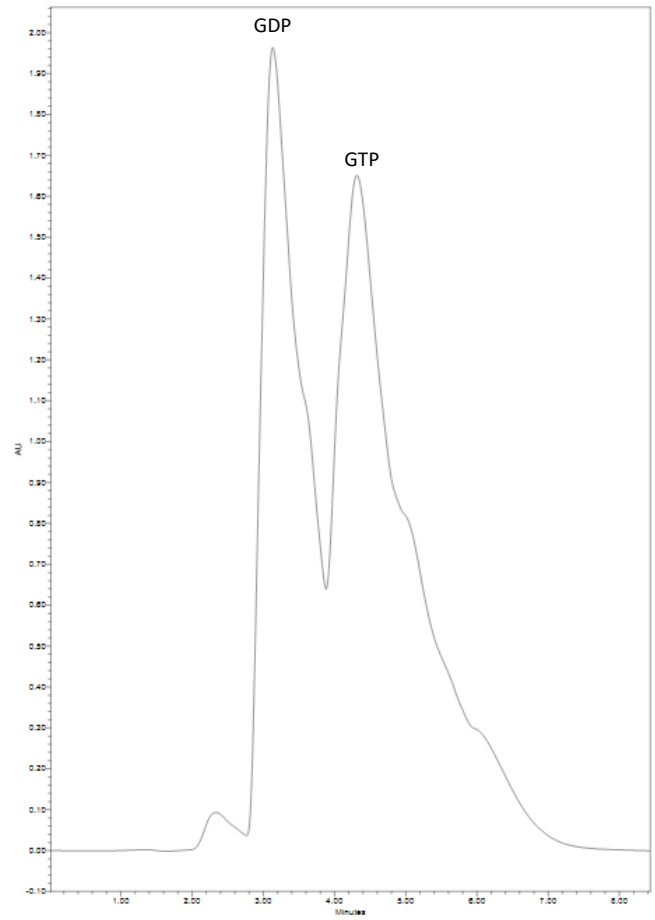

B

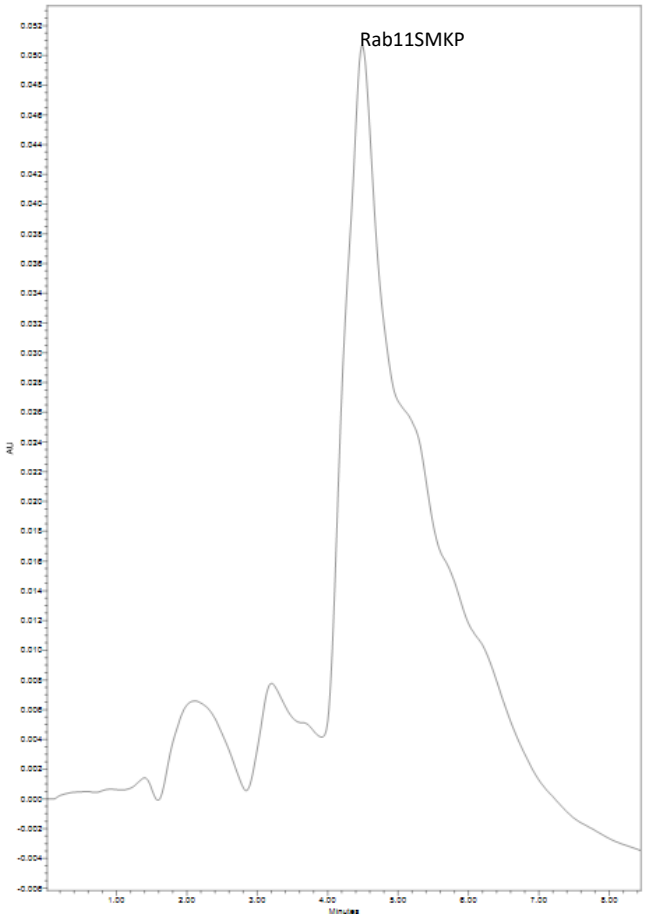

Figure 3.2.16 HPLC Analysis of Rab11SM,KP. Panel A (overleaf) shows GDP/GTP standards analysed by reverse phase HPLC. Panel B shows nucleotide extracted from Rab11SMKP analysed in a similar fashion. The X-axis shows the time in minuites and the Y-axis shows the absorbance in AU. Protein samples were taken from those Rabs which were prepared for ITC analysis. A similar proportion of GDP:GTP is reflected in this experiment as demonstrated in the previous experiment (Figure 3.2.15). The Rab protein is shown to be, for the major part, in the active GTP bound state and the percentage area under the GTP peak is similar to or slightly higher than that of the constitutively active (QL) sample.

Rab11SMKP: GDP- 11%, GTP- 83.7%

It follows the mutant Rab11SMKP has a similar percentage active state to the Rab11QL sample and variation in the binding affinity is a result of the mutations introduced into the protein.

3.3 Discussion

Initial preparation for biophysical analysis of Rab11 involved the introduction of a number of mutations into Rab11 in order to introduce Rab14 character to the protein. Rab14 retains the ability to bind Class I FIPs. However, it is important to remember that Rab14 is not a Rab11 family member, but rather a more divergent group II Rab with a distinct functional niche. As such, distinct structural and sequence differences exist between Rab14 and Rab11 family members, which are extremely similar in sequence, particularly within the switch regions. The most obvious, and perhaps the most interesting of these differences is a unique intramolecular disulphide that is defined in the crystal structure of Rab14-RCP. This disulphide bond is formed between C26 and C40 near switch I [284]. In the Rab11-FIP2 complex, switch I of Rab11 is embedded between the two helices of FIP2 [204]. It is possible that the unique cysteine residue in switch I of Rab14, which is shown to form a disulphide in the Rab14-RCP crystal structure, may influence the affinity of Rab14 for the effector. With this in mind, a single cysteine mutation and a double cysteine mutation were generated in constitutively active Rab11. These mutants were analysed by SDS PAGE under non-reducing conditions and were found to have significant differences in mobility. Interestingly, the single cysteine mutant was found to run as a double band under SDS PAGE, suggesting that two species are formed or that the protein moving between states found in native Rab11 and the double cysteine mutant.

Having established a significant difference between the Rab11 and the cysteine mutants, biophysical analysis was performed to examine any influence the mutations may have on Rab11 affinity. Surprisingly, no significant influence on affinity was measured in either the single cysteine mutation or the double mutation. We must conclude that, although the GTP dependent disulphide present in Rab14 is a distinct and unique feature of the Rab, it does not play a major role in influencing its affinity for FIP2.

Further distinct features between the Rabs were examined. A combination of mutations, S20M and K41P, were introduced into a constitutively active Rab11. The affinity of this construct for FIP2 was found to be significantly

reduced in comparison to Rab11. It is likely that these residues contribute to the reduced affinity of Rab14 for FIP2 in comparison to Rab11 family members. This quantitative data provides good evidence that these seemingly minor sequence changes have a significant influence of the affinity of the interaction. The S20M mutation is positioned in the P-loop. A serine residue found in Rab11 family members is instead a methionine in Rab14. In fact Rab14 is the only Rab with a large hydrophobic side chain at this position. This methionine causes the switch II region to adopt an alternative backbone conformation.

In Rab11 family members residue 41 is a positively charged lysine (Rab11a/b) or arginine (Rab25) residue. However, in Rab14, this position is replaced by a proline residue which is both uncharged and represents a significantly different side chain conformation. In their interactions with Rab11 family members the charged residues at position 41 interact with a conserved glutamate in FIP effectors. This interaction is abolished in Rab14 and contributes to a lack of electrostatic parity.

Our evidence suggests that a lack of electrostatic parity and a shift in the conformation of switch II has a significant influence on the affinity of Rab14 for FIP2. However, it should be noted that these differences are not sufficient to account for the affinity of Rab14 for FIP2 which is reported in the literature as approximately tenfold weaker than that of Rab11 [284]. It must be concluded that Rab-effector specificity and affinity are multifactorial issues, which are influenced by multiple sequence elements.

Our aim in generating a series of constitutively active (Q70L) Rab mutants was to ensure that titrations and biophysical analysis would be carried out on Rab in the active, GTP bound form. The GTP bound Rab is the biological effector for FIP. In this state, the Rab is membrane localised and will carry out its effector functions. The Rabs used for biophysical analysis were tested for the presence and proportion of nucleotide after titrations were performed in order to ensure that the ITC experiments were performed on biologically active Rab. HPLC analysis confirmed that Rabs were, in the majority, GTP bound, with a minor fraction in the GDP bound state. The proportion of

GTP;GDP bound was similar for all Rabs, indicating that our comparisons of affinity are valid.

Chapter 4:

Purification and Crystallisation of FIP2

4.1 Introduction

FIP2 is a member of the Rab11 family interacting proteins (FIPs). These are a conserved family of effectors which bind to a subset of Rabs and Arfs. The FIPs are characterised by their ability to bind the Rab11 subfamily of proteins through their C-terminal RBDs.

The FIPs can be divided into two groups. The class I FIPs all contain C2 domains and they include Rip11(aka FIP5), FIP2 and RCP (aka FIP1) [232]. The class II FIPs; FIP3 and FIP4, are known to interact with Arfs. They contain ERM domains, EF hands and a proline- rich region [236]. FIP1 one does not contain any of these identifying motifs and therefore is not categorised into either of the subgroups [278]. In complex with their effectors, the FIPs form dimeric alpha helical coiled coils, providing two symmetrical Rab binding sites at their C-termini and domains which can modulate other functions at their N-termini.

FIP2 is a member of the class I FIPs. It may bind to the members of the Rab11 subfamily, but also to a closely related Rab, Rab14. The Rab11 family members are associated with recycling endosomes (REs) and have functions in the recycling of early endosomes (EEs) to the *trans*-Golgi network (TGN) [237]. The FIPs have roles at multiple points in these events. FIP2 functions in regulating transcytosis [245], apical targeting [277] and in regulating recycling systems [231].

Along with Rab14, FIP2 has been implicated in the progression of chlamydial infection. FIP2 has been shown to be recruited to chlamydial inclusions. The protein and its Rab interacting proteins have been implicated in chlamydial infection. However no other member of the FIPs have been shown to be localised to these structures [230, 278]. FIP2 silencing decreases the bacterial progeny demonstrating its importance for bacterial replication. FIP2 binds to Rab11 at the inclusion membrane. The bound FIP2 then favours the recruitment of Rab14. It is likely that the bacteria recruits FIP2 to hijack host intracellular trafficking in order to redirect vesicles full of nutrients to the inclusion [279].

4.1.2 Scientific Objectives

- To solve the structure of FIP2 in complex with Rab14, in order to further understand the specificity of Rab14 for class I FIPs
- To solve the structure of FIP2 (uncomplexed), in order to understand the structure of the pre-binding state of the effector. Currently there are no crystal structures of uncomplexed Class I or Class II FIPs.

4.2 Results

Initial crystallographic trials focused on obtaining crystals of the Rab14:FIP2 protein complex. Truncated Rab14 and FIP2 constructs extant in the lab were chosen. These constructs have been shown, through previous work, to be well expressed in *E.coli* culture and stable in solution for a long enough period of time, and at a sufficient concentration, to allow them to be suitable candidates for crystallisation trials. The initial purification strategy for the complex involved purifying FIP2 (441-498) and Rab14 (7-175) separately by nickel affinity chromatography followed by cleavage of the His tag, and then further purifying the proteins by ion exchange to ensure their homogeneity. After the ion exchange step, the proteins were combined and subjected to gel filtration chromatography. However the Rab14:FIP complex did not separate well from the excess FIP2. The two Gaussian peaks expected to form under gel filtration chromatography were merged and therefore the fractions containing Rab14 also contained a non-stoichiometric amount of FIP2. The final sample, which was set up in a crystallisation trial, was biassed towards FIP2. Despite this obvious disadvantage, some crystals were obtained. Crystal growth occurred after approximately two weeks post set up, at a protein concentration of 6 mg/ml. The hit condition consisted of 0.01 M Cobalt chloride 0.1 M Na acetate pH 4.6 1.0 M 1,6-Hexanediol from the sparce matrix screen Structure Screen I and II (Hampton Research).These crystals were tested at the APS beamline and found to diffract to 2.37-2.29 Å. Initial attempts at molecular replacement from these crystals were unsuccessful.

The initial crystals produced in sparse matrix screening were replicated in hanging drop 24 well screens. These crystals were produced in a much larger volume of 4 µL drops and were accordingly much larger is size. Their increased size allowed for the crystal composition to be analysed by SDS PAGE. This analysis indicated that the crystals were formed exclusively from FIP2 and any Rab14 in the solution was excluded from the crystal. With this knowledge, further attempts to optimise the crystallisation strategy of FIP2 were made, excluding Rab14 from the purification. Optimised crystals were produced from these more homogenous protein preparations and crystals of a more regular morphology were obtained in a similar crystallisation

condition. Slight adjustments of the pH of the sodium acetate crystallisation buffer resulted in crystals of varying morphology. At pH 4.6, clumps of crystals were formed around a single nucleation point. At pH 4.8, multiple nucleation points allowed for the development of showers of single crystals.

In order to obtain phase information to rectify problems with molecular replacement, an attempt was made to produce crystals using selenomehtionine derivatised FIP2. The selenomethionine derivatised FIP2 was well expressed and purified to a sufficient concentration of homogenous protein. However, no crystals were formed in the native crystal condition, or when subjected to sparce matrix screening.

In order to gain some phase information an alternative strategy was adopted. Upon data collection at Synchotron Soleil, an anomalous data set was collected from native crystals along the cobalt energy edge. The presence of cobalt chloride is required for crystal growth. Therefore, a reasonable assumption was made that cobalt atoms occupied specific sites within the crystal lattice. It was possible to obtain some phase information from the cobalt atoms. Crystals produced in optimised, hanging drop screens were tested at the Synchrotron Soleil facility and found to diffract to 3.5 Å. An anomalous data set was also collected along the cobalt energy edge. The data was anomalous to approximately 5 Å. Attempts to use this data set to provide phasing information were, unfortunately, not successful.

Following these setbacks, the original data collected at APS beamline was re-examined. A novel molecular replacement strategy using the programme Arcimboldo was adopted. In this strategy, short poly-alanine alpha helices were used as molecular replacement models and connected to build larger alpha-helical segments. Four molecules of FIP2 were built by Arcimboldo using only the reflection file as the starting point for *ab initio* structure determination [286].

4.2.1 Crystallisation of FIP2

The starting aim of this project was to achieve crystallisation of the Rab14:FIP2 complex. With this aim in mind, Rab14 (7-175) and FIP2(441-498) were expressed with a His tag in BL21 DE3 *E.coli* cells and purified by nickel affinity purification (see Figure 4.2.1). Both proteins were well expressed in a soluble form. The proteins were cleaved of their His tags. However, the cleavage efficiency of Rab14 was poor and resulted in a relatively small volume of dilute protein in comparison to that of FIP2. Following affinity chromatography from cell lysate and subsequent cleavage, the proteins were further purified by anion exchange chromatography using a monoQ column to ensure their homogeneity as shown in figures 4.2.2-4.2.5. The Rab14 and FIP2 were then combined and run over a superdex75 16/60 gel filtration chromatography column. It was expected that the gel filtration column would separate out the Rab14:FIP2 complex from the excess FIP2 resulting in a stoichiometric complex. However, the two species were not sufficiently separated and eluted from the column in two overlapping peaks (see Figures 4.2.6 and 4.2.7). It is possible that, due to the non-spherical coiled coil configuration of the FIP2, the protein eluted from the column at a point which would represent a larger molecular weight than when visualised under the denaturing conditions of an SDS PAGE. The purification strategy resulted in a Rab14:FIP2 solution that was heavily biassed towards FIP2, the solution also contained a significant impurity of around 30kDa (see Figure 4.2.8). Despite these disadvantages, protein crystals appeared under sparse matrix screening (Structure Screen, Hampton Research). The hit condition consisted of 0.01 M Cobalt chloride 0.1 M Na acetate pH 4.6 1.0 M 1,6-Hexanediol from the sparce matrix screen Structure Screen I and II (Hampton Research), with a protein concentration of 6 mg/ml. The crystals appeared after approximately 14 days. The crystals were shard like in nature with an irregular, jagged appearance. The crystals appeared to have nucleated from a brown protein precipitate which formed soon after the plate was set up.

These crystals were analysed at the Advance Photon Source (APS) beamline and were found to diffract to 2.37-2.29 Å. Initial attempts at molecular replacement were not successful. It was suspected that the composition of the

crystals was not Rab14:FIP2 complex and further investigation as to their composition ensued (see section 5.2.2).

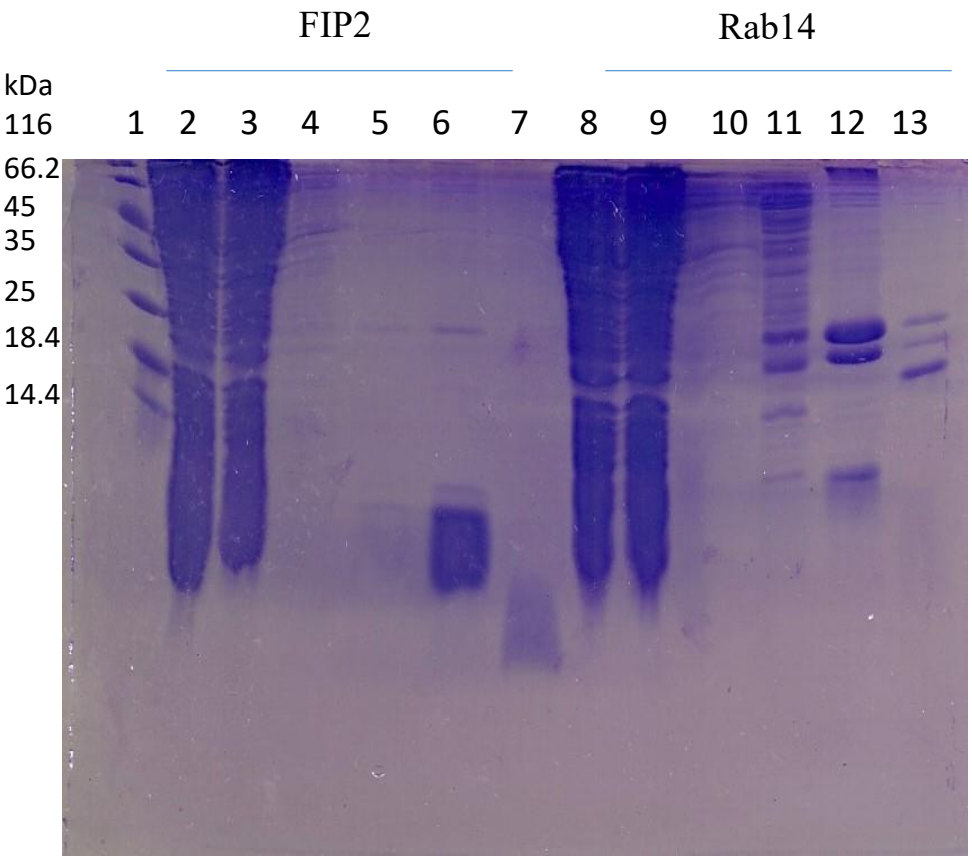

Lane 1. Ladder
Lane 2. FIP2 HB10C supernatant
Lane 3. Flow through, not bound to column
Lane 4. 10 mM imidazole wash
Lane 5. 30 mM imidazole wash
Lane 6. 200 mM imidazole elute
Lane 7. Second nickel purified, cleaved protein
Lane 8. Rab14 supernatant
Lane 9. Rab14 flow through, not bound to column
Lane 10. Rab14 10mM imidazole wash
Lane 11. Rab14 30mM imidazole wash
Lane 12. Rab14 200 mM elute
Lane 13. Second nickel purified, cleaved protein

Figure 4.2.1 Nickel Affinity Chromatography and Cleavage. Lanes 2-7 show FIP2 purified from cell lysate by nickel affinity chromatography and subsequent cleavage with rTEV protease. Lanes 8-13 show a similar purification strategy for recombinant Rab14

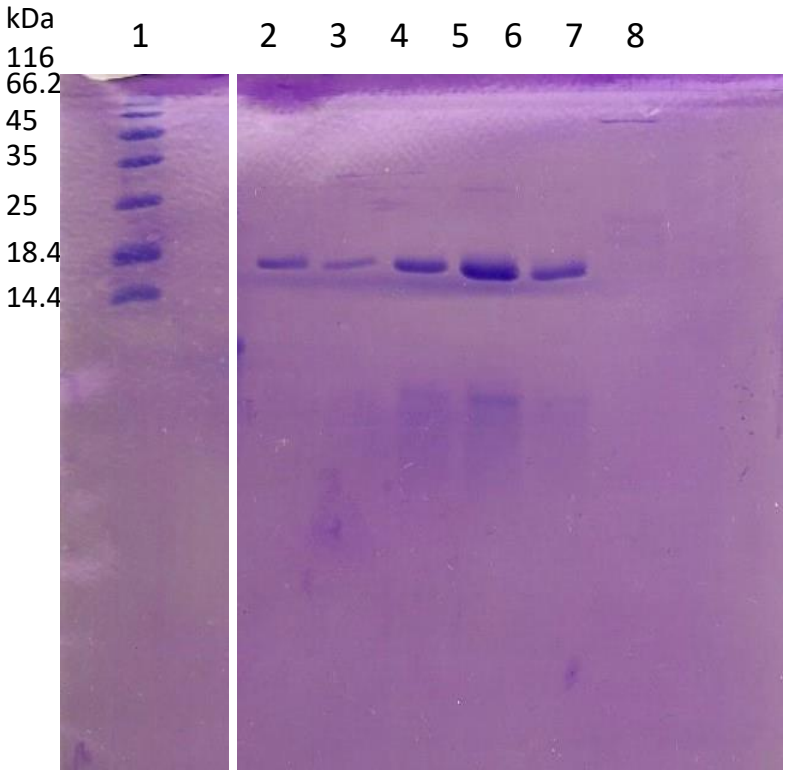

Lane 1. Ladder
Lane 2. Mono Q elute 9 ml
Lane 3. Mono Q elute 10 ml
Lane 4. Mono Q elute 11.5 ml
Lane 5. Mono Q elute 13 ml
Lane 6. Mono Q elute 14 ml
Lane 7. Mono Q elute 26.5 ml
Lane 8. Waste

Figure 4.2.2 Ion Exchange Purification of Rab14. Lanes 2-7 represent a series of Gaussian peaks produced by ion exchange chromatography purification of Rab14 analysed by SDS PAGE. Lane 8 shows the material which did not stick to the ion exchange column.

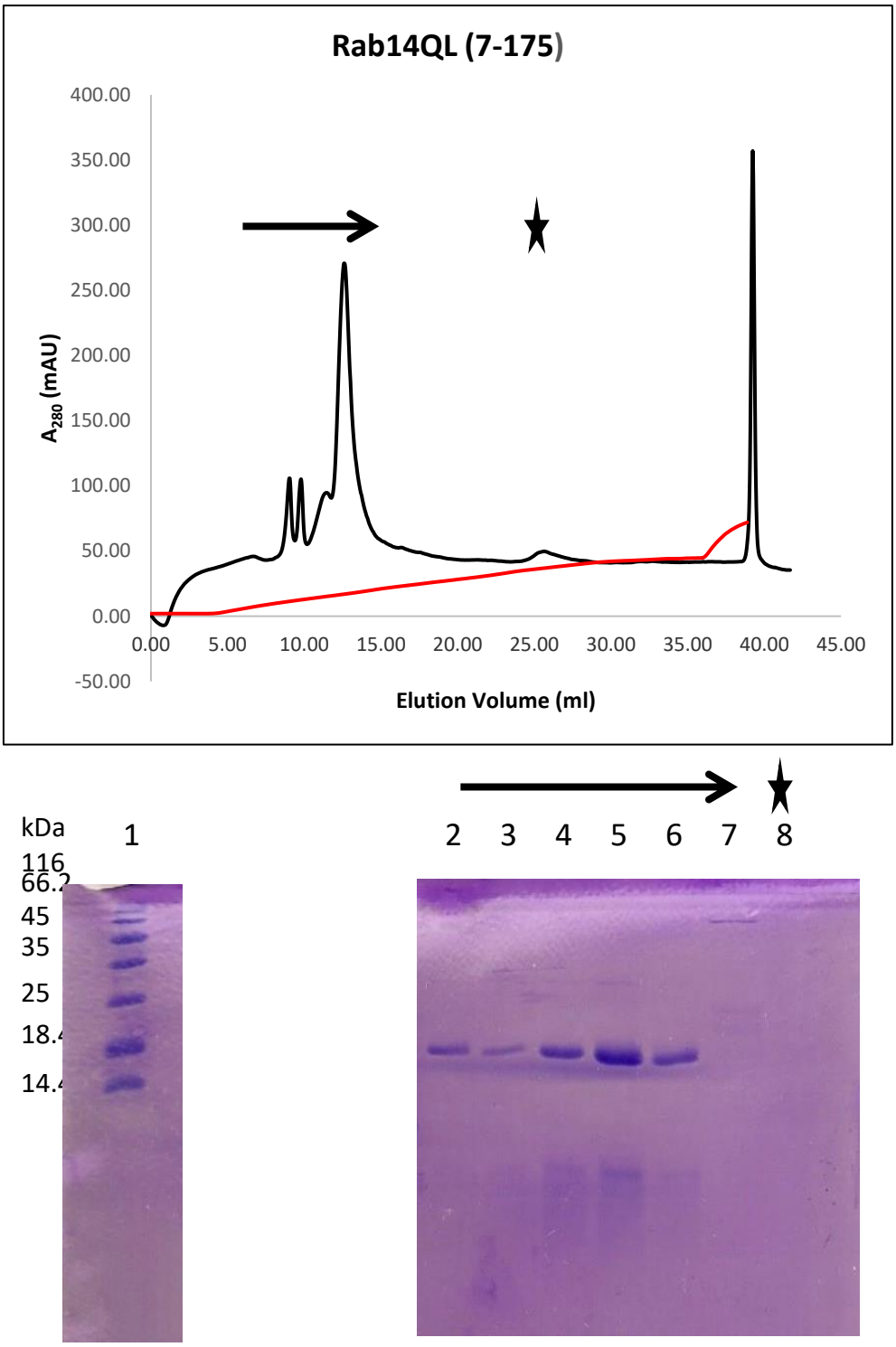

Figure 4.2.3 Ion Exchange Purification of Rab14. The figure above (top panel) shows a series of Gaussian peaks produced by Mono Q purification of Rab14. The black line represents the absorbance at 280 nm and the red line denotes the conductance in mS. The black arrow above the graph indicates the distribution of the samples taken and analysed by SDS PAGE in the lower panel. Similarly the black star indicates a sample taken from a peak eluting in higher salt. As reflected in the SDS gel, this peak does not contain significant quantities of protein.

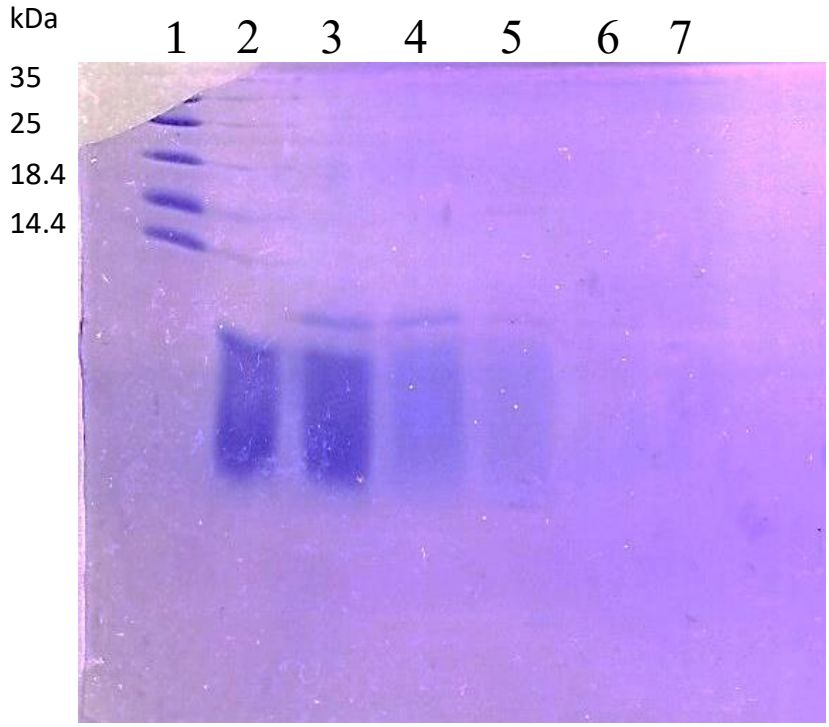

Lane 1. Ladder
Lane 2. Mono Q elute Q 9.5 ml
Lane 3. Mono Q elute 10 ml
Lane 4. Mono Q elute 11 ml
Lane 5. Mono Q elute 22.5 ml
Lane 6. Mono Q elute 24 ml
Lane 7. Mono Q elute 14.5 ml
Lane 8. Waste

Figure 4.2.4 Ion Exchange Purification of FIP2. Lanes 2-7 consist of samples taken from a single peak of FIP2 eluted from a Mono Q column and analysed by SDS PAGE. Initially the cleaved product of FIP2 is eluted (lane 1), followed by FIP2 contaminated by the uncleaved His tagged precursor. Further optimised purification strategies have managed to increase the cleavage efficiency and increase the level of separation between the two species via ion exchange. Lane 8 shows the material which did not stick to the ion exchange column

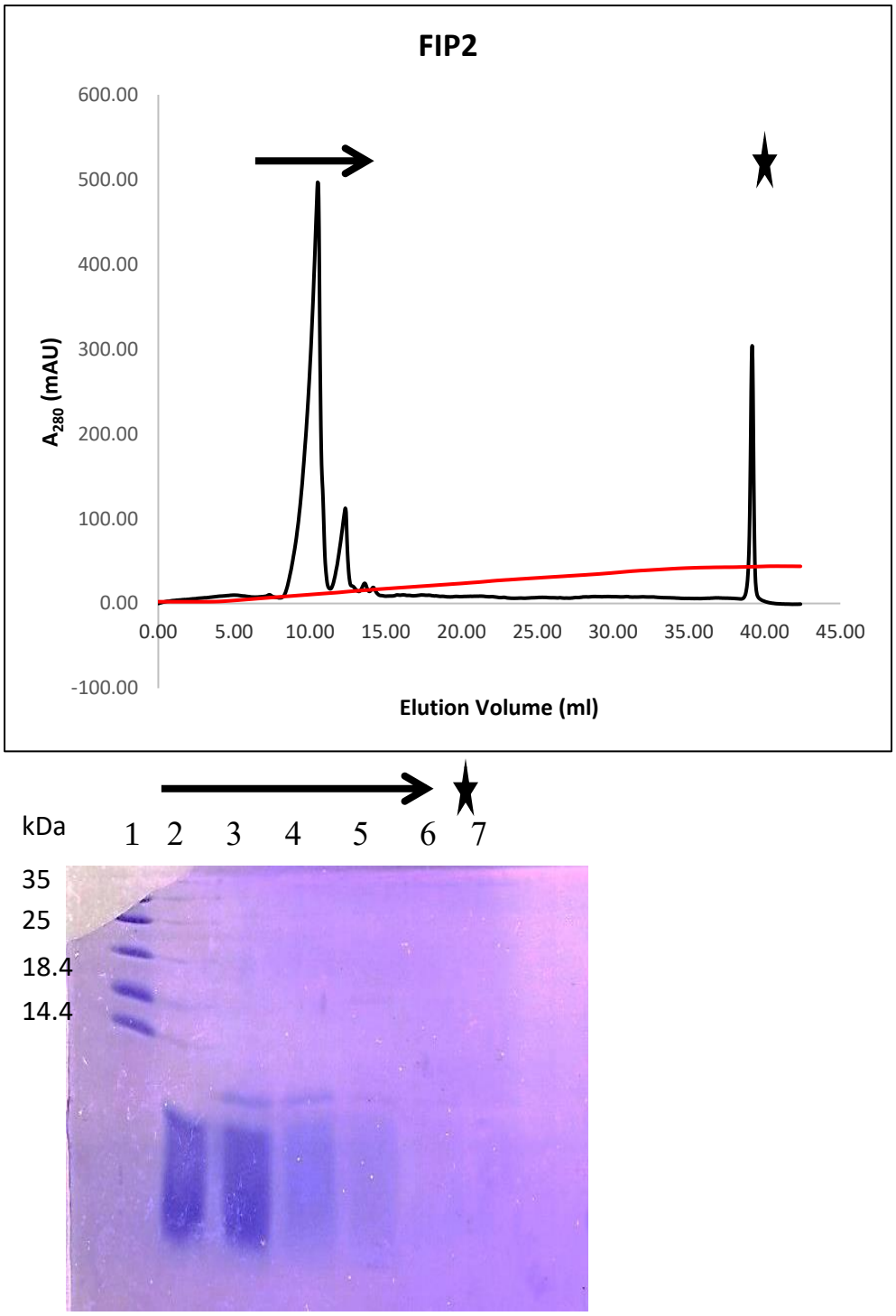

Figure 4.2.5 Ion Exchange Purification of FIP2. The top panel of the figure overleaf shows a series of peaks produced by ion exchange purification of FIP2 on a mono Q column. The black line represents the absorbance at 280 nm and the red line denotes the conductance in mS. The bottom panel shows an SDS PAGE analysis of the purification, as described in figure 4.2.4. The black arrow indicates the range of samples taken across the peak under the corresponding black arrow in the top panel, the black star indicates a sample taken from the peak elution later in the profile under higher salt concentrations. No useful target protein is found to be eluting in this peak.

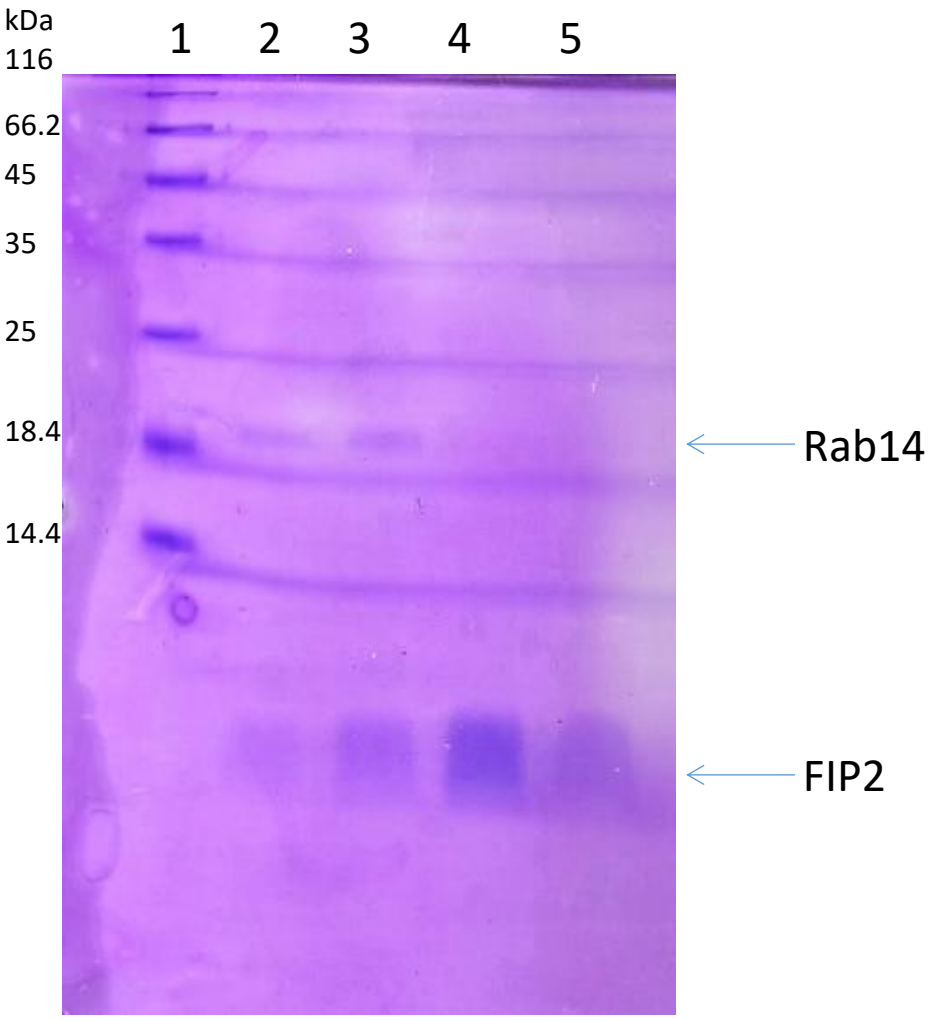

Lane 1. Ladder
Lane 2. Gel Filtration elute 73 ml
Lane 3. Gel Filtration elute 74.5 ml
Lane 4. Gel Filtration elute 79 ml
Lane 5. Gel Filtration elute 82.5ml
Lane 6. Gel Filtration elute 105 ml

Figure 4.2.6 Co-Gel Filtration of Rab14-FIP2. The two proteins shown were combined in non-stoichiometric amounts. When run on an sx75 gel filtration column, the complex and FIP dimer peaks do not separate sufficiently. This is illustrated in the SDS PAGE shown above where Rab14 is only present in the fractions shown in lanes 2-3, representing the first half of the peak (see Figure 5.2.7). The SDS gel itself has flaws running at similar heights to the protein ladder. This is likely a result of an error during loading of the gel.

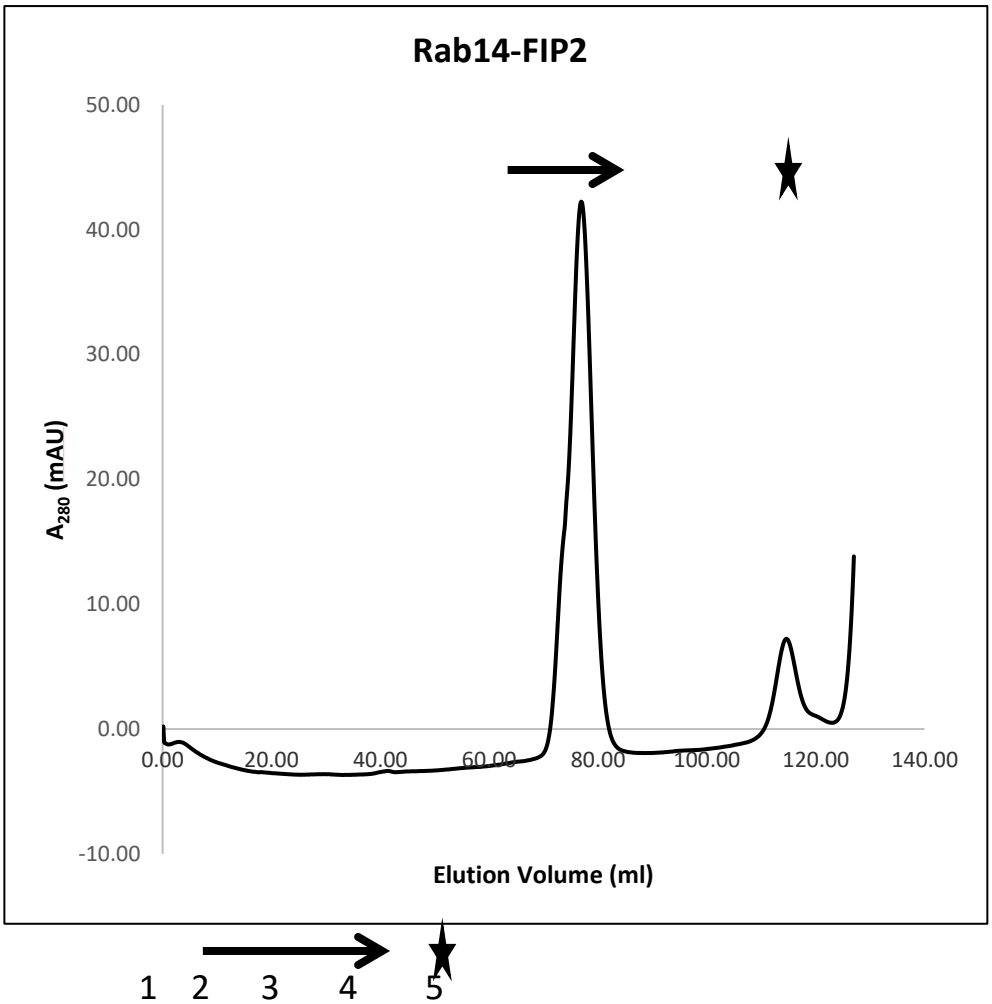

Figure 4.2.7 Co-Gel Filtration of Rab14-FIP2. As discussed in figure 4.2.6, the gel filtration elution profile (top panel) and corresponding SDS gel analysis (bottom panel) shown in the panels above represent the result of combining non-stoichiometric amounts of FIP2 and Rab14 and subjecting the complex to gel filtration chromatography using a Superdex 75 16/60 column. The black arrow corresponds to samples taken from the single peak eluted in the profile. The peak displays a hump on the left side. SDS PAGE analysis in the bottom panel shows that all the Rab14 in the sample is localised to this side of the peak, indicating that a Gaussian peak containing the complex and a separate peak containing the FIP2 dimer exist and have not separated correctly. This results in the fractions containing the complex having an excess of FIP2.

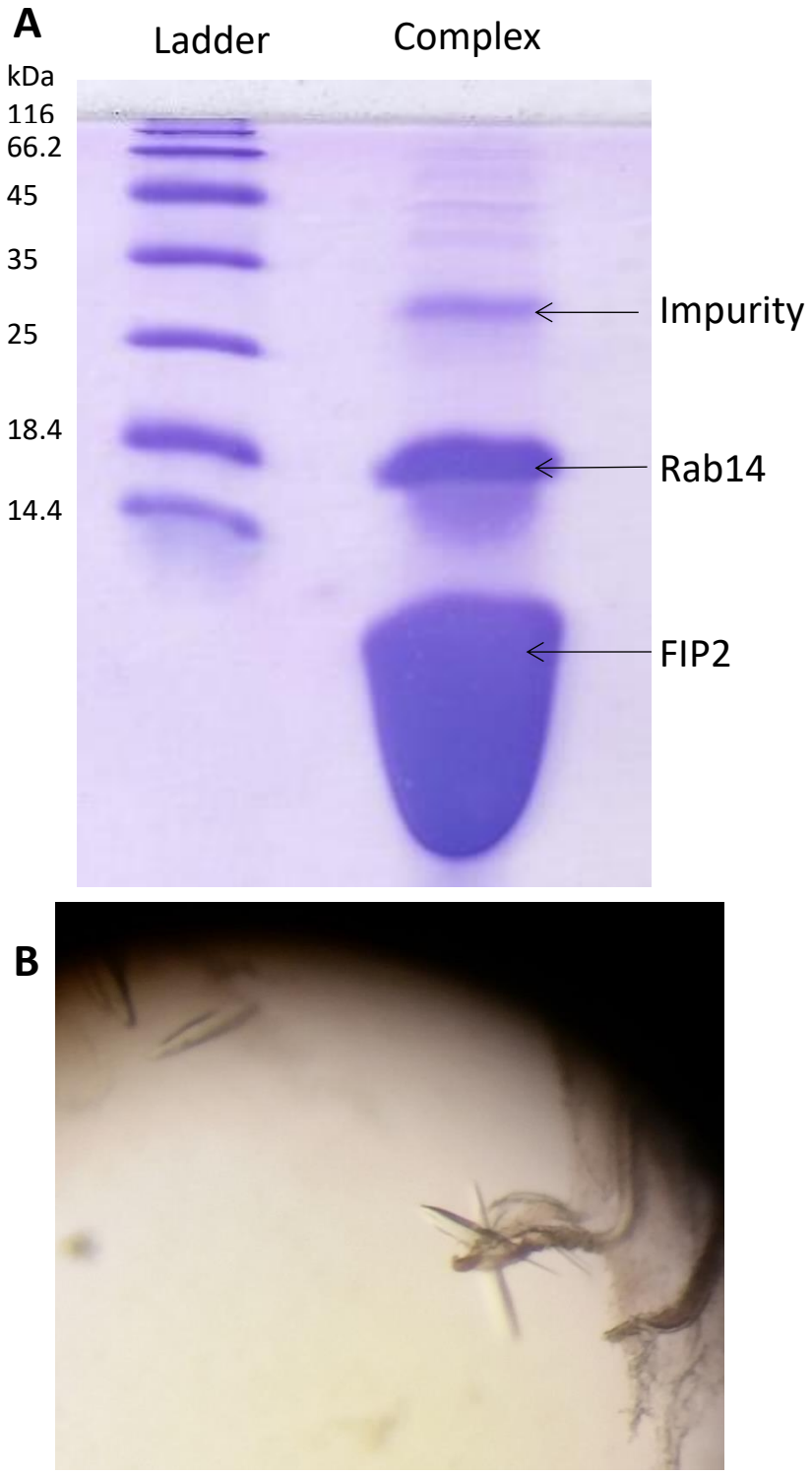

Figure 4.2.8 Crystallisation Trials. The purified complex shown in panel A contains some impurities, the most significant of which runs at a molecular weight between the 25 kDa and the 35 kDa markers. Furthermore the complex appears to have a significant stoichiometric bias towards FIP2. Despite these obvious drawbacks, some irregularly shaped crystals were obtained under sparse matrix screening (panel B). These crystals appeared after two weeks, and were nucleated from a brown protein precipitate. Crystals appeared in the sparse matrix screen Structure Screen I and II (Hampton Research) in the condition 0.01 M Cobalt Chloride, 0.1M Sodium Acetate pH 4.6, 1 M 1,6-Hexanediol.

4.2.2 Crystal Replication and Optimisation

From the results of the initial diffraction experiments, the composition of the crystals was called into question. It became important to replicate and optimise the crystals in order to analyse them to establish their composition, and also to optimise the diffraction. The morphology, size and internal order of a crystal all play a role in the quality of diffraction data produced.

The initial replication strategy followed an identical procedure to that undertaken during the production of the initial crystals. This purification scheme produced protein of a similar composition and concentration to the initial crystallisation experiment. Hanging drop screens were set up in a 24 well grid format, maintaining similar crystallisation conditions to those in the initial sparse matrix screen, (0.01 M Cobalt Chloride, 0.1M Sodium Acetate pH 4.6, 1 M 1,6-Hexanediol) but with slight variations in pH. Crystal screens were incubated at 16 ˚C for two weeks before crystal growth was observed. Replicated crystals developed at a varied pH to the initial condition (0.01 M Cobalt Chloride, 0.1M Sodium Acetate pH 4.7, 1 M 1,6-Hexanediol). The crystals appeared to have formed from a central nucleation site and had a clumped morphology with protruding spikes (see Figure 4.2.10). The replicated crystals were larger than the initial crystallisation hit, reflecting the larger drop size and volume of protein in the screen. These crystals were analysed by SDS PAGE analysis and found to contain only FIP2, with Rab14 being excluded from the crystal. Further attempts at molecular replacement using the FIP2 seen in the Rab11:FIP2 complex were not successful. Therefore optimising the crystals for improved data collection became an important goal.

In an attempt to optimise crystal growth, screening of multiple conditions were undertaken. The purification strategy for the crystallisation experiment was altered to exclude the Rab14 from the protein solution. As a result the solution also contained fewer non-specific protein impurities and a more homogeneous solution of concentrated FIP2 was obtained. Variations in the salt, precipitant, buffer and pH were all attempted (see Table 4.2.9). Of these variations, crystal growth was only observed following a small change in the pH of the sodium acetate buffer (0.01 M Cobalt Chloride, 0.1 M Sodium

Acetate pH 4.8, 1 M 1,6-Hexanediol). The morphology of the optimised crystals was strikingly different to the crystals produced under sparse matrix screening and to the crystals replicated in 24 well screens using the initial purification strategy. Multiple nucleation sites allowed for the growth of many, individual crystals. This was unlike previous efforts where crystals appear to grow from a single or few nucleation sites resulting in clumps of crystals. The morphology of the crystals was more regular with well-defined sharp edges and faces (see Figure 4.2.11).

The quality of the crystals declined over time. Therefore crystals were harvested promptly after their formation and stored in liquid nitrogen. Crystals were cryo-protected using 25% glycerol. After harvesting, new crystal growth appeared in re-sealed drops. In this case few, large, individual crystals appeared. This is in contrast to the showers of crystals that appeared in the fresh drop. The growth of new crystals in a re-sealed drop was a good indicator that crystal seeding would be a useful strategy to obtain single, large crystals. However all attempts at streak seeding and micro-seeding were unsuccessful.

Optimisation of Crystallisation Conditions:

	Salt	**Buffer**	**Precipitant**
Initial Hit	**0.01 M Cobalt Chloride**	**0.1M Sodium Acetate pH 4.6**	**1 M 1,6-Hexanediol**
Hit	0.01 M Cobalt Chloride	0.1M Sodium Acetate pH 4.7	1 M 1,6-Hexanediol
Hit	0.01 M Cobalt Chloride	0.1M Sodium Acetate pH 4.8	1 M 1,6-Hexanediol
Variation	0.01 M Sodium Chloride	0.1M Sodium Acetate pH 4.6	1 M 1,6-Hexanediol
Variation	0.01 M Magnesium Chloride	0.1M Sodium Acetate pH 4.7	1 M 1,6-Hexanediol
Variation	0.01 M Calcium Chloride	0.1M Sodium Acetate pH 4.6	1 M 1,6-Hexanediol
Variation	0.01 M Cobalt Chloride	0.1M Sodium Acetate pH 5	1 M 1,6-Hexanediol
Variation	0.01 M Cobalt Chloride	0.1M Sodium Acetate pH 4.6	11.8% Isopropanol
Variation	0.01 M Cobalt Chloride	0.1M Sodium Acetate pH 4.6	11.8% Ethanol
Variation	0.01 M Cobalt Chloride	0.1M Sodium Acetate pH 4.8	0.6 M 1,6-Hexanediol
Variation	0.01 M Cobalt Chloride	0.1M Sodium Acetate pH 4.8	0.8 M 1,6-Hexanediol
Variation	0.01 M Cobalt Chloride	0.1M Sodium Acetate pH 4.8	1.2 M 1,6-Hexanediol
Variation	0.01 M Cobalt Chloride	0.1M Zinc Acetate pH 4.8	1 M 1,6-Hexanediol
Variation	0.0025 M Cobalt Chloride	None	1 M 1,6-Hexanediol
Variation	0.005 M Cobalt Chloride	None	1 M 1,6-Hexanediol

Variation	0.01 M Cobalt Chloride		None	1 M 1,6-Hexanediol
Variation	0.02 M Cobalt Chloride		None	1 M 1,6-Hexanediol
Variation	0.01 M Cobalt Chloride		0.1M MES pH 6	1 M 1,6-Hexanediol

Table 4.2.9 Optimisation of Crystallisation Conditions. The table overleaf lists the crystal conditions trialled in an attempt to optimise the crystallisation of FIP2. The initial hit condition produced under sparse matrix screening is shown in bold. Of the novel conditions, only two which were similar to the initial hit (except for slight variations in the pH) produced crystals. These conditions were: 0.01 M Cobalt Chloride, 0.1M Sodium Acetate pH 4.7, 1 M 1,6-Hexanediol and 0.01 M Cobalt Chloride, 0.1M Sodium Acetate pH 4.8, 1 M 1,6-Hexanediol. The condition with a pH of 4.7 produced clumps of crystals growing out of a nucleus of protein precipitation. The condition with a pH of 4.8 produced showers of single crystals.

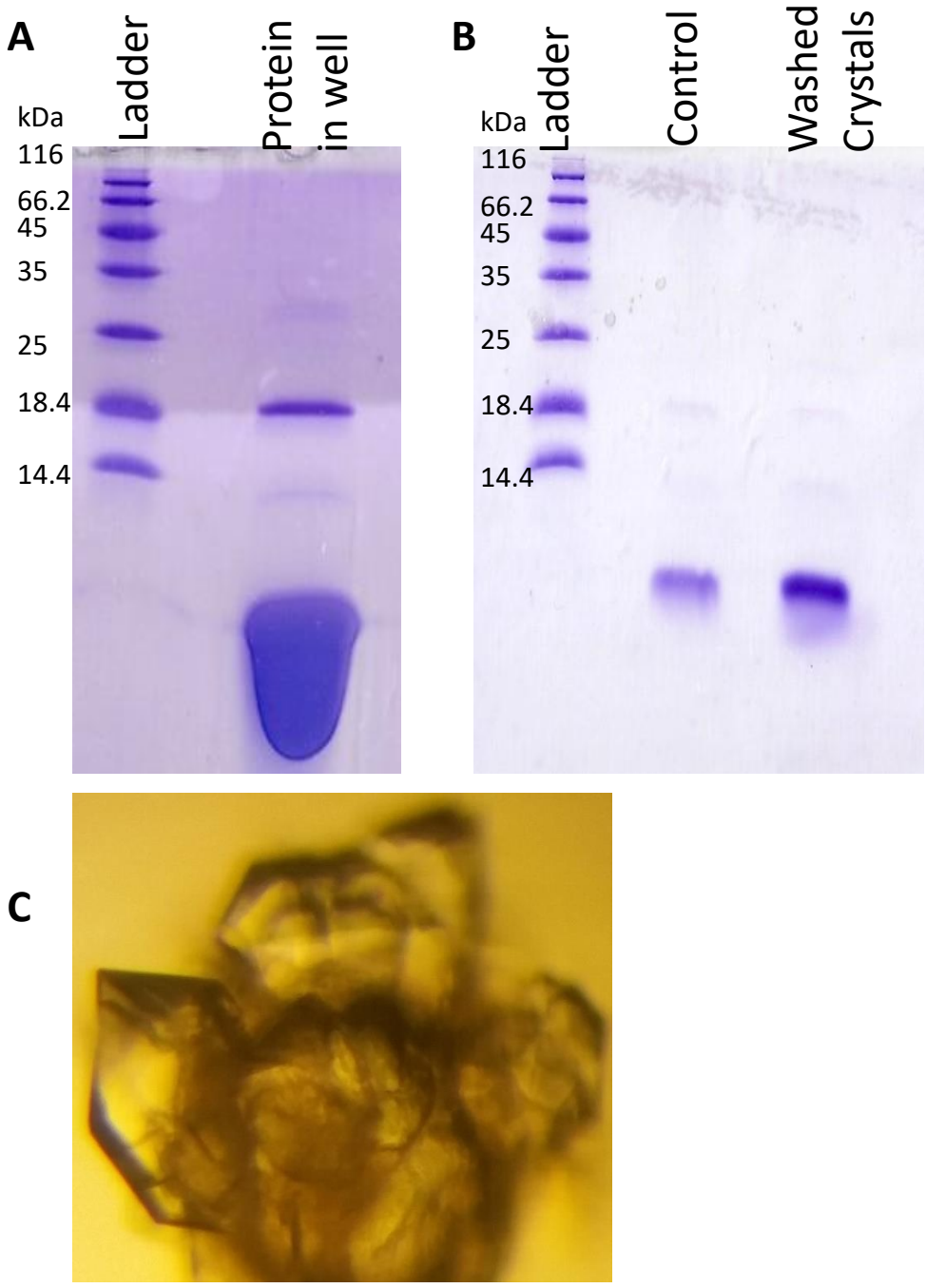

Figure 4.2.10 Replication of Crystals in 24 Well Screens. Initial attempts at replicating crystal growth in hanging drop screens followed a purification strategy similar to that undertaken for the original crystallisation hit. Panel A shows the protein which was set up in the hanging drop experiment. Similar to the initial hit condition, the protein solution contained a non-stoichiometric amount of Rab14. Crystal replication was successful and a crystal sample was washed and analysed by SDS PAGE. Panel B shows the SDS gel of the washed protein crystals. The Control lane is protein from the drop solution. The Washed Crystals lane shows the crystals washed in buffer and run on an SDS PAGE. Panel C shows the morphology of the crystals produced in the condition: 0.01 M Cobalt Chloride, 0.1 M Sodium Acetate pH 4.7, 1 M 1,6-Hexanediol. The crystals produced nucleated from a central point and had a clumped, jagged morphology.

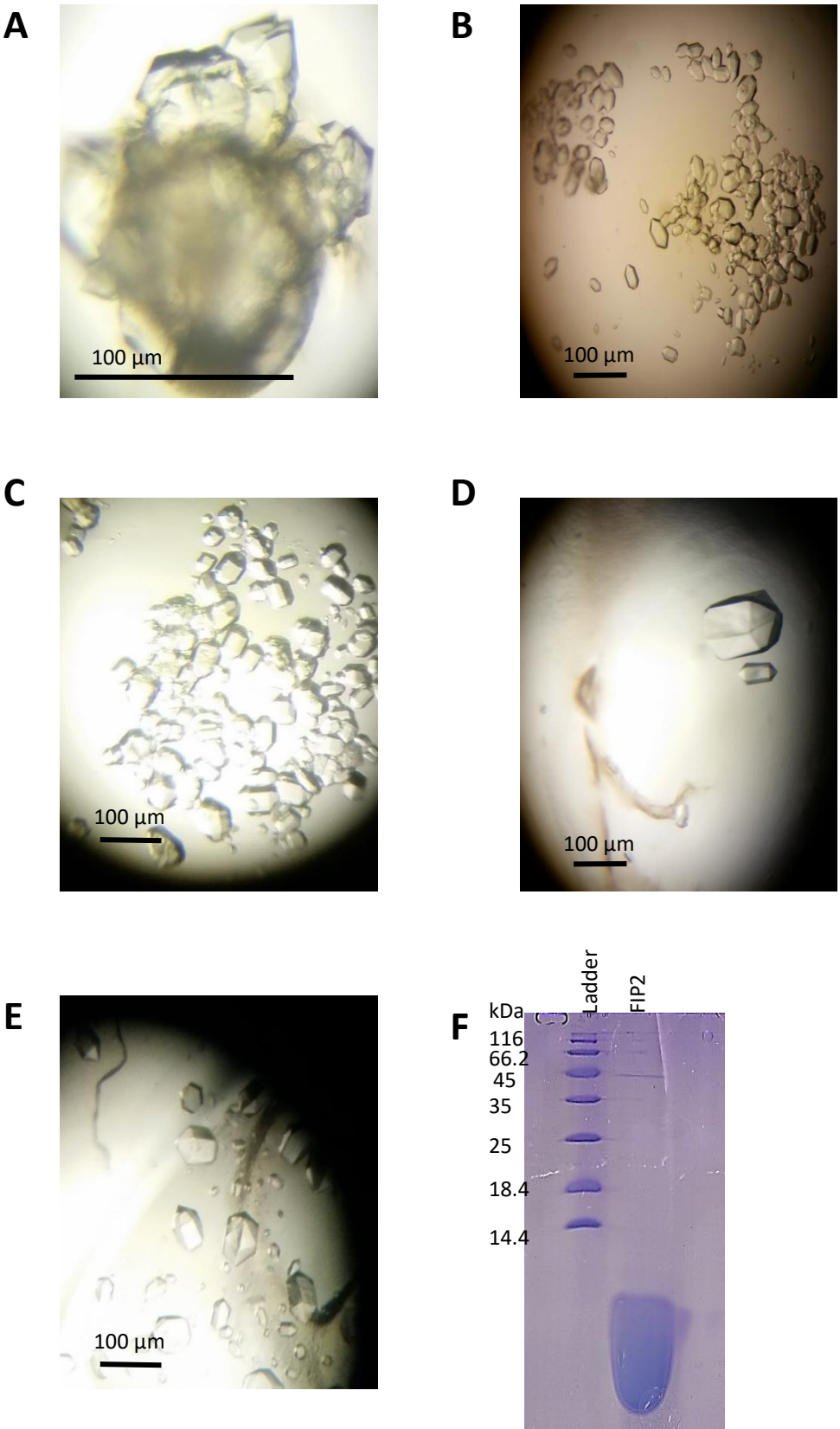
A
100 µm
B
100 µm
C
100 µm
D
100 µm
E
100 µm
F
kDa
Ladder
FIP2
116
66.2
45
35
25
18.4
14.4

Figure 4.2.11 FIP2 Crystal Optimisation. Shown above are the results of crystal optimisation. The crystals in panel A were formed in the condition 0.01 M $CoCl_2$, 0.1 M Na Acetate pH 4.7, 1 M 1,6-Hexanediol from protein purifications containing FIP2 and a non-stiochiometric amount of Rab14. These crystals nucleate from a single point and have a less regular morphology. The crystals in panels B-E were formed in the condition 0.01 M $CoCl_2$, 0.1 M Na Acetate pH 4.8, 1 M 1,6-Hexanediol. These crystals represent growth from multiple nucleation sites and are largely singular well defined crystals. The large individual crystal shown in panel D is an example of a crystal which developed from a drop that had been re-sealed after the crystals which formed earlier had been harvested. This crystal is much larger than previous crystal growth. Panel F shows the purity of the protein set up in the trials which produced the crystals in panel B-E. Unlike the protein solution in figure 4.2.10, Rab14 was excluded from the purification strategy resulting in much improved homogeneity and purity of FIP2

4.2.3 Data Collection

Optimised crystals were analysed at Synchrotron Soleil, Paris, France. Native data sets were collected to a resolution of 3.5 Å. This did not represent an improvement on the original data set collected at APS.

Due to the difficulty in achieving successful molecular replacement data, attempts were made at producing selenomethionine substituted crystals (see Figure 4.2.12). Although milligram amounts of purified selenomethionine FIP2 were obtained, crystallisation was not successful. Therefore, a strategy to obtain phase information using the cobalt chloride in the crystallisation condition was employed. It was found to be possible to use the cobalt in the crystallisation solution to obtain anomalous diffraction data at Synchrotron Solei. Given that crystal formation appears to be dependent on cobalt, it was postulated that the cobalt ions may occupy specific points in the lattice and be useful in providing phase information. Further experiments were run at APS using crystals which had been soaked in a solution similar to the mother liquor but excluding the cobalt. This process may have aided in removing non-specific cobalt from the crystal, leaving those cobalt ions which occupy specific points in the lattice. Some anomalous data was obtained, to a resolution of 5 Å. However, this was not sufficient for molecular replacement.

At this point, the first data set obtained at APS was re-examined. Structure determination was achieved from this data using the programme Acrimboldo. Short, poly-alanine α-helices were used as molecular replacement models and connected to build larger helical segments (see Figure 4.2.13). Four molecules of FIP2 were built by Arcimboldo, using only the reflection file as the starting point for *ab initio* structure determination [286].

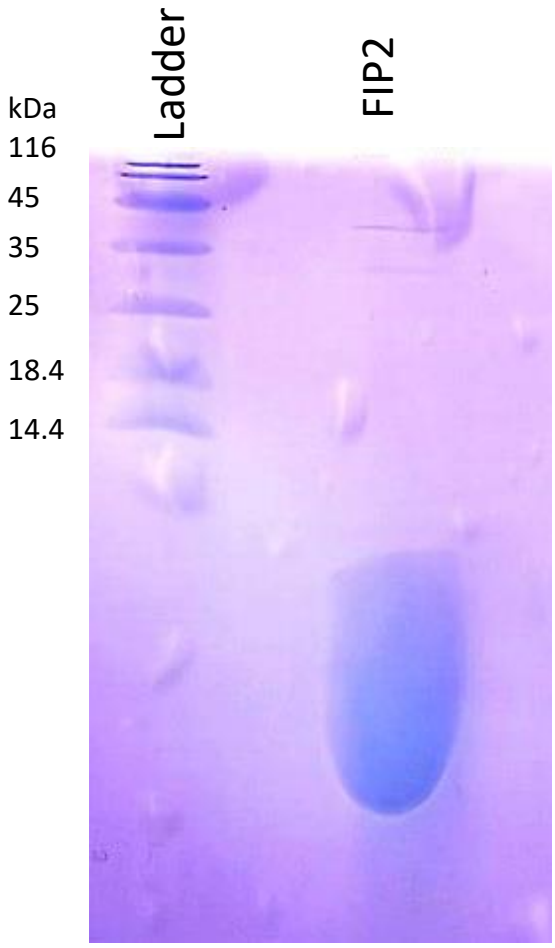

Figure 4.2.12 Selenomethionine Derivatised FIP2. Figure shows purified FIP2 substituted with selenomethionine. Crystallisation trials were set up in the same manner as native FIP2 in 24 well hanging drop format screening around similar conditions to the native hit condition. These trials did not yield any crystals. Further attempts were made to re-screen using sparse matrix screening. These attempts also proved unsuccessful.

Table 4.2.13 Statistics of Data Collection and Reduction

FIP2 – Rab-binding domain

Resolution range (Å)	46.16-2.29 (2.37-2.29)
Space group	C 2 2 21
Unit cell (Å)	62.54 68.43 172.09 90 90 90
Total reflections	72768 (6855)
Unique reflections	16934 (1611)
Multiplicity	4.3 (4.3)
Completeness (%)	99.4 (95.3)
Mean I/sigma(I)	8.8 (1.7)
R-merge	0.111 (0.924)
R-meas	0.126 (1.048)
R-pim	0.059 (0.483)

Values in parentheses are for the highest resolution shell

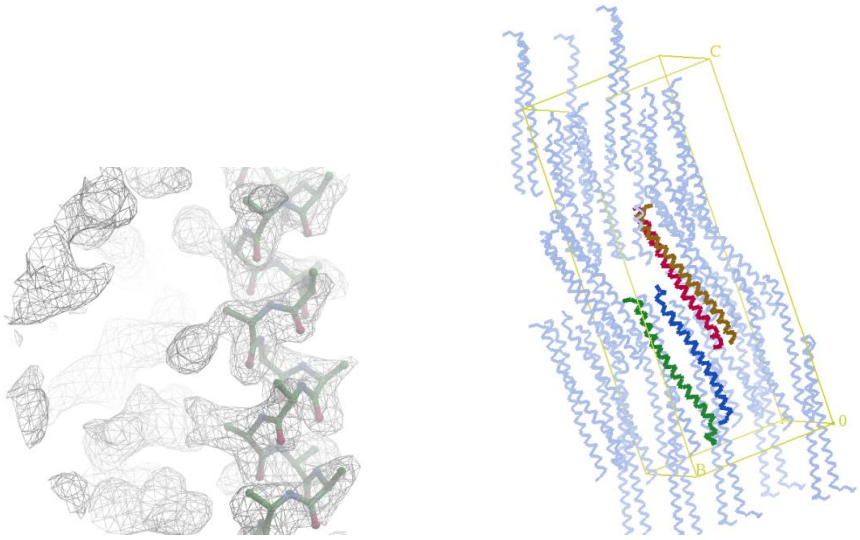

Figure 4.2.13 Crystal Structure of the Uncomplexed FIP2 RBD. Although traditional molecular replacement failed, the structure was determined using the programme Arcimboldo. Short poly-alanine α-helices were used as molecular replacement models and connected to build larger α-helical segments. The bottom left panel shows the electron density map of the final model showing side-chains beyond alanine, which provide evidence for correctness of the initial model. The bottom right panel shows packing in a section of the crystal, with the unit cell shown as yellow lines. Four molecules of FIP2 (red, green, brown and blue) were built by Arcimboldo, using only the reflection file as the starting point for *ab initio* structure determination [286].

4.3 Discussion

Initial crystallisation attempts were focused on the complex Rab14-FIP2. Rab14-FIP2 interactions pose an interesting question in that the complex formed between them has a lower affinity than a complex formed between FIP and Rab11 family members [284]. What elements of this new structure could underpin to the individual affinities produced between two group II Rabs with a common, shared effector. The purification strategy for these attempts was flawed, in that the complex produced was heavily biassed towards FIP2. Protein crystals produced from sparse matrix screening were replicated in 24 well screens and determined to be composed of FIP2 and independent of Rab14. This allowed us the opportunity to examine the structure of a class I FIP independent of a bound Rab. No such crystal structure currently exists and the structure of the unbound effector may reveal elements of conformational change which occur upon binding. The challenge of molecular replacement from the original FIP2 data was significant, therefore multiple attempts at replicating the crystals to obtain better diffraction data and phase information were undertaken.

Replicated crystals of FIP2 were produced in a similar condition to the original hit (pH 4.7). These crystals formed from protein precipitate and adopted a clumped 'fist-like' morphology. Optimised crystals, produced from an updated crystallisation strategy excluding Rab14 and at a slightly higher pH of 4.8, formed showers of crystals of various sizes. These crystals, although being of a more regular morphology and formed from FIP2 solutions of significantly better homogeneity, did not diffract to higher resolution than the original crystals produced under sparse matrix screening.

In an attempt to alleviate the challenge of molecular replacement, attempts at producing selenomethionine derivitised crystals were made. These however were unsuccessful. Nevertheless some phase information was obtained from the native crystals by taking advantage of the dependency of crystal formation on the presence of cobalt in the crystallisation condition. Although anomalous data was collected, it was not of sufficient resolution to be of significant help to structure resolution.

The issue of structure resolution was finally resolved by a novel approach using the programme Arcimboldo [286]. This was achieved by Dr Khan using computing facilities at Harvard University. The resulting structure indicates that the structure of the uncomplexed effector is significantly different to the structure visualised in complex with the Rab11 family members. Further analysis and discussion of this structure was performed and is discussed in Chapter 5 of this work.

Chapter 5:

Structural Analysis of Uncomplexed FIP2

5.1. Introduction

Existing crystal structures of Class I and II FIPs all show the structure of the effector in complex with its cognate Rab [202, 204, 284, 285]. In contrast, as outlined in Chapter 4, we have successfully crystallised and refined the structure of FIP2, independent of its Rab binding partner.

In the case of Rab11:FIP2, the complex forms a central symmetric coiled coil of FIP2 with Rab binding sites on either side. Switch I of Rab11 is embedded between the FIP dimer and forms hydrophobic interactions while the switch II of the Rab molecule is in a more flexible conformation than switch I which is unique to Rab11 [281].

The novel structure discussed in this chapter is significantly different from the Rab:FIP structures existing in the literature. Here, we will examine the novel FIP2 structure and analyse its relevance in comparison to previous structures of FIP2.

5.1.2 Scientific Objectives

- To analyse the novel crystal structure of FIP2 in comparison to existing structures.

5.2 Results

5.2. Structure Comparison of Novel FIP2 Structure with FIP2 as seen in the Rab11:FIP2 Complex.

Major differences can be seen in the structure of the uncomplexed FIP2 in comparison to the structure of FIP2 when in complex with Rab11 family members. We examined, for comparison, the structure of the Rab11:FIP2 complex in contrast with the novel FIP2 structure [281].

In complex with Rab11, FIP2 forms a centrosymmetric parallel coiled coil. In the case of the uncomplexed effector, two non-parallel pairs of FIP2 molecules form the asymmetric unit of the crystal lattice. One of the molecules of FIP2 is inverted with respect to the other and further crystal contacts exist between the FIP2 pairs. Some differences in the length of the defined FIP2 molecules exist. In the case of Rab11:FIP2, the pdb structure, 2gzh, has FIP2 residues defined from 447-503 (shown in Figure 5.2.4). However, in the case of the novel FIP2 structure, 4 molecules of FIP2 are refined with slightly different boundaries (shown in Figure 5.2.5). For the purposes of this comparison, we will examine molecule A, the most fully defined FIP2 protomer which is refined from residue 445-497. Upon further inspection, the 'dimers' in the novel FIP2 structure appear loosened, with the two molecules bowed away from each other when compared to the structure of the FIP2 dimer in complex with Rab11. It is possible that the structure actually represents four monomers of FIP2 which have formed these dimers under the high protein concentration of the crystallisation condition.

Analysis of the structures by the Protein Interfaces, Surfaces and Assemblies (PISA) server reinforces the hypothesis that the novel FIP2 structure is not representative of a strict dimer. The buried surface area between the protomers shows a significant difference between the novel structure and the FIP2 dimer formed in the Rab11:FIP2 complex. Analysis by PISA indicates a buried surface area between FIP protomers A and D of the novel structure of 586.6 $Å^2$. In contrast the two protomers of the FIP2 dimer in the complex have a higher buried surface area of 1659.7 $Å^2$ (see Table 5.2.1). Furthermore, significant differences in the predicted Gibbs free energy for the formation of

the interfaces exist, -20 kcal/mol for the FIP2 dimer as seen in the complex, in contrast to 0.8kcal/mol for the novel structure, indicating that the dimer formation is less energetically favourable. There are also differences in the calculated complexation significance score. This value reflects the significance of the interface for assembly formation. The score for the novel structure is lower than that of the FIP2 dimer as seen in the complex, again indicating that stable dimerisation is not supported in the novel structure. Furthermore, DLS analysis shows that the radius of the FIP2 particles in solution is roughly halved in accordance with lowering the pH to that similar to the crystallisation condition (see Table 5.2.2).

Circular Dichroism analysis of FIP2 at a range of pH values

In order to investigate the change in orientation between the coiled coil in the Rab11:FIP2 structure (and other similar Rab11:FIP structures) and the novel FIP2 structure, circular dichroism analysis was applied to a solution of FIP2 at a range of pH values. The CD measurements trend towards increased helicity at more physiological pH values. The decrease in helicity measured at less physiological pH may indicate an 'unwinding' of the coiled coil as the protomers change conformation and orientation (see Figure 5.2.3).

Further evidence for this theory can be found from examination of the structures by superimposition. Superimpositions of the novel FIP2 'A' protomer with the structure of FIP2 in complex were performed using Pymol. An image of the superimposition is shown in figure 5.2.6.. These *in silico* comparisons indicate that there is some similarity between the structures of the FIP2 protomers in their α-helical segment between residues 454-491 with a RMSD of 1.46. In contrast, when including the N and C-termini of the structures, the RMSD rises to 6.07. In conclusion, there are significant differences in the structures of the protomers, the most dramatic of which are localised at the N and C termini of the FIP2. In the complex the direction of the polypeptide reverses to orient the C-terminus towards the second protomer of the dimer which serves to re-inforce the dimerisation of FIP2. The C-terminus of the uncomplexed FIP2 is truncated with respect to the complexed form, ending at a residue 497 as opposed to residue 502. The C-

terminal portion of both forms represent the end of the α-helix followed by a short helical segment which is roughly perpendicular to the α-helix. The nucleation of the second helix is mediated by a proline residue, P493, which is conserved in all FIPs. In the complex form, another proline residue, P499, changes the direction of the polypeptide and allows the protomers to wrap around each other and reinforce the dimerisation. There are interactions between the side chain of Tyr500 and Glu491 and also between the phenyl ring of Try500 lying below the guanidine group of Arg487, forming a cation-π interaction. However, in the uncomplexed form, these reinforcing interactions do not exist with the polypeptide ending at residue 497. The position of the short helical segment is displaced relative to its position in the FIP2 dimer in complex. Furthermore, the section bends away from the partner molecule and does not provide any contacts which would stabilise a dimer.

Table 5.2.1 PISA Analysis of FIP2

Interfacing structures	Buried Surface Area (Å^2)	ΔG (kcal/mol)	Salt Bridge	Hydrogen Bond	Complexation Significance Score
FIP2 dimer (Rab11:FIP)	1659.7	-20.5	6	13	0.657
FIP2 A:D interface	586.6	0.8	16	11	0.178

Table 5.2.1 PISA Analysis of FIP2. Analysis shows significant differences in the predicted buried surface area, Gibbs free energy (ΔG) and complexation significance score between the FIP2 interface in the novel structure and in the complex with Rab11. The lanes labelled salt bridge and hydrogen bond represent predicted numbers of each interaction between the protomers.

Table 5.2.2 DLS Measurements of FIP2

sample	% mass	Radius (nm)
FIP2 pH 7.5	100	3
FIP2 pH 4.8	99.2	1.4

Table 5.2.2 DLS Measurements of FIP2. DLS measurements were performed on FIP2 which had been diluted into buffer at pH7.5 and pH4.8, similar to the ratios used in the crystallisation set up. The table above shows that the radius of the FIP2 particles has approximately halved at the lowered pH.

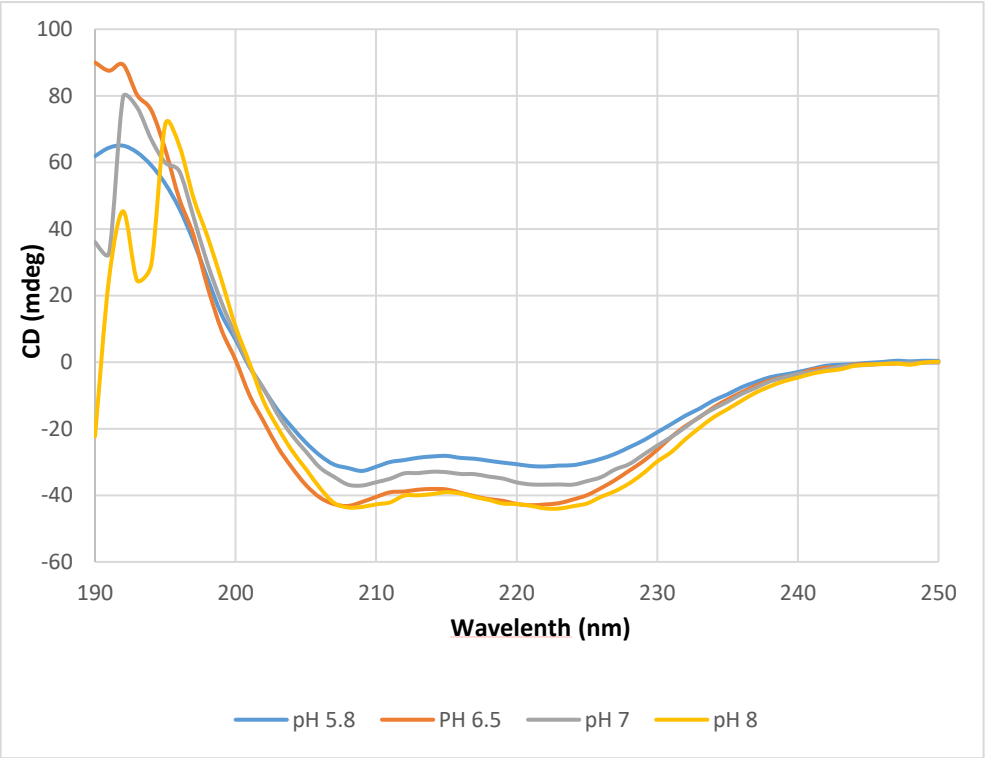

Figure 5.2.3 FIP Circular Dichroism Analysis. The CD spectra for FIP2 were measured at a range of pH values: 5.8, 6.5, 7 and 8. The spectra indicate that FIP2 forms an α-helical secondary structure consistent with the crystallisation data. Increasing helicity is seen at pH values closer to physiological pH whereas, at pH 5.8, decreased helicity of the FIP2 molecule is shown. The noise level increases at lower wavelengths.

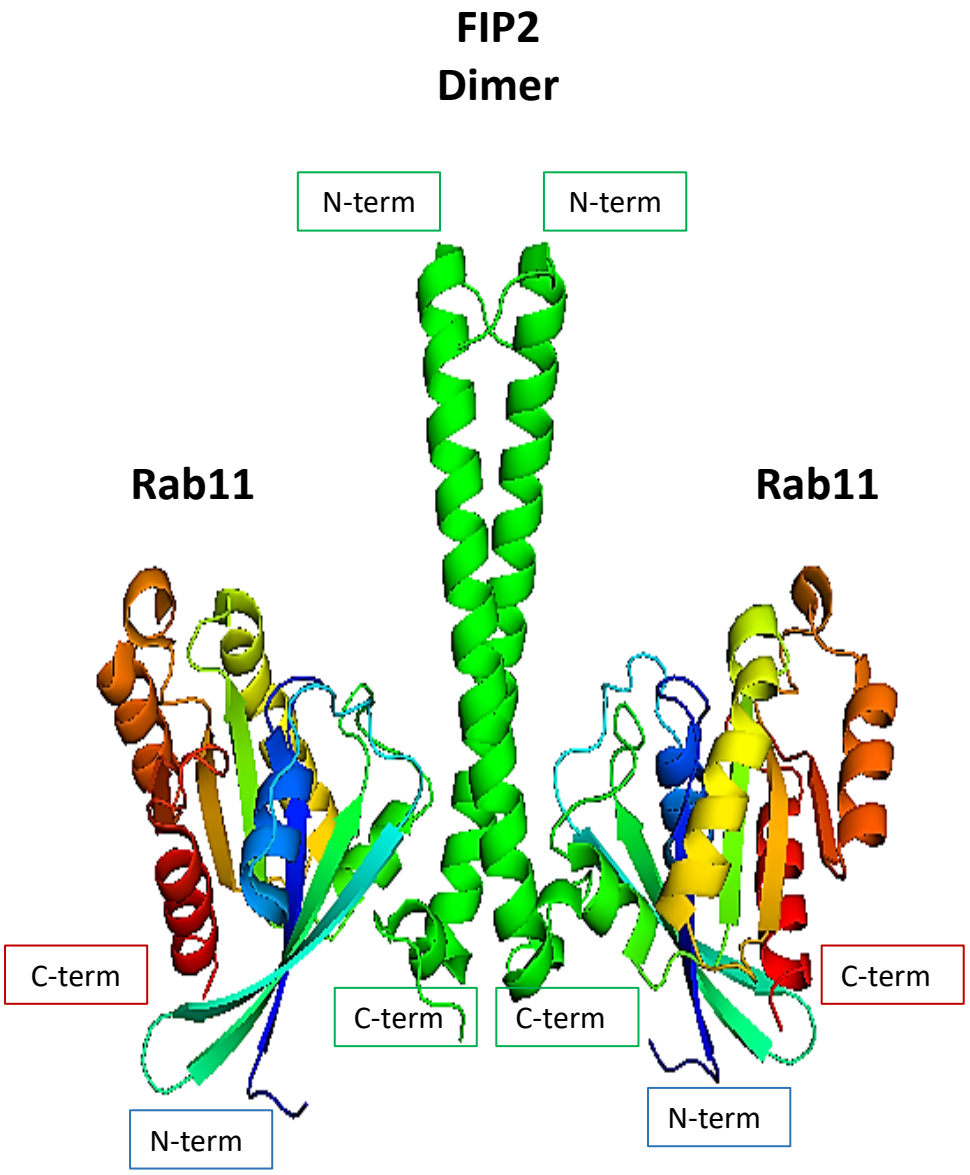

Figure 5.2.4 Rab11:FIP2 Crystal Structure. The figure above shows the structure formed between Rab11 and FIP2. A dimer of FIP2 forms a centrosymmetric coiled coil (shown in green). FIP2 forms a parallel coiled coil with the Rab11 binding site at the C-terminus. At the C-terminus, the α-helix terminates and a short 3_{10} helix is nucleated. A proline residue at position 499 changes the direction of the polypeptide and allows the protomers to wrap around each other and reinforce the dimerisation. Two Rab11 binding sites are formed on either side of the FIP2 dimer. Both helices of the FIP2 are involved in the RBD.

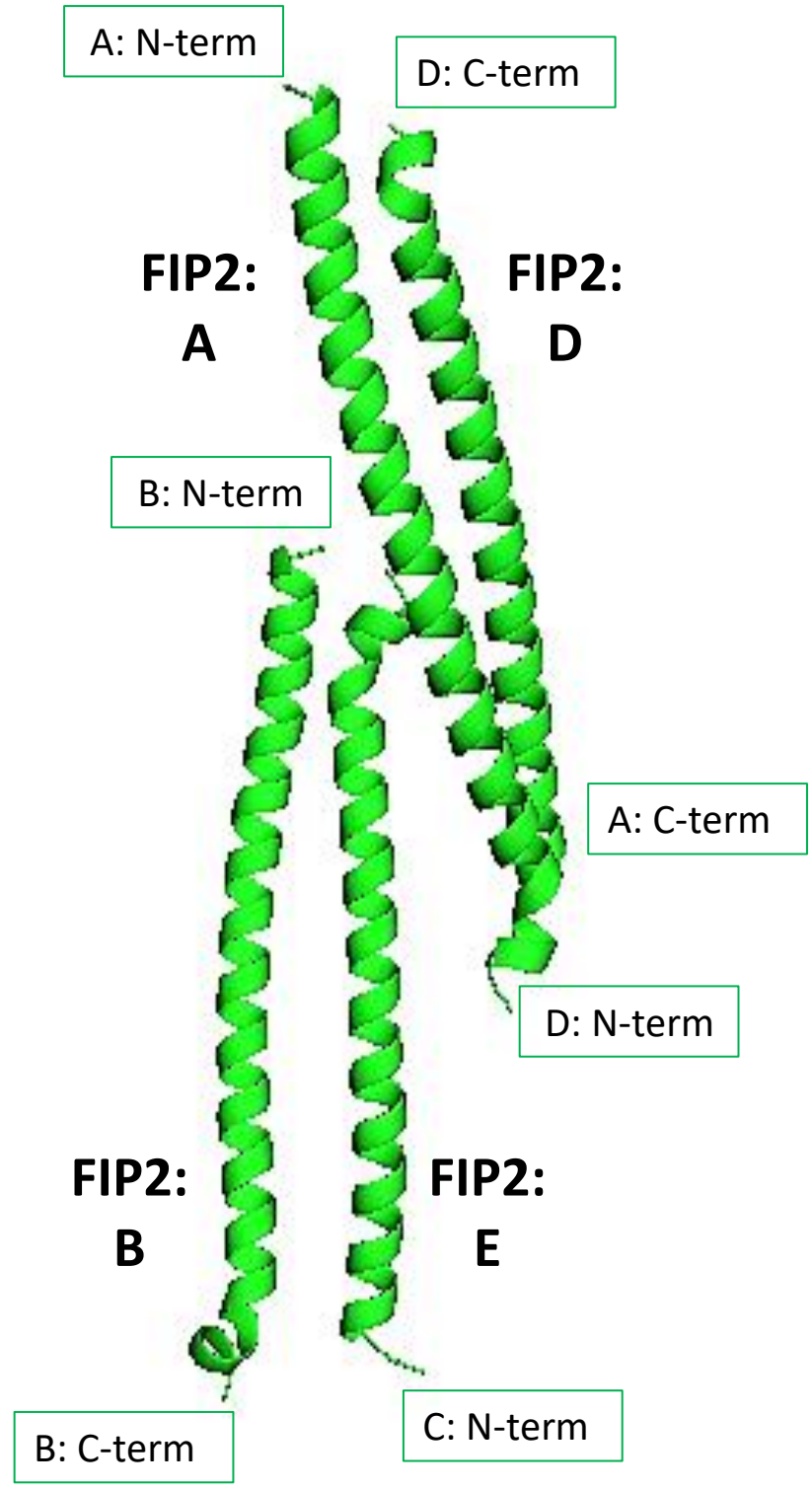

Figure 5.2.5 FIP2 Crystal Structure. The figure above shows the novel FIP2 effector crystal structure independent of a bound Rab. Four molecules of FIP2 are refined in the crystal structure. The molecules are labelled A, D, B, E. Molecules A and D and B and E appear to be arranged in pairs in an antiparallel fashion. Figure made using Pymol [2].

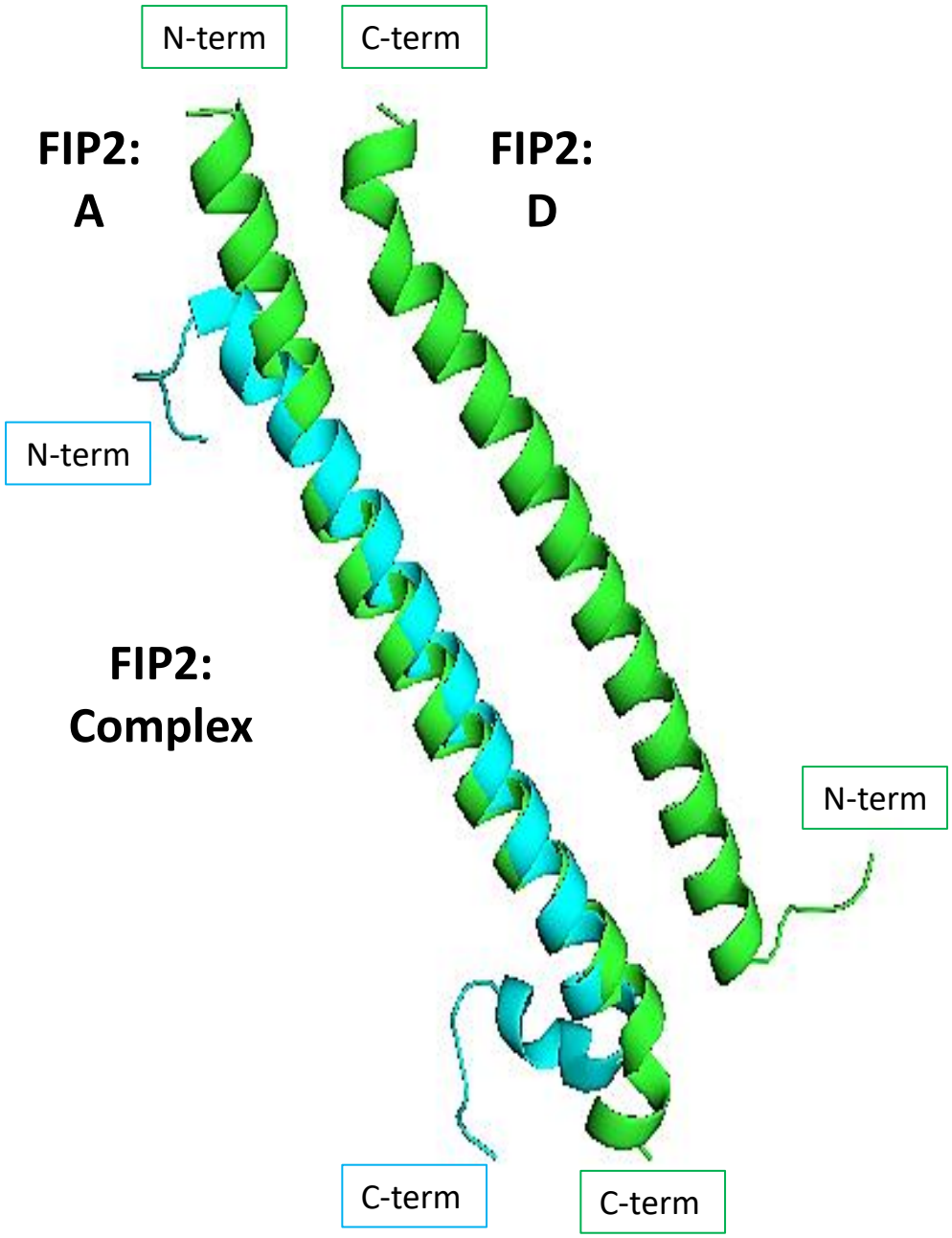

Figure 5.2.6 Superposition of the Novel FIP2 Crystal Structure with a FIP2 Protomer from the Rab11:FIP2 Complex. The figure above shows the novel FIP2 effector crystal structure (green helices) superimposed onto a FIP2 protomer as seen in the crystal structure of Rab11:FIP2 (shown in cyan). Residues 454-491 are superimposed with a RMSD of 1.46. In the complex structure, the FIP2 forms a parallel coiled coil whereas, in the novel structure the FIP2 molecules form an anti-parallel pairs. For this reason the second protomer in the complex form has been excluded from the figure as sequence alignment for both FIP2 molecules simultaneously is impossible. The superimposition shows major differences in the structure of the FIP2 protomers, particularly evident at the N-terminus and C-terminus of the molecules. Figure made using Pymol [2].

5.3 Discussion

It can be concluded that major differences exist between the existing structures of Rab11:FIPs present in the literature and the novel structure resolved in this work. Overall, the binding site of Rab11 is abolished in the structure. In the complex, switch I of Rab11, residues 44-46 are buried between the two helices of the FIP2 dimer with both protomers of FIP2 interacting with the Rab11 molecule. The RBD involves both protomers of FIP2 and due to the inversion of the coiled coil in the novel crystal lattice, the Rab binding site is no longer present. Furthermore, as indicated by PISA analysis and supported by CD and DLS data, it is possible and indeed likely that the novel structure actually represents the structure of monomers of FIP2 in solution. PISA analysis indicates that the dimerisation indicated in the crystal structure is not energetically favourable with a low CSS. DLS data show a decrease in the radius of the FIP2 particles consistent with a dimer to monomer shift. CD data indicates a lowering of helicity in pH values closer to the crystallisation condition and analysis of the structure itself indicates a loss of reinforcing interactions which exist at the C-terminus of the dimer in the complex structure. All of this evidence suggests that the asymmetric unit formed in the crystal is not indicative of stable dimers of FIP2.

The question of why the novel structure is so different to structure of FIP effectors crystallised in complex remains. One possible reason is that the non-physiological conditions of the crystallisation experiment are contributing to the altered conformation of FIP2. This appears to be supported by CD analysis, with the FIP2 showing decreased helicity at pH 5.8 in comparison to pH8. However, the crystallisation conditions of Rab11:FIP2 complex, used here for comparison, range from pH4.8-5.5 [204]. It is possible that FIP2 favours the monomeric form at lowered pH, and that the dimer conformation of FIP2 is captured and stabilised by Rab binding. Another possibility is that the truncation of FIP2 in the novel crystal structure (ending residue 497) is contributing to the lack of dimerisation. In the complex, further contacts exist at the C-terminus which re-inforce the interaction between protomers.

Chapter 6:

Discussion and Conclusions

6.1 Rab11/ Rab14 Show Different Affinities for their Shared Effectors, the Class I FIPS

Rab proteins all contain the same basic fold, yet they associate specifically with a large number of structurally diverse effectors [196]. By studying the underlying mechanisms by which Rabs encode effector specificity, we may contribute towards unravelling the mechanisms behind the larger questions of what determines protein-protein specificity and affinity.

The Rab11 subfamily is comprised of a set of three closely related Rabs (Rab11a, Rab11b and Rab25) which share a high level of sequence similarity. This Rab family shares a set of effectors - the Rab11FIPs [230]. Multiple structures of Rab11 family members and their FIP effectors exist in the literature [204, 208, 244, 284, 285]. Interestingly, Rab14, a Rab of the same functional group as Rab11, shares the ability to interact with a subset of FIP effectors, namely the class I FIPs [233]. Rab14 interacts with FIPs with distinct specificity and affinity. By examining the literature, we see that Rab14 interacts with FIP2 with an affinity that is approximately tenfold weaker than the interaction between Rab11a and FIP2 [284]. This raises the questions as to which factors allow Rab14 to retain FIP-binding characteristics, and which factors influence the specificity and affinity of these interactions. Although the structure of Rab14-FIP2 has not been solved, we can examine the structure of another Rab14-FIP interaction which is present in the literature for clues as to the factors which may account for Rab14 and Rab11 displaying such variable affinities for class I FIPs.

Crystal structures of both Rab11 and Rab14, in complex with their FIP effectors, allow for well-reasoned arguments to be presented for a number of factors which may influence this differential affinity. However, currently no thorough experimental investigation is present in the literature [204, 231, 284]. From the structure of Rab14-RCP, we see that a number of distinct features exist. The most unusual of these features is an intramolecular disulphide bond which exists between residue 26 and residue 40 which is in the switch I region of Rab14. This is disulphide thought to be GTP dependent. It is present in the structure of Rab14-RCP but not in the structure of Rab14 (GDP) [199, 284]. If these structures are true representations of the *in vivo*

nucleotide state of Rab14, it follows that the disulphide is present during the membrane localised interactions between Rab14 and FIP2. It is possible that this bond is of significance to the interaction and we aimed to establish whether this unique feature is an influencing feature for Rab14-FIP2 affinity.

We introduced a single cysteine mutation and, subsequently, a double cysteine mutation into Rab11 in order to examine its effect on the structure and affinity for FIP2. We demonstrated that, although the mutants have an effect on the molecular characteristics of Rab11, as demonstrated by analysis by SDS PAGE under non-reducing conditions, no significant change in affinity is recorded between mutant and wild type Rab11. We must conclude that this unique feature of Rab14 is not an important factor in determining its affinity to class I FIPS. Furthermore, our SDS PAGE results do not prove the existence of a disulphide bond. It is possible that variations seen under SDS PAGE analysis are merely due to different oxidation states of the cysteine residue and that the intramolecular disulphide shown in the Rab14:RCP structure is an artefact of the crystallisation condition. Further structural analysis, including the structural solution of the Rab14:FIP2 complex would shed light on this issue. However, this study clearly shows that this feature is not a determining factor in the affinity of Rab14 for FIPs.

The question of which factors are important in influencing effector affinity remained unsolved. However, further experiments showed that, although we initially hypothesised them to be of secondary concern to the disulphide bond, two amino acid differences between Rab14 and Rab11 family members are instrumental in governing the affinity of Rab14-FIP. We examined a Rab11 mutant which introduced these two amino acid substitutions, namely a serine at position 20, which is substituted for a methionine in Rab14, and a lysine at position 41, which is substituted for a proline in Rab14. The differences between Rab11 and Rab14 at these particular positions are illustrated in figure 6.1.1. After introducing both of these mutations into Rab11, a threefold decrease in affinity for FIP2 was measured. We can see from comparing the crystal structures of Rab11-FIP2 and Rab14-RCP that the S20M mutation in a P-loop residue causes a knock-on effect in the switch II region of the Rab. The altered conformation induced by the S20M mutation may contribute to

the reduced affinity of Rab14-FIP2. Alternatively, or as a combining factor, the K41P mutation in the switch I region of Rab14 may contribute to the reduced affinity for the effector. Although the conformation of switch I seen in the crystal structures is similar in Rab14-RCP and Rab11-FIPs, this mutation contributes to a lack of electrostatic parity between the Rab and the effector. In the case of Rab14, a conserved glutamate in the FIP effector has no electrostatic partner, whereas, in the Rab11 subfamily members, it is met with a lysine or arginine at position 41 [281, 284].

Our experiments show that the influencing factors in the specificity of Rab14-FIP2 and, with some extrapolation, the specificity of Rab14-FIPs do not include the unique disulphide present in Rab14. Rather, other residues which have an influence on the electrostatic parity of the complex as well as the conformation of the switch II region affect the affinity. However, these regions are not sufficient to explain the reduction of affinity outlined in the literature. We must conclude that Rab-effector specificity is a multifactorial process that is influenced by the cumulative effect of small sequence differences in non-conserved residues which differ between Rabs.

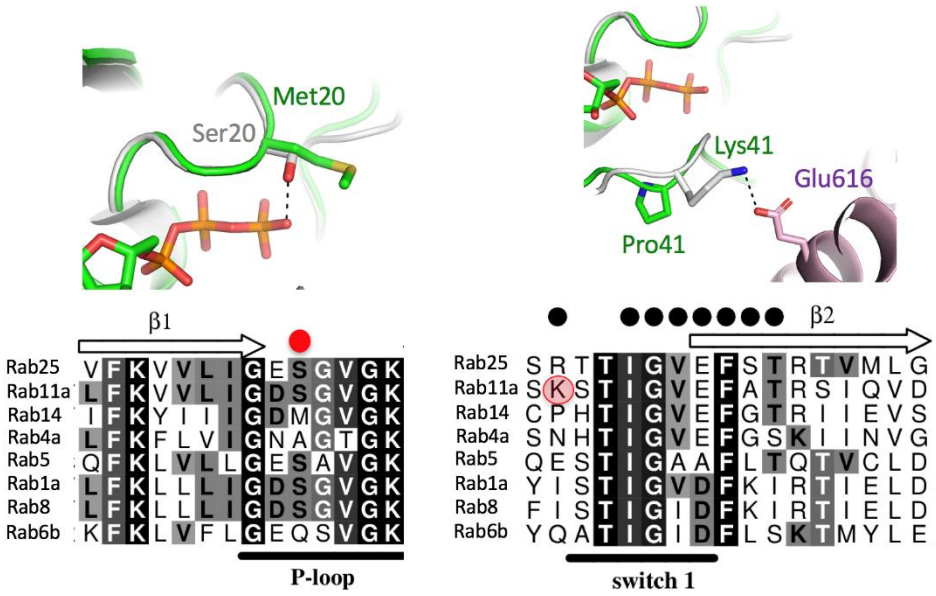

Figure 6.1.1 Structural determinants of Rab affinity for FIP2. The two red circles (filled and transparent) denote the site of Rab11 mutations, S20M and K41P (bottom panel). Rab14 is shown in green cartoons and sticks, while Rab11 is grey, FIP2 is shown in violet. GTP from Rab11 is shown in orange stick models. The figure was made using Pymol [2] by Dr A.Khan.

6.2 Structural Determination of FIP2

Our initial aim in crystallisation experiments was to solve the structure of the Rab14-FIP2 complex. By doing this we aimed to reinforce and confirm the structure of Rab14 in complex with class I FIPs and highlight differences in structure which may underpin the differential specificity of Rab14-FIPs in comparison to Rab11-FIPs. Indeed, we expected to produce another 'butterfly' shaped structure, reminiscent of Rab11-FIPs in which the FIP forms a central symmetric coiled coil with equivalent Rab binding sites on either side. Serendipitously, we instead crystallised FIP2 independent of Rab. This afforded us the opportunity to address a more interesting question- what is the structure of FIP2 independent of Rab? No crystal structure for a FIP effector independent of Rab is currently present in the literature.

Multiple challenges presented during attempts at structure resolution. The helical structure of FIP2 complicated matters, as fitting a molecular replacement structure to the correct helix pitch was difficult. In order to aid this process, FIP2 crystals were replicated in an effort to produce higher resolution data sets. Multiple FIP2 crystals were replicated with increasingly regular and attractive morphology. Crystal production was improved from jagged, shard-like crystals to regularly shaped, large, individual crystals as crystallisation conditions were optimised. However, these apparent improvements were not reflected in the resolution of diffraction data and molecular replacement was not possible. Attempts were made at producing selenomethionine derivatised crystals. However, although some spherulites were produced, no crystals of diffraction quality were obtained. A more innovative strategy was adopted in an attempt to generate phase information. The growth condition of the crystals required the presence of cobalt. We postulated that the cobalt may occupy specific positions in the crystal lattice and that perhaps some phase information could be gleaned from collecting diffraction data at the cobalt absorption edge. Although this strategy was partially successful, the anomalous data was not of sufficient resolution to be useful for structure determination. Finally a successful structure solution was achieved by Dr Khan using the programme Arcimboldo and computer facilities at Harvard University. The programme is named after the painter

Giuseppe Archimboldo, whose paintings use multiple objects, often fruit, to create images of human faces. In a similar fashion, the programme used short multi-alanine helices to build longer alpha helices and solve a structure [286].

The structure of FIP2 features four α-helices which appear to interact in pairs. However, the helices are not reminiscent of the coiled coil formed in the Rab11-FIP structures. Most dramatically, one helix in the pair is flipped relative to the other, forming anti-parallel pairs of helices. This flipping abolishes the reinforcing C-terminal interactions which are important to the structure of Rab11-FIP2. In the case of Rab11-FIP2, these interactions form contacts with a β-strand in the Rab structure. More dramatically still, the Rab binding site is completely abolished by the change in helix orientation. In complex, the Rab makes contact with both helices of the FIP2 dimer. Analysis by PISA and DLS indicates that the pairs in the crystal structure are not truly representative of a dimer, but rather monomers of FIP2 arranged in this fashion in the high protein concentration of the crystallisation condition.

What factors have caused this large conformational change between the novel structure of FIP2 and the structure of FIP2 in complex with Rab? It is possible that the C-terminally truncated FIP2 used for crystallisation contributes to the lack of reinforcing contacts of the dimer. Another explanation for the dramatically different conformation of FIP2 could be the artificially low pH of the crystallisation condition. The protein crystallises at a maximum pH4.8. CD analysis and DLS reinforce the hypothesis that destabilisation of the dimer is increased as the pH is lowered. However, the Rab11-FIP2 structure itself was crystallised at low pH in 0.3 M ammonium phosphate pH 4.8 [281]. We conclude that the monomeric form of FIP2 resolved in the crystal structure becomes more favourable as the pH is lowered and that dimer formation is stabilised by Rab binding.

An NMR structure of the C-terminal region of FIP2 has been published. The structure shows FIP2 as a slightly curved alpha helix from Thr452 to Asn483. The region resolved in this structure is C-terminally truncated and does not retain the ability to bind to Rab, calling into question the relevance of the structure. Wei et al show that the dimer retains a coiled coil structure with

some fraying of the coil at the C-terminus [287]. The authors suggest that a preformed helix is not necessary for Rab11 binding. However, the interactions between the switch regions of the Rab and the binding surface of FIP2 are formed by both helices of the coiled coil dimer. Furthermore, additional Rab contacts and reinforcement of the homodimer occur at the C-terminus. Therefore, we feel that a pre-formed helix must be a requirement of Rab binding. The analysis of our FIP2 construct, which retains Rab-binding ability, supports the hypothesis that Rab reinforces the dimer conformation of FIP2.

6.3 Future Perspectives

Future work would aim to expand on the biophysical work shown here. While this work serves to rule out the intramolecular disulphide bond which exists in Rab14 as a factor in its reduced affinity for class I FIPs, further work to identify those sites in Rab14 which contribute to the lowered affinity is necessary. This work has begun the process of elucidating these factors. Here, we have identified two mutations which together account for a threefold reduction in affinity of Rab14:FIP2 in comparison to Rab11:FIP2. To further this work, individual mutations at these residues (S40M and K41P) should be generated to further examine the significance of the proline, which contributes to a lack of electrostatic parity, and the methionine, which contributes to the altered conformation of switch II. It is possible that one of these mutations contributes more to the lowered affinity than the other. Furthermore, the effect of these particular mutations on Rab14 interactions with other class I FIPs should be analysed to reinforce the importance of these mutations on interactions between Rab14 and the remaining FIP family members.

Our study has only identified sites which account for a threefold decrease in the affinity of Rab14:FIP2 in comparison to Rab11:FIP2. However, the literature indicates a tenfold difference in affinity between the complexes. Further analysis to identify other important residues which differ between the complexes and may have influence on their affinities should be considered.

Structural questions also remain. Our biophysical work would be further supported by determining the structure of Rab14:FIP2 with the aim of analysing the electron density to determine if the novel disulphide bond present in Rab14:RCP is also present in other Rab14:FIP complexes. Perhaps, this feature of the Rab14:RCP complex is an artefact of the crystallisation condition and not truly representative of the complex *in vivo*.

In tandem with biophysical and structural work, it is important that our results be supported by cell biology studies. The S20M and K41P mutations, which have been identified as important, should be expressed in cell culture both as double mutation and single mutation variants in order to examine any possible effect they may have on the localisation of Rab11 and its FIP2 effector. Do these mutations infer Rab14-like character in a cellular environment? If so, we may determine whether our biophysical studies have functional relevance *in vivo.*

Appendix

pET28b	
Source/Vendor:	EMD Biosciences
Alt Name:	pET28b
Plasmid Type:	Bacterial Expression
Expression Level:	High
Size:	5368
5' Sequencing 1 Primer:	T7 Fwd
Tag 1:	His (Nterm and Cterm)
Bacterial Resistance:	Kanamycin
Notes:	Nterm thrombin cleavage site
Stable:	Transient
Constitutive:	Constitutive
Viral/Non-Viral:	Nonviral

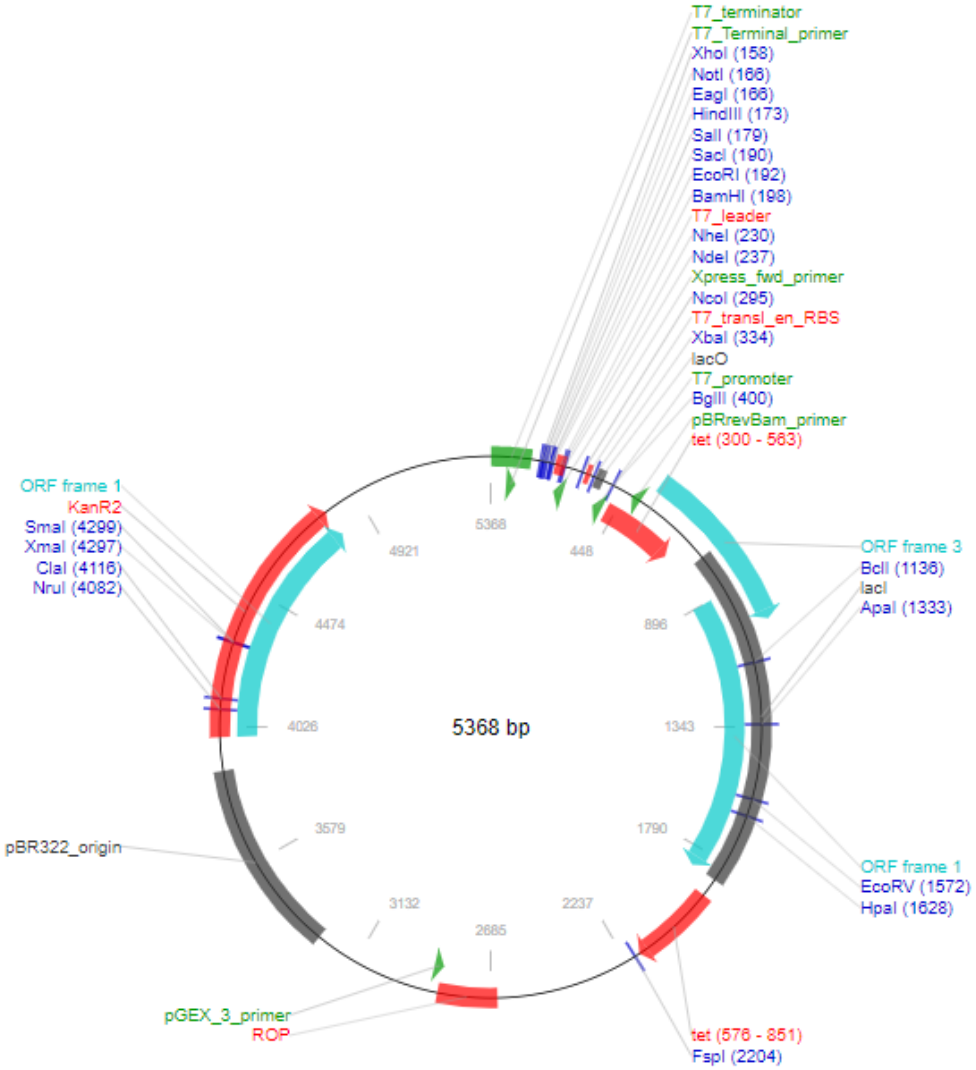

pET15b	
Source/Vendor:	Novagen (EMD Millipore)
Alt Name:	pET15b
Plasmid Type:	Bacterial Expression
Promotor:	AmpR, lac1
Expression Level:	High
Size:	5708
5' Sequencing 1 Primer:	T7 Fwd
Tag 1:	His (Nterm)
Bacterial Resistance:	Ampicillin
Notes:	Nterm thrombin cleavage site
Stable:	Transient
Constitutive:	Constitutive
Viral/Non-Viral:	Nonviral

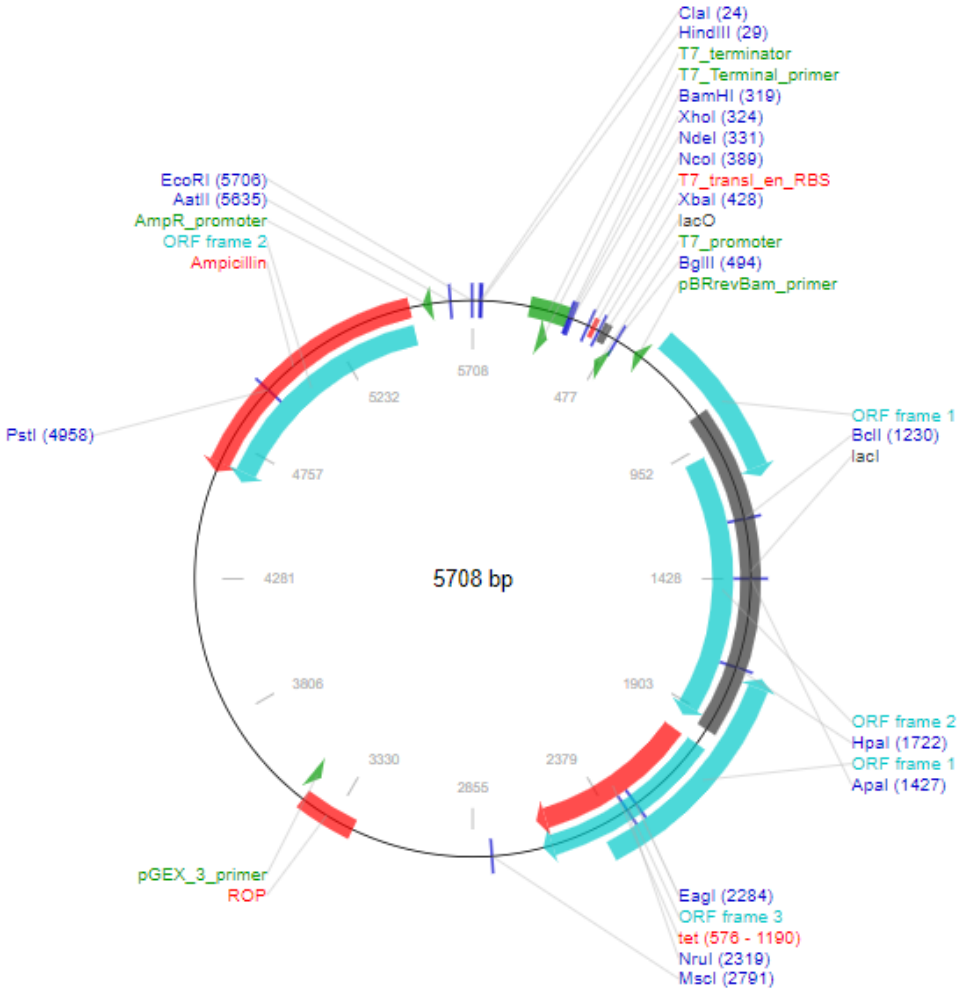

pNIC BSA4	
Vector backbone:	pET28a
Backbone manufacturer	Novagen
Vector Type:	Bacterial Expression
Promotor:	AmpR, lac1
Growth Strain:	DH5alpha
Cloning Method:	Restriction enzyme
Size:	7284 bp
5' Sequencing 1 Primer:	T7 Fwd
Tag 1:	His (Nterm)
Bacterial Resistance:	Kanamycin
Notes:	His – TEV (N-terminal on backbone)
Viral/Non-Viral:	Nonviral
Citation	[288]

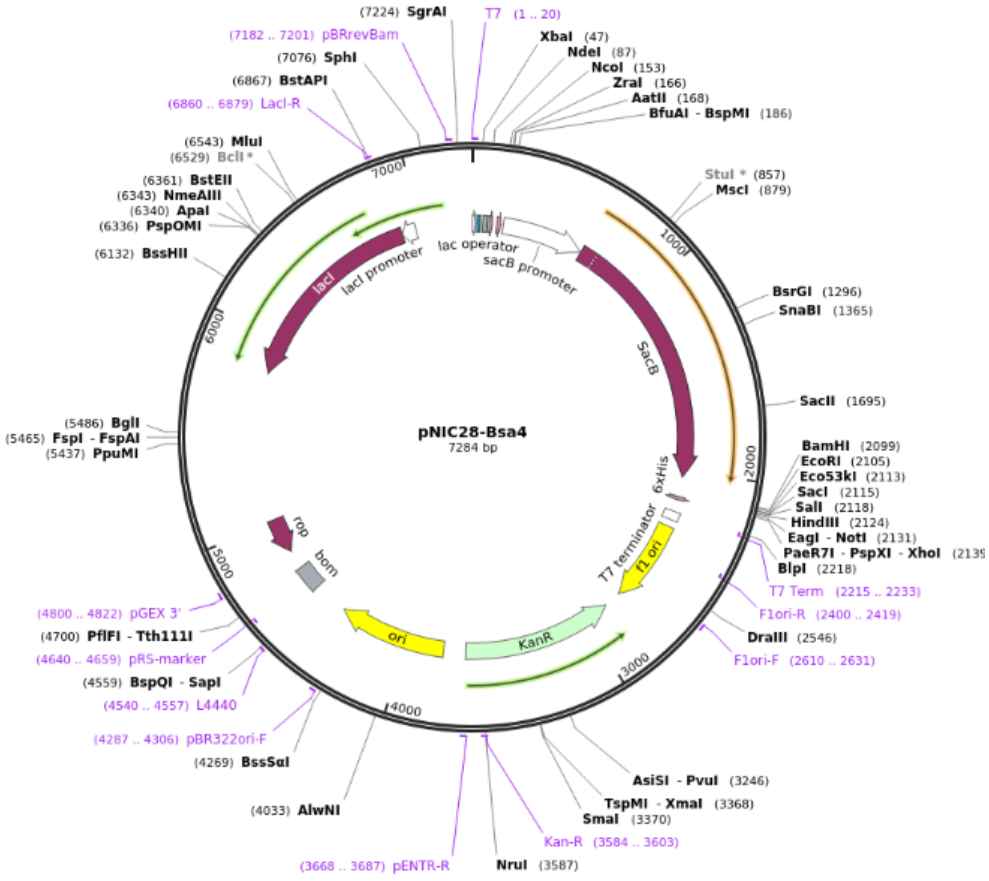

All plasmid maps are sourced from Addgene

Bibliography

1. Pereira-Leal, J.B. and M.C. Seabra, *Evolution of the Rab family of small GTP-binding proteins.* J Mol Biol, 2001. **313**(4): p. 889-901.
2. The PyMOL Molecular Graphics System, V.S., LLC.
3. Stenmark, H., *Rab GTPases as coordinators of vesicle traffic.* Nat Rev Mol Cell Biol, 2009. **10**(8): p. 513-25.
4. Kastritis, P.L. and A.M. Bonvin, *On the binding affinity of macromolecular interactions: daring to ask why proteins interact.* J R Soc Interface, 2013. **10**(79): p. 20120835.
5. Saraste, M., P.R. Sibbald, and A. Wittinghofer, *The P-loop--a common motif in ATP- and GTP-binding proteins.* Trends Biochem Sci, 1990. **15**(11): p. 430-4.
6. Gorbalenya, A.E. and E.V. Koonin, *Superfamily of UvrA-related NTP-binding proteins. Implications for rational classification of recombination/repair systems.* J Mol Biol, 1990. **213**(4): p. 583-91.
7. Milner-White, E.J., J.R. Coggins, and I.A. Anton, *Evidence for an ancestral core structure in nucleotide-binding proteins with the type A motif.* J Mol Biol, 1991. **221**(3): p. 751-4.
8. Schweins, T. and A. Wittinghofer, *GTP-binding proteins. Structures, interactions and relationships.* Curr Biol, 1994. **4**(6): p. 547-50.
9. Vetter, I.R. and A. Wittinghofer, *Nucleoside triphosphate-binding proteins: different scaffolds to achieve phosphoryl transfer.* Q Rev Biophys, 1999. **32**(1): p. 1-56.
10. Walker, J.E., et al., *Distantly related sequences in the alpha- and beta-subunits of ATP synthase, myosin, kinases and other ATP-requiring enzymes and a common nucleotide binding fold.* EMBO J, 1982. **1**(8): p. 945-51.
11. Rodnina, M.V., et al., *GTPases mechanisms and functions of translation factors on the ribosome.* Biol Chem, 2000. **381**(5-6): p. 377-87.
12. Takai, Y., T. Sasaki, and T. Matozaki, *Small GTP-binding proteins.* Physiol Rev, 2001. **81**(1): p. 153-208.
13. Pai, E.F., et al., *Structure of the guanine-nucleotide-binding domain of the Ha-ras oncogene product p21 in the triphosphate conformation.* Nature, 1989. **341**(6239): p. 209-14.
14. Pai, E.F., et al., *Refined crystal structure of the triphosphate conformation of H-ras p21 at 1.35 A resolution: implications for the mechanism of GTP hydrolysis.* EMBO J, 1990. **9**(8): p. 2351-9.
15. Milburn, M.V., et al., *Molecular switch for signal transduction: structural differences between active and inactive forms of protooncogenic ras proteins.* Science, 1990. **247**(4945): p. 939-45.
16. Karnoub, A.E. and R.A. Weinberg, *Ras oncogenes: split personalities.* Nat Rev Mol Cell Biol, 2008. **9**(7): p. 517-31.
17. Heasman, S.J. and A.J. Ridley, *Mammalian Rho GTPases: new insights into their functions from in vivo studies.* Nat Rev Mol Cell Biol, 2008. **9**(9): p. 690-701.
18. Zerial, M. and H. McBride, *Rab proteins as membrane organizers.* Nat Rev Mol Cell Biol, 2001. **2**(2): p. 107-17.
19. Wennerberg, K., K.L. Rossman, and C.J. Der, *The Ras superfamily at a glance.* J Cell Sci, 2005. **118**(Pt 5): p. 843-6.
20. Cox, A.D. and C.J. Der, *Ras history: The saga continues.* Small GTPases, 2010. **1**(1): p. 2-27.

21. Olivier, J.P., et al., *A Drosophila SH2-SH3 adaptor protein implicated in coupling the sevenless tyrosine kinase to an activator of Ras guanine nucleotide exchange, Sos.* Cell, 1993. **73**(1): p. 179-91.
22. Simon, M.A., G.S. Dodson, and G.M. Rubin, *An SH3-SH2-SH3 protein is required for p21Ras1 activation and binds to sevenless and Sos proteins in vitro.* Cell, 1993. **73**(1): p. 169-77.
23. Egan, S.E., et al., *Association of Sos Ras exchange protein with Grb2 is implicated in tyrosine kinase signal transduction and transformation.* Nature, 1993. **363**(6424): p. 45-51.
24. Gale, N.W., et al., *Grb2 mediates the EGF-dependent activation of guanine nucleotide exchange on Ras.* Nature, 1993. **363**(6424): p. 88-92.
25. Li, N., et al., *Guanine-nucleotide-releasing factor hSos1 binds to Grb2 and links receptor tyrosine kinases to Ras signalling.* Nature, 1993. **363**(6424): p. 85-8.
26. Buday, L. and J. Downward, *Epidermal growth factor regulates p21ras through the formation of a complex of receptor, Grb2 adapter protein, and Sos nucleotide exchange factor.* Cell, 1993. **73**(3): p. 611-20.
27. Chardin, P., et al., *Human Sos1: a guanine nucleotide exchange factor for Ras that binds to GRB2.* Science, 1993. **260**(5112): p. 1338-43.
28. Rozakis-Adcock, M., et al., *The SH2 and SH3 domains of mammalian Grb2 couple the EGF receptor to the Ras activator mSos1.* Nature, 1993. **363**(6424): p. 83-5.
29. Gallego, C., et al., *Mitogen-activated protein kinase activation resulting from selective oncogene expression in NIH 3T3 and rat 1a cells.* Proc Natl Acad Sci U S A, 1992. **89**(16): p. 7355-9.
30. Dent, P., et al., *Activation of mitogen-activated protein kinase kinase by v-Raf in NIH 3T3 cells and in vitro.* Science, 1992. **257**(5075): p. 1404-7.
31. Kyriakis, J.M., et al., *Raf-1 activates MAP kinase-kinase.* Nature, 1992. **358**(6385): p. 417-21.
32. Howe, L.R., et al., *Activation of the MAP kinase pathway by the protein kinase raf.* Cell, 1992. **71**(2): p. 335-42.
33. Harden, T.K. and J. Sondek, *Regulation of phospholipase C isozymes by ras superfamily GTPases.* Annu Rev Pharmacol Toxicol, 2006. **46**: p. 355-79.
34. Repasky, G.A., E.J. Chenette, and C.J. Der, *Renewing the conspiracy theory debate: does Raf function alone to mediate Ras oncogenesis?* Trends Cell Biol, 2004. **14**(11): p. 639-47.
35. Trahey, M. and F. McCormick, *A cytoplasmic protein stimulates normal N-ras p21 GTPase, but does not affect oncogenic mutants.* Science, 1987. **238**(4826): p. 542-5.
36. Oceguera-Yanez, F., et al., *Ect2 and MgcRacGAP regulate the activation and function of Cdc42 in mitosis.* J Cell Biol, 2005. **168**(2): p. 221-32.
37. Hirose, K., et al., *MgcRacGAP is involved in cytokinesis through associating with mitotic spindle and midbody.* J Biol Chem, 2001. **276**(8): p. 5821-8.
38. Seguin, L., et al., *CUX1 and E2F1 regulate coordinated expression of the mitotic complex genes Ect2, MgcRacGAP, and MKLP1 in S phase.* Mol Cell Biol, 2009. **29**(2): p. 570-81.
39. Su, L., J.M. Agati, and S.J. Parsons, *p190RhoGAP is cell cycle regulated and affects cytokinesis.* J Cell Biol, 2003. **163**(3): p. 571-82.
40. Matthews, H.K., et al., *Changes in Ect2 localization couple actomyosin-dependent cell shape changes to mitotic progression.* Dev Cell, 2012. **23**(2): p. 371-83.

41. Mali, P., D. Wirtz, and P.C. Searson, *Interplay of RhoA and motility in the programmed spreading of daughter cells postmitosis.* Biophys J, 2010. **99**(11): p. 3526-34.
42. Maddox, A.S. and K. Burridge, *RhoA is required for cortical retraction and rigidity during mitotic cell rounding.* J Cell Biol, 2003. **160**(2): p. 255-65.
43. Rodriguez-Fraticelli, A.E., et al., *The Cdc42 GEF Intersectin 2 controls mitotic spindle orientation to form the lumen during epithelial morphogenesis.* J Cell Biol, 2010. **189**(4): p. 725-38.
44. Kodani, A., et al., *GM130-dependent control of Cdc42 activity at the Golgi regulates centrosome organization.* Mol Biol Cell, 2009. **20**(4): p. 1192-200.
45. Kamijo, K., et al., *Dissecting the role of Rho-mediated signaling in contractile ring formation.* Mol Biol Cell, 2006. **17**(1): p. 43-55.
46. Drechsel, D.N., et al., *A requirement for Rho and Cdc42 during cytokinesis in Xenopus embryos.* Curr Biol, 1997. **7**(1): p. 12-23.
47. Jantsch-Plunger, V., et al., *CYK-4: A Rho family gtpase activating protein (GAP) required for central spindle formation and cytokinesis.* J Cell Biol, 2000. **149**(7): p. 1391-404.
48. Kishi, K., et al., *Regulation of cytoplasmic division of Xenopus embryo by rho p21 and its inhibitory GDP/GTP exchange protein (rho GDI).* J Cell Biol, 1993. **120**(5): p. 1187-95.
49. Piekny, A., M. Werner, and M. Glotzer, *Cytokinesis: welcome to the Rho zone.* Trends Cell Biol, 2005. **15**(12): p. 651-8.
50. Yuce, O., A. Piekny, and M. Glotzer, *An ECT2-centralspindlin complex regulates the localization and function of RhoA.* J Cell Biol, 2005. **170**(4): p. 571-82.
51. Bement, W.M., H.A. Benink, and G. von Dassow, *A microtubule-dependent zone of active RhoA during cleavage plane specification.* J Cell Biol, 2005. **170**(1): p. 91-101.
52. Yonemura, S., K. Hirao-Minakuchi, and Y. Nishimura, *Rho localization in cells and tissues.* Exp Cell Res, 2004. **295**(2): p. 300-14.
53. Yoshizaki, H., et al., *Activity of Rho-family GTPases during cell division as visualized with FRET-based probes.* J Cell Biol, 2003. **162**(2): p. 223-32.
54. Donaldson, J.G. and C.L. Jackson, *ARF family G proteins and their regulators: roles in membrane transport, development and disease.* Nat Rev Mol Cell Biol, 2011. **12**(6): p. 362-75.
55. Suzuki, T., et al., *Crucial role of the small GTPase ARF6 in hepatic cord formation during liver development.* Mol Cell Biol, 2006. **26**(16): p. 6149-56.
56. D'Souza-Schorey, C. and P. Chavrier, *ARF proteins: roles in membrane traffic and beyond.* Nat Rev Mol Cell Biol, 2006. **7**(5): p. 347-58.
57. Grant, B.D. and J.G. Donaldson, *Pathways and mechanisms of endocytic recycling.* Nat Rev Mol Cell Biol, 2009. **10**(9): p. 597-608.
58. Montagnac, G., et al., *Decoupling of activation and effector binding underlies ARF6 priming of fast endocytic recycling.* Curr Biol, 2011. **21**(7): p. 574-9.
59. Osmani, N., et al., *Cdc42 localization and cell polarity depend on membrane traffic.* J Cell Biol, 2010. **191**(7): p. 1261-9.
60. Ikenouchi, J. and M. Umeda, *FRMD4A regulates epithelial polarity by connecting Arf6 activation with the PAR complex.* Proc Natl Acad Sci U S A, 2010. **107**(2): p. 748-53.

61. Hiroi, T., et al., *GEP100/BRAG2: activator of ADP-ribosylation factor 6 for regulation of cell adhesion and actin cytoskeleton via E-cadherin and alpha-catenin.* Proc Natl Acad Sci U S A, 2006. **103**(28): p. 10672-7.
62. Haas, A.K., et al., *Analysis of GTPase-activating proteins: Rab1 and Rab43 are key Rabs required to maintain a functional Golgi complex in human cells.* J Cell Sci, 2007. **120**(Pt 17): p. 2997-3010.
63. Koo, T.H., B.A. Eipper, and J.G. Donaldson, *Arf6 recruits the Rac GEF Kalirin to the plasma membrane facilitating Rac activation.* BMC Cell Biol, 2007. **8**: p. 29.
64. Gorlich, D. and U. Kutay, *Transport between the cell nucleus and the cytoplasm.* Annu Rev Cell Dev Biol, 1999. **15**: p. 607-60.
65. Stewart, M., *Molecular mechanism of the nuclear protein import cycle.* Nat Rev Mol Cell Biol, 2007. **8**(3): p. 195-208.
66. Stewart, M., et al., *Molecular mechanism of translocation through nuclear pore complexes during nuclear protein import.* FEBS Lett, 2001. **498**(2-3): p. 145-9.
67. Andrade, M.A., et al., *Comparison of ARM and HEAT protein repeats.* J Mol Biol, 2001. **309**(1): p. 1-18.
68. Bischoff, F.R. and H. Ponstingl, *Catalysis of guanine nucleotide exchange on Ran by the mitotic regulator RCC1.* Nature, 1991. **354**(6348): p. 80-2.
69. Bischoff, F.R. and H. Ponstingl, *Mitotic regulator protein RCC1 is complexed with a nuclear ras-related polypeptide.* Proc Natl Acad Sci U S A, 1991. **88**(23): p. 10830-4.
70. Klebe, C., et al., *Interaction of the nuclear GTP-binding protein Ran with its regulatory proteins RCC1 and RanGAP1.* Biochemistry, 1995. **34**(2): p. 639-47.
71. Becker, J., et al., *RNA1 encodes a GTPase-activating protein specific for Gsp1p, the Ran/TC4 homologue of Saccharomyces cerevisiae.* J Biol Chem, 1995. **270**(20): p. 11860-5.
72. Bischoff, F.R., et al., *RanGAP1 induces GTPase activity of nuclear Ras-related Ran.* Proc Natl Acad Sci U S A, 1994. **91**(7): p. 2587-91.
73. Ribbeck, K., et al., *NTF2 mediates nuclear import of Ran.* EMBO J, 1998. **17**(22): p. 6587-98.
74. Smith, A., A. Brownawell, and I.G. Macara, *Nuclear import of Ran is mediated by the transport factor NTF2.* Curr Biol, 1998. **8**(25): p. 1403-6.
75. Rexach, M. and G. Blobel, *Protein import into nuclei: association and dissociation reactions involving transport substrate, transport factors, and nucleoporins.* Cell, 1995. **83**(5): p. 683-92.
76. Gorlich, D., et al., *Identification of different roles for RanGDP and RanGTP in nuclear protein import.* EMBO J, 1996. **15**(20): p. 5584-94.
77. Izaurralde, E., et al., *The asymmetric distribution of the constituents of the Ran system is essential for transport into and out of the nucleus.* EMBO J, 1997. **16**(21): p. 6535-47.
78. Moore, J.D., *The Ran-GTPase and cell-cycle control.* Bioessays, 2001. **23**(1): p. 77-85.
79. Sazer, S. and M. Dasso, *The ran decathlon: multiple roles of Ran.* J Cell Sci, 2000. **113 (Pt 7)**: p. 1111-8.
80. Gruss, O.J., et al., *Ran induces spindle assembly by reversing the inhibitory effect of importin alpha on TPX2 activity.* Cell, 2001. **104**(1): p. 83-93.
81. Nachury, M.V., et al., *Importin beta is a mitotic target of the small GTPase Ran in spindle assembly.* Cell, 2001. **104**(1): p. 95-106.

82. Wiese, C., et al., *Role of importin-beta in coupling Ran to downstream targets in microtubule assembly.* Science, 2001. **291**(5504): p. 653-6.
83. Pfeffer, S., *A model for Rab GTPase localization.* Biochem Soc Trans, 2005. **33**(Pt 4): p. 627-30.
84. Grosshans, B.L., D. Ortiz, and P. Novick, *Rabs and their effectors: achieving specificity in membrane traffic.* Proc Natl Acad Sci U S A, 2006. **103**(32): p. 11821-7.
85. Wandinger-Ness, A. and M. Zerial, *Rab proteins and the compartmentalization of the endosomal system.* Cold Spring Harb Perspect Biol, 2014. **6**(11): p. a022616.
86. Leung, K.F., R. Baron, and M.C. Seabra, *Thematic review series: lipid posttranslational modifications. geranylgeranylation of Rab GTPases.* J Lipid Res, 2006. **47**(3): p. 467-75.
87. Goody, R.S., A. Rak, and K. Alexandrov, *The structural and mechanistic basis for recycling of Rab proteins between membrane compartments.* Cell Mol Life Sci, 2005. **62**(15): p. 1657-70.
88. Pfeffer, S. and D. Aivazian, *Targeting Rab GTPases to distinct membrane compartments.* Nat Rev Mol Cell Biol, 2004. **5**(11): p. 886-96.
89. Segev, N., *Ypt and Rab GTPases: insight into functions through novel interactions.* Curr Opin Cell Biol, 2001. **13**(4): p. 500-11.
90. Mott, H.R. and D. Owen, *Structures of Ras superfamily effector complexes: What have we learnt in two decades?* Crit Rev Biochem Mol Biol, 2015. **50**(2): p. 85-133.
91. Pereira-Leal, J.B. and M.C. Seabra, *The mammalian Rab family of small GTPases: definition of family and subfamily sequence motifs suggests a mechanism for functional specificity in the Ras superfamily.* J Mol Biol, 2000. **301**(4): p. 1077-87.
92. Hutagalung, A.H. and P.J. Novick, *Role of Rab GTPases in membrane traffic and cell physiology.* Physiol Rev, 2011. **91**(1): p. 119-49.
93. Rink, J., et al., *Rab conversion as a mechanism of progression from early to late endosomes.* Cell, 2005. **122**(5): p. 735-49.
94. Maxfield, F.R. and T.E. McGraw, *Endocytic recycling.* Nat Rev Mol Cell Biol, 2004. **5**(2): p. 121-32.
95. Gallon, M. and P.J. Cullen, *Retromer and sorting nexins in endosomal sorting.* Biochem Soc Trans, 2015. **43**(1): p. 33-47.
96. Dennis, M.K., et al., *BLOC-1 and BLOC-3 regulate VAMP7 cycling to and from melanosomes via distinct tubular transport carriers.* J Cell Biol, 2016. **214**(3): p. 293-308.
97. Dennis, M.K., et al., *BLOC-2 targets recycling endosomal tubules to melanosomes for cargo delivery.* J Cell Biol, 2015. **209**(4): p. 563-77.
98. Wang, J., et al., *The Arf GAP ASAP1 provides a platform to regulate Arf4- and Rab11-Rab8-mediated ciliary receptor targeting.* EMBO J, 2012. **31**(20): p. 4057-71.
99. Ward, H.H., et al., *A conserved signal and GTPase complex are required for the ciliary transport of polycystin-1.* Mol Biol Cell, 2011. **22**(18): p. 3289-305.
100. Nielsen, E., et al., *Rab5 regulates motility of early endosomes on microtubules.* Nat Cell Biol, 1999. **1**(6): p. 376-82.
101. Bananis, E., et al., *Microtubule-dependent movement of late endocytic vesicles in vitro: requirements for Dynein and Kinesin.* Mol Biol Cell, 2004. **15**(8): p. 3688-97.

102. Barbero, P., L. Bittova, and S.R. Pfeffer, *Visualization of Rab9-mediated vesicle transport from endosomes to the trans-Golgi in living cells.* J Cell Biol, 2002. **156**(3): p. 511-8.
103. Cantalupo, G., et al., *Rab-interacting lysosomal protein (RILP): the Rab7 effector required for transport to lysosomes.* EMBO J, 2001. **20**(4): p. 683-93.
104. Johansson, M., et al., *Activation of endosomal dynein motors by stepwise assembly of Rab7-RILP-p150Glued, ORP1L, and the receptor betalll spectrin.* J Cell Biol, 2007. **176**(4): p. 459-71.
105. Jordens, I., et al., *The Rab7 effector protein RILP controls lysosomal transport by inducing the recruitment of dynein-dynactin motors.* Curr Biol, 2001. **11**(21): p. 1680-5.
106. Agola, J.O., et al., *Rab GTPases as regulators of endocytosis, targets of disease and therapeutic opportunities.* Clin Genet, 2011. **80**(4): p. 305-18.
107. Lapierre, L.A., et al., *Myosin vb is associated with plasma membrane recycling systems.* Mol Biol Cell, 2001. **12**(6): p. 1843-57.
108. Lindsay, A.J., et al., *Identification and characterization of multiple novel Rab-myosin Va interactions.* Mol Biol Cell, 2013. **24**(21): p. 3420-34.
109. Gautreau, A., K. Oguievetskaia, and C. Ungermann, *Function and regulation of the endosomal fusion and fission machineries.* Cold Spring Harb Perspect Biol, 2014. **6**(3).
110. Solinger, J.A. and A. Spang, *Tethering complexes in the endocytic pathway: CORVET and HOPS.* FEBS J, 2013. **280**(12): p. 2743-57.
111. Weber, T., et al., *SNAREpins: minimal machinery for membrane fusion.* Cell, 1998. **92**(6): p. 759-72.
112. McNew, J.A., et al., *Close is not enough: SNARE-dependent membrane fusion requires an active mechanism that transduces force to membrane anchors.* J Cell Biol, 2000. **150**(1): p. 105-17.
113. Jahn, R. and R.H. Scheller, *SNAREs--engines for membrane fusion.* Nat Rev Mol Cell Biol, 2006. **7**(9): p. 631-43.
114. Zimmerberg, J. and K. Gawrisch, *The physical chemistry of biological membranes.* Nat Chem Biol, 2006. **2**(11): p. 564-7.
115. Wickner, W. and R. Schekman, *Membrane fusion.* Nat Struct Mol Biol, 2008. **15**(7): p. 658-64.
116. Nielsen, E., et al., *Rabenosyn-5, a novel Rab5 effector, is complexed with hVPS45 and recruited to endosomes through a FYVE finger domain.* J Cell Biol, 2000. **151**(3): p. 601-12.
117. Carr, C.M. and J. Rizo, *At the junction of SNARE and SM protein function.* Curr Opin Cell Biol, 2010. **22**(4): p. 488-95.
118. Rizo, J. and T.C. Sudhof, *The membrane fusion enigma: SNAREs, Sec1/Munc18 proteins, and their accomplices--guilty as charged?* Annu Rev Cell Dev Biol, 2012. **28**: p. 279-308.
119. Gonzalez-Gaitan, M., *Signal dispersal and transduction through the endocytic pathway.* Nat Rev Mol Cell Biol, 2003. **4**(3): p. 213-24.
120. Piddini, E. and J.P. Vincent, *Modulation of developmental signals by endocytosis: different means and many ends.* Curr Opin Cell Biol, 2003. **15**(4): p. 474-81.
121. Duran, R.V. and M.N. Hall, *Regulation of TOR by small GTPases.* EMBO Rep, 2012. **13**(2): p. 121-8.
122. Sturgill, T.W., et al., *TOR1 and TOR2 have distinct locations in live cells.* Eukaryot Cell, 2008. **7**(10): p. 1819-30.

123. Berchtold, D. and T.C. Walther, *TORC2 plasma membrane localization is essential for cell viability and restricted to a distinct domain.* Mol Biol Cell, 2009. **20**(5): p. 1565-75.
124. Yonehara, R., et al., *Structural basis for the assembly of the Ragulator-Rag GTPase complex.* Nat Commun, 2017. **8**(1): p. 1625.
125. Li, L., et al., *Regulation of mTORC1 by the Rab and Arf GTPases.* J Biol Chem, 2010. **285**(26): p. 19705-9.
126. Flinn, R.J., et al., *The late endosome is essential for mTORC1 signaling.* Mol Biol Cell, 2010. **21**(5): p. 833-41.
127. Rojas, A.M., et al., *The Ras protein superfamily: evolutionary tree and role of conserved amino acids.* J Cell Biol, 2012. **196**(2): p. 189-201.
128. Kondrashov, F.A., et al., *Selection in the evolution of gene duplications.* Genome Biol, 2002. **3**(2): p. RESEARCH0008.
129. Erdman, R.A., et al., *Rab24 is an atypical member of the Rab GTPase family. Deficient GTPase activity, GDP dissociation inhibitor interaction, and prenylation of Rab24 expressed in cultured cells.* J Biol Chem, 2000. **275**(6): p. 3848-56.
130. Valencia, A., et al., *GTPase domains of ras p21 oncogene protein and elongation factor Tu: analysis of three-dimensional structures, sequence families, and functional sites.* Proc Natl Acad Sci U S A, 1991. **88**(12): p. 5443-7.
131. Lazar, T., M. Gotte, and D. Gallwitz, *Vesicular transport: how many Ypt/Rab-GTPases make a eukaryotic cell?* Trends Biochem Sci, 1997. **22**(12): p. 468-72.
132. Vetter, I.R. and A. Wittinghofer, *The guanine nucleotide-binding switch in three dimensions.* Science, 2001. **294**(5545): p. 1299-304.
133. Cherfils, J. and M. Zeghouf, *Regulation of small GTPases by GEFs, GAPs, and GDIs.* Physiol Rev, 2013. **93**(1): p. 269-309.
134. Kamerlin, S.C., et al., *Why nature really chose phosphate.* Q Rev Biophys, 2013. **46**(1): p. 1-132.
135. Duarte, F., et al., *Resolving apparent conflicts between theoretical and experimental models of phosphate monoester hydrolysis.* J Am Chem Soc, 2015. **137**(3): p. 1081-93.
136. Lassila, J.K., J.G. Zalatan, and D. Herschlag, *Biological phosphoryl-transfer reactions: understanding mechanism and catalysis.* Annu Rev Biochem, 2011. **80**: p. 669-702.
137. Scheffzek, K., et al., *The Ras-RasGAP complex: structural basis for GTPase activation and its loss in oncogenic Ras mutants.* Science, 1997. **277**(5324): p. 333-8.
138. Klahn, M., E. Rosta, and A. Warshel, *On the mechanism of hydrolysis of phosphate monoesters dianions in solutions and proteins.* J Am Chem Soc, 2006. **128**(47): p. 15310-23.
139. Langen, R., T. Schweins, and A. Warshel, *On the mechanism of guanosine triphosphate hydrolysis in ras p21 proteins.* Biochemistry, 1992. **31**(37): p. 8691-6.
140. Schweins, T., et al., *Substrate-assisted catalysis as a mechanism for GTP hydrolysis of p21ras and other GTP-binding proteins.* Nat Struct Biol, 1995. **2**(1): p. 36-44.
141. Martin-Garcia, F., et al., *The Role of Gln61 in HRas GTP hydrolysis: a quantum mechanics/molecular mechanics study.* Biophys J, 2012. **102**(1): p. 152-7.

142. Brunger, A.T., et al., *Crystal structure of an active form of RAS protein, a complex of a GTP analog and the HRAS p21 catalytic domain.* Proc Natl Acad Sci U S A, 1990. **87**(12): p. 4849-53.
143. Gideon, P., et al., *Mutational and kinetic analyses of the GTPase-activating protein (GAP)-p21 interaction: the C-terminal domain of GAP is not sufficient for full activity.* Mol Cell Biol, 1992. **12**(5): p. 2050-6.
144. Adamczyk, A.J. and A. Warshel, *Converting structural information into an allosteric-energy-based picture for elongation factor Tu activation by the ribosome.* Proc Natl Acad Sci U S A, 2011. **108**(24): p. 9827-32.
145. Schweins, T., R. Langen, and A. Warshel, *Why have mutagenesis studies not located the general base in ras p21.* Nat Struct Biol, 1994. **1**(7): p. 476-84.
146. Zor, T., et al., *Rescue of a mutant G-protein by substrate-assisted catalysis.* Eur J Biochem, 1997. **249**(1): p. 330-6.
147. Topol, I.A., et al., *Quantum chemical modeling of the GTP hydrolysis by the RAS-GAP protein complex.* Biochim Biophys Acta, 2004. **1700**(1): p. 125-36.
148. Grigorenko, B.L., et al., *QM/MM modeling the Ras-GAP catalyzed hydrolysis of guanosine triphosphate.* Proteins, 2005. **60**(3): p. 495-503.
149. Khrenova, M.G., et al., *Modeling the role of G12V and G13V Ras mutations in the Ras-GAP-catalyzed hydrolysis reaction of guanosine triphosphate.* Biochemistry, 2014. **53**(45): p. 7093-9.
150. Shurki, A. and A. Warshel, *Why does the Ras switch "break" by oncogenic mutations?* Proteins, 2004. **55**(1): p. 1-10.
151. Glennon, T.M., J. Villa, and A. Warshel, *How does GAP catalyze the GTPase reaction of Ras? A computer simulation study.* Biochemistry, 2000. **39**(32): p. 9641-51.
152. Buss, J.E. and B.M. Sefton, *Direct identification of palmitic acid as the lipid attached to p21ras.* Mol Cell Biol, 1986. **6**(1): p. 116-22.
153. Rocks, O., et al., *An acylation cycle regulates localization and activity of palmitoylated Ras isoforms.* Science, 2005. **307**(5716): p. 1746-52.
154. Antonny, B., et al., *N-terminal hydrophobic residues of the G-protein ADP-ribosylation factor-1 insert into membrane phospholipids upon GDP to GTP exchange.* Biochemistry, 1997. **36**(15): p. 4675-84.
155. Liu, Y., R.A. Kahn, and J.H. Prestegard, *Structure and membrane interaction of myristoylated ARF1.* Structure, 2009. **17**(1): p. 79-87.
156. Liu, Y., R.A. Kahn, and J.H. Prestegard, *Dynamic structure of membrane-anchored Arf*GTP.* Nat Struct Mol Biol, 2010. **17**(7): p. 876-81.
157. Hillig, R.C., et al., *Structural and biochemical properties show ARL3-GDP as a distinct GTP binding protein.* Structure, 2000. **8**(12): p. 1239-45.
158. Pasqualato, S., et al., *The structural GDP/GTP cycle of human Arf6.* EMBO Rep, 2001. **2**(3): p. 234-8.
159. Pasqualato, S., L. Renault, and J. Cherfils, *Arf, Arl, Arp and Sar proteins: a family of GTP-binding proteins with a structural device for 'front-back' communication.* EMBO Rep, 2002. **3**(11): p. 1035-41.
160. Leung, K.F., et al., *Rab GTPases containing a CAAX motif are processed post-geranylgeranylation by proteolysis and methylation.* J Biol Chem, 2007. **282**(2): p. 1487-97.
161. Andres, D.A., et al., *cDNA cloning of component A of Rab geranylgeranyl transferase and demonstration of its role as a Rab escort protein.* Cell, 1993. **73**(6): p. 1091-9.

162. Guo, Z., et al., *Structures of RabGGTase-substrate/product complexes provide insights into the evolution of protein prenylation.* EMBO J, 2008. **27**(18): p. 2444-56.
163. Rak, A., et al., *Structure of the Rab7:REP-1 complex: insights into the mechanism of Rab prenylation and choroideremia disease.* Cell, 2004. **117**(6): p. 749-60.
164. Pylypenko, O., et al., *Structure of Rab escort protein-1 in complex with Rab geranylgeranyltransferase.* Mol Cell, 2003. **11**(2): p. 483-94.
165. Wu, Y.W., et al., *Structure of the disordered C terminus of Rab7 GTPase induced by binding to the Rab geranylgeranyl transferase catalytic complex reveals the mechanism of Rab prenylation.* J Biol Chem, 2009. **284**(19): p. 13185-92.
166. Larijani, B., et al., *Multiple factors contribute to inefficient prenylation of Rab27a in Rab prenylation diseases.* J Biol Chem, 2003. **278**(47): p. 46798-804.
167. Pylypenko, O., et al., *Structure of doubly prenylated Ypt1:GDI complex and the mechanism of GDI-mediated Rab recycling.* EMBO J, 2006. **25**(1): p. 13-23.
168. Wu, Y.W., et al., *Interaction analysis of prenylated Rab GTPase with Rab escort protein and GDP dissociation inhibitor explains the need for both regulators.* Proc Natl Acad Sci U S A, 2007. **104**(30): p. 12294-9.
169. Muller, M.P. and R.S. Goody, *Molecular control of Rab activity by GEFs, GAPs and GDI.* Small GTPases, 2017: p. 1-17.
170. Ali, B.R., et al., *Multiple regions contribute to membrane targeting of Rab GTPases.* J Cell Sci, 2004. **117**(Pt 26): p. 6401-12.
171. Li, F., et al., *The role of the hypervariable C-terminal domain in Rab GTPases membrane targeting.* Proc Natl Acad Sci U S A, 2014. **111**(7): p. 2572-7.
172. Wu, Y.W., et al., *Membrane targeting mechanism of Rab GTPases elucidated by semisynthetic protein probes.* Nat Chem Biol, 2010. **6**(7): p. 534-40.
173. Gerondopoulos, A., et al., *BLOC-3 mutated in Hermansky-Pudlak syndrome is a Rab32/38 guanine nucleotide exchange factor.* Curr Biol, 2012. **22**(22): p. 2135-9.
174. Blumer, J., et al., *RabGEFs are a major determinant for specific Rab membrane targeting.* J Cell Biol, 2013. **200**(3): p. 287-300.
175. Carney, D.S., B.A. Davies, and B.F. Horazdovsky, *Vps9 domain-containing proteins: activators of Rab5 GTPases from yeast to neurons.* Trends Cell Biol, 2006. **16**(1): p. 27-35.
176. Burd, C.G., et al., *A yeast protein related to a mammalian Ras-binding protein, Vps9p, is required for localization of vacuolar proteins.* Mol Cell Biol, 1996. **16**(5): p. 2369-77.
177. Horiuchi, H., et al., *A novel Rab5 GDP/GTP exchange factor complexed to Rabaptin-5 links nucleotide exchange to effector recruitment and function.* Cell, 1997. **90**(6): p. 1149-59.
178. Marat, A.L., H. Dokainish, and P.S. McPherson, *DENN domain proteins: regulators of Rab GTPases.* J Biol Chem, 2011. **286**(16): p. 13791-800.
179. Koch, D., et al., *A pull-down procedure for the identification of unknown GEFs for small GTPases.* Small GTPases, 2016. **7**(2): p. 93-106.

180. Lippe, R., et al., *Functional synergy between Rab5 effector Rabaptin-5 and exchange factor Rabex-5 when physically associated in a complex.* Mol Biol Cell, 2001. **12**(7): p. 2219-28.
181. Nottingham, R.M. and S.R. Pfeffer, *Defining the boundaries: Rab GEFs and GAPs.* Proc Natl Acad Sci U S A, 2009. **106**(34): p. 14185-6.
182. Dong, G., et al., *A catalytic coiled coil: structural insights into the activation of the Rab GTPase Sec4p by Sec2p.* Mol Cell, 2007. **25**(3): p. 455-62.
183. Delprato, A. and D.G. Lambright, *Structural basis for Rab GTPase activation by VPS9 domain exchange factors.* Nat Struct Mol Biol, 2007. **14**(5): p. 406-12.
184. Langemeyer, L., et al., *Diversity and plasticity in Rab GTPase nucleotide release mechanism has consequences for Rab activation and inactivation.* Elife, 2014. **3**: p. e01623.
185. Cai, Y., et al., *The structural basis for activation of the Rab Ypt1p by the TRAPP membrane-tethering complexes.* Cell, 2008. **133**(7): p. 1202-13.
186. Esters, H., et al., *High-resolution crystal structure of S. cerevisiae Ypt51(DeltaC15)-GppNHp, a small GTP-binding protein involved in regulation of endocytosis.* J Mol Biol, 2000. **298**(1): p. 111-21.
187. Huber, S.K. and A.J. Scheidig, *High resolution crystal structures of human Rab4a in its active and inactive conformations.* FEBS Lett, 2005. **579**(13): p. 2821-9.
188. Rensland, H., et al., *Substrate and product structural requirements for binding of nucleotides to H-ras p21: the mechanism of discrimination between guanosine and adenosine nucleotides.* Biochemistry, 1995. **34**(2): p. 593-9.
189. Fukuda, M., *TBC proteins: GAPs for mammalian small GTPase Rab?* Biosci Rep, 2011. **31**(3): p. 159-68.
190. Nagano, F., et al., *Molecular cloning and characterization of the noncatalytic subunit of the Rab3 subfamily-specific GTPase-activating protein.* J Biol Chem, 1998. **273**(38): p. 24781-5.
191. Rivera-Molina, F.E. and P.J. Novick, *A Rab GAP cascade defines the boundary between two Rab GTPases on the secretory pathway.* Proc Natl Acad Sci U S A, 2009. **106**(34): p. 14408-13.
192. Suda, Y., et al., *Rab GAP cascade regulates dynamics of Ypt6 in the Golgi traffic.* Proc Natl Acad Sci U S A, 2013. **110**(47): p. 18976-81.
193. Pan, X., et al., *TBC-domain GAPs for Rab GTPases accelerate GTP hydrolysis by a dual-finger mechanism.* Nature, 2006. **442**(7100): p. 303-6.
194. Mihai Gazdag, E., et al., *Mechanism of Rab1b deactivation by the Legionella pneumophila GAP LepB.* EMBO Rep, 2013. **14**(2): p. 199-205.
195. Dirac-Svejstrup, A.B., T. Sumizawa, and S.R. Pfeffer, *Identification of a GDI displacement factor that releases endosomal Rab GTPases from Rab-GDI.* EMBO J, 1997. **16**(3): p. 465-72.
196. Khan, A.R. and J. Menetrey, *Structural biology of Arf and Rab GTPases' effector recruitment and specificity.* Structure, 2013. **21**(8): p. 1284-97.
197. Lucas, M., et al., *Structural basis for the recruitment and activation of the Legionella phospholipase VipD by the host GTPase Rab5.* Proc Natl Acad Sci U S A, 2014. **111**(34): p. E3514-23.
198. Zhu, G., et al., *Structural basis of Rab5-Rabaptin5 interaction in endocytosis.* Nat Struct Mol Biol, 2004. **11**(10): p. 975-83.

199. Eathiraj, S., et al., *Structural basis of family-wide Rab GTPase recognition by rabenosyn-5.* Nature, 2005. **436**(7049): p. 415-9.
200. Mishra, A., et al., *Structural basis for Rab GTPase recognition and endosome tethering by the C2H2 zinc finger of Early Endosomal Autoantigen 1 (EEA1).* Proc Natl Acad Sci U S A, 2010. **107**(24): p. 10866-71.
201. Merithew, E., et al., *Structural plasticity of an invariant hydrophobic triad in the switch regions of Rab GTPases is a determinant of effector recognition.* J Biol Chem, 2001. **276**(17): p. 13982-8.
202. Shiba, T., et al., *Structural basis for Rab11-dependent membrane recruitment of a family of Rab11-interacting protein 3 (FIP3)/Arfophilin-1.* Proc Natl Acad Sci U S A, 2006. **103**(42): p. 15416-21.
203. Eathiraj, S., et al., *Structural basis for Rab11-mediated recruitment of FIP3 to recycling endosomes.* J Mol Biol, 2006. **364**(2): p. 121-35.
204. Jagoe, W.N., et al., *Crystal structure of rab11 in complex with rab11 family interacting protein 2.* Structure, 2006. **14**(8): p. 1273-83.
205. Pylypenko, O., et al., *Structural basis of myosin V Rab GTPase-dependent cargo recognition.* Proc Natl Acad Sci U S A, 2013. **110**(51): p. 20443-8.
206. Pylypenko, O., et al., *Coordinated recruitment of Spir actin nucleators and myosin V motors to Rab11 vesicle membranes.* Elife, 2016. **5**.
207. Pylypenko, O., et al., *Rab GTPases and their interacting protein partners: Structural insights into Rab functional diversity.* Small GTPases, 2017: p. 1-27.
208. Vetter, M., et al., *Structure of Rab11-FIP3-Rabin8 reveals simultaneous binding of FIP3 and Rabin8 effectors to Rab11.* Nat Struct Mol Biol, 2015. **22**(9): p. 695-702.
209. Burke, J.E., et al., *Structures of PI4KIIIbeta complexes show simultaneous recruitment of Rab11 and its effectors.* Science, 2014. **344**(6187): p. 1035-8.
210. de Graaf, P., et al., *Phosphatidylinositol 4-kinasebeta is critical for functional association of rab11 with the Golgi complex.* Mol Biol Cell, 2004. **15**(4): p. 2038-47.
211. Wilson, G.M., et al., *The FIP3-Rab11 protein complex regulates recycling endosome targeting to the cleavage furrow during late cytokinesis.* Mol Biol Cell, 2005. **16**(2): p. 849-60.
212. Sechi, S., et al., *GOLPH3 is essential for contractile ring formation and Rab11 localization to the cleavage site during cytokinesis in Drosophila melanogaster.* PLoS Genet, 2014. **10**(5): p. e1004305.
213. Morrow, A.A., et al., *The lipid kinase PI4KIIIbeta is highly expressed in breast tumors and activates Akt in cooperation with Rab11a.* Mol Cancer Res, 2014. **12**(10): p. 1492-508.
214. Knodler, A., et al., *Coordination of Rab8 and Rab11 in primary ciliogenesis.* Proc Natl Acad Sci U S A, 2010. **107**(14): p. 6346-51.
215. Wang, J. and D. Deretic, *The Arf and Rab11 effector FIP3 acts synergistically with ASAP1 to direct Rabin8 in ciliary receptor targeting.* J Cell Sci, 2015. **128**(7): p. 1375-85.
216. Hyvola, N., et al., *Membrane targeting and activation of the Lowe syndrome protein OCRL1 by rab GTPases.* EMBO J, 2006. **25**(16): p. 3750-61.

217. Dambournet, D., et al., *Rab35 GTPase and OCRL phosphatase remodel lipids and F-actin for successful cytokinesis.* Nat Cell Biol, 2011. **13**(8): p. 981-8.
218. Cauvin, C., et al., *Rab35 GTPase Triggers Switch-like Recruitment of the Lowe Syndrome Lipid Phosphatase OCRL on Newborn Endosomes.* Curr Biol, 2016. **26**(1): p. 120-8.
219. Hou, X., et al., *A structural basis for Lowe syndrome caused by mutations in the Rab-binding domain of OCRL1.* EMBO J, 2011. **30**(8): p. 1659-70.
220. Hagemann, N., et al., *Crystal structure of the Rab binding domain of OCRL1 in complex with Rab8 and functional implications of the OCRL1/Rab8 module for Lowe syndrome.* Small GTPases, 2012. **3**(2): p. 107-10.
221. de Renzis, S., B. Sonnichsen, and M. Zerial, *Divalent Rab effectors regulate the sub-compartmental organization and sorting of early endosomes.* Nat Cell Biol, 2002. **4**(2): p. 124-33.
222. Deneka, M. and P. van der Sluijs, *'Rab'ing up endosomal membrane transport.* Nat Cell Biol, 2002. **4**(2): p. E33-5.
223. Navaroli, D.M., et al., *Rabenosyn-5 defines the fate of the transferrin receptor following clathrin-mediated endocytosis.* Proc Natl Acad Sci U S A, 2012. **109**(8): p. E471-80.
224. Recacha, R., et al., *Structural basis for recruitment of Rab6-interacting protein 1 to Golgi via a RUN domain.* Structure, 2009. **17**(1): p. 21-30.
225. Ostermeier, C. and A.T. Brunger, *Structural basis of Rab effector specificity: crystal structure of the small G protein Rab3A complexed with the effector domain of rabphilin-3A.* Cell, 1999. **96**(3): p. 363-74.
226. Lapierre, L.A., et al., *Rab11b resides in a vesicular compartment distinct from Rab11a in parietal cells and other epithelial cells.* Exp Cell Res, 2003. **290**(2): p. 322-31.
227. Goldenring, J.R., et al., *Rab11 is an apically located small GTP-binding protein in epithelial tissues.* Am J Physiol, 1996. **270**(3 Pt 1): p. G515-25.
228. Goldenring, J.R., et al., *Identification of a small GTP-binding protein, Rab25, expressed in the gastrointestinal mucosa, kidney, and lung.* J Biol Chem, 1993. **268**(25): p. 18419-22.
229. Prekeris, R., J. Klumperman, and R.H. Scheller, *A Rab11/Rip11 protein complex regulates apical membrane trafficking via recycling endosomes.* Mol Cell, 2000. **6**(6): p. 1437-48.
230. Hales, C.M., et al., *Identification and characterization of a family of Rab11-interacting proteins.* J Biol Chem, 2001. **276**(42): p. 39067-75.
231. Lindsay, A.J., et al., *Rab coupling protein (RCP), a novel Rab4 and Rab11 effector protein.* J Biol Chem, 2002. **277**(14): p. 12190-9.
232. Lindsay, A.J. and M.W. McCaffrey, *The C2 domains of the class I Rab11 family of interacting proteins target recycling vesicles to the plasma membrane.* J Cell Sci, 2004. **117**(Pt 19): p. 4365-75.
233. Kelly, E.E., et al., *Class I Rab11-family interacting proteins are binding targets for the Rab14 GTPase.* Biol Cell, 2009. **102**(1): p. 51-62.
234. Junutula, J.R., et al., *Rab14 is involved in membrane trafficking between the Golgi complex and endosomes.* Mol Biol Cell, 2004. **15**(5): p. 2218-29.
235. Fukuda, M., et al., *Large scale screening for novel rab effectors reveals unexpected broad Rab binding specificity.* Mol Cell Proteomics, 2008. **7**(6): p. 1031-42.

236. Hickson, G.R., et al., *Arfophilins are dual Arf/Rab 11 binding proteins that regulate recycling endosome distribution and are related to Drosophila nuclear fallout.* Mol Biol Cell, 2003. **14**(7): p. 2908-20.
237. Ullrich, O., et al., *Rab11 regulates recycling through the pericentriolar recycling endosome.* J Cell Biol, 1996. **135**(4): p. 913-24.
238. Li, J., et al., *Differential regulation of amyloid-beta endocytic trafficking and lysosomal degradation by apolipoprotein E isoforms.* J Biol Chem, 2012. **287**(53): p. 44593-601.
239. Li, X., et al., *Aberrant Rab11-dependent trafficking of the neuronal glutamate transporter EAAC1 causes oxidative stress and cell death in Huntington's disease.* J Neurosci, 2010. **30**(13): p. 4552-61.
240. Li, X., et al., *Deficient Rab11 activity underlies glucose hypometabolism in primary neurons of Huntington's disease mice.* Biochem Biophys Res Commun, 2012. **421**(4): p. 727-30.
241. Bryant, N.J., R. Govers, and D.E. James, *Regulated transport of the glucose transporter GLUT4.* Nat Rev Mol Cell Biol, 2002. **3**(4): p. 267-77.
242. Mosesson, Y., G.B. Mills, and Y. Yarden, *Derailed endocytosis: an emerging feature of cancer.* Nat Rev Cancer, 2008. **8**(11): p. 835-50.
243. Green, E.G., et al., *Rab11 is associated with transferrin-containing recycling compartments in K562 cells.* Biochem Biophys Res Commun, 1997. **239**(2): p. 612-6.
244. Baetz, N.W. and J.R. Goldenring, *Rab11-family interacting proteins define spatially and temporally distinct regions within the dynamic Rab11a-dependent recycling system.* Mol Biol Cell, 2013. **24**(5): p. 643-58.
245. Ducharme, N.A., et al., *Rab11-FIP2 regulates differentiable steps in transcytosis.* Am J Physiol Cell Physiol, 2007. **293**(3): p. C1059-72.
246. Brock, S.C., J.R. Goldenring, and J.E. Crowe, Jr., *Apical recycling systems regulate directional budding of respiratory syncytial virus from polarized epithelial cells.* Proc Natl Acad Sci U S A, 2003. **100**(25): p. 15143-8.
247. Boal, F., et al., *Insulin promotes Rip11 accumulation at the plasma membrane by inhibiting a dynamin- and PI3-kinase-dependent, but Akt-independent, internalisation event.* Cell Signal, 2016. **28**(1): p. 74-82.
248. Muretta, J.M., I. Romenskaia, and C.C. Mastick, *Insulin releases Glut4 from static storage compartments into cycling endosomes and increases the rate constant for Glut4 exocytosis.* J Biol Chem, 2008. **283**(1): p. 311-23.
249. Brewer, P.D., et al., *Insulin-regulated Glut4 translocation: membrane protein trafficking with six distinctive steps.* J Biol Chem, 2014. **289**(25): p. 17280-98.
250. Brewer, P.D., et al., *Loss of AS160 Akt substrate causes Glut4 protein to accumulate in compartments that are primed for fusion in basal adipocytes.* J Biol Chem, 2011. **286**(30): p. 26287-97.
251. Habtemichael, E.N., et al., *Kinetic evidence that Glut4 follows different endocytic pathways than the receptors for transferrin and alpha2-macroglobulin.* J Biol Chem, 2011. **286**(12): p. 10115-25.
252. Brewer, P.D., et al., *Glut4 Is Sorted from a Rab10 GTPase-independent Constitutive Recycling Pathway into a Highly Insulin-responsive Rab10 GTPase-dependent Sequestration Pathway after Adipocyte Differentiation.* J Biol Chem, 2016. **291**(2): p. 773-89.
253. Zeigerer, A., M.K. McBrayer, and T.E. McGraw, *Insulin stimulation of GLUT4 exocytosis, but not its inhibition of endocytosis, is dependent on RabGAP AS160.* Mol Biol Cell, 2004. **15**(10): p. 4406-15.

254. Sano, H., et al., *Rab10, a target of the AS160 Rab GAP, is required for insulin-stimulated translocation of GLUT4 to the adipocyte plasma membrane.* Cell Metab, 2007. **5**(4): p. 293-303.
255. Sano, H., et al., *Rab10 in insulin-stimulated GLUT4 translocation.* Biochem J, 2008. **411**(1): p. 89-95.
256. Chen, Y., et al., *Rab10 and myosin-Va mediate insulin-stimulated GLUT4 storage vesicle translocation in adipocytes.* J Cell Biol, 2012. **198**(4): p. 545-60.
257. Sadacca, L.A., et al., *Specialized sorting of GLUT4 and its recruitment to the cell surface are independently regulated by distinct Rabs.* Mol Biol Cell, 2013. **24**(16): p. 2544-57.
258. Ishikura, S., P.J. Bilan, and A. Klip, *Rabs 8A and 14 are targets of the insulin-regulated Rab-GAP AS160 regulating GLUT4 traffic in muscle cells.* Biochem Biophys Res Commun, 2007. **353**(4): p. 1074-9.
259. Reed, S.E., et al., *A role for Rab14 in the endocytic trafficking of GLUT4 in 3T3-L1 adipocytes.* J Cell Sci, 2013. **126**(Pt 9): p. 1931-41.
260. Brewer, P.D., et al., *Rab14 limits the sorting of Glut4 from endosomes into insulin-sensitive regulated secretory compartments in adipocytes.* Biochem J, 2016. **473**(10): p. 1315-27.
261. Schiel, J.A., C. Childs, and R. Prekeris, *Endocytic transport and cytokinesis: from regulation of the cytoskeleton to midbody inheritance.* Trends Cell Biol, 2013. **23**(7): p. 319-27.
262. Fielding, A.B., et al., *Rab11-FIP3 and FIP4 interact with Arf6 and the exocyst to control membrane traffic in cytokinesis.* EMBO J, 2005. **24**(19): p. 3389-99.
263. Schiel, J.A., et al., *Endocytic membrane fusion and buckling-induced microtubule severing mediate cell abscission.* J Cell Sci, 2011. **124**(Pt 9): p. 1411-24.
264. Schiel, J.A., et al., *FIP3-endosome-dependent formation of the secondary ingression mediates ESCRT-III recruitment during cytokinesis.* Nat Cell Biol, 2012. **14**(10): p. 1068-78.
265. Prekeris, R., *Analyzing the functions of Rab11-effector proteins during cell division.* Methods Cell Biol, 2015. **130**: p. 19-34.
266. Simon, G.C., et al., *Sequential Cyk-4 binding to ECT2 and FIP3 regulates cleavage furrow ingression and abscission during cytokinesis.* EMBO J, 2008. **27**(13): p. 1791-803.
267. Schafer, J.C., et al., *Rab11-FIP2 interaction with MYO5B regulates movement of Rab11a-containing recycling vesicles.* Traffic, 2014. **15**(3): p. 292-308.
268. Abdelrahman, Y.M. and R.J. Belland, *The chlamydial developmental cycle.* FEMS Microbiol Rev, 2005. **29**(5): p. 949-59.
269. Beagley, K.W. and P. Timms, *Chlamydia trachomatis infection: incidence, health costs and prospects for vaccine development.* J Reprod Immunol, 2000. **48**(1): p. 47-68.
270. Saka, H.A. and R.H. Valdivia, *Acquisition of nutrients by Chlamydiae: unique challenges of living in an intracellular compartment.* Curr Opin Microbiol, 2010. **13**(1): p. 4-10.
271. Rzomp, K.A., et al., *Rab GTPases are recruited to chlamydial inclusions in both a species-dependent and species-independent manner.* Infect Immun, 2003. **71**(10): p. 5855-70.

272. Rejman Lipinski, A., et al., *Rab6 and Rab11 regulate Chlamydia trachomatis development and golgin-84-dependent Golgi fragmentation.* PLoS Pathog, 2009. **5**(10): p. e1000615.
273. Rzomp, K.A., A.R. Moorhead, and M.A. Scidmore, *The GTPase Rab4 interacts with Chlamydia trachomatis inclusion membrane protein CT229.* Infect Immun, 2006. **74**(9): p. 5362-73.
274. Fields, K.A. and T. Hackstadt, *The chlamydial inclusion: escape from the endocytic pathway.* Annu Rev Cell Dev Biol, 2002. **18**: p. 221-45.
275. Scidmore, M.A., E.R. Fischer, and T. Hackstadt, *Restricted fusion of Chlamydia trachomatis vesicles with endocytic compartments during the initial stages of infection.* Infect Immun, 2003. **71**(2): p. 973-84.
276. Capmany, A. and M.T. Damiani, *Chlamydia trachomatis intercepts Golgi-derived sphingolipids through a Rab14-mediated transport required for bacterial development and replication.* PLoS One, 2010. **5**(11): p. e14084.
277. Ducharme, N.A., et al., *Rab11-FIP2 influences multiple components of the endosomal system in polarized MDCK cells.* Cell Logist, 2011. **1**(2): p. 57-68.
278. Wallace, D.M., et al., *The novel Rab11-FIP/Rip/RCP family of proteins displays extensive homo- and hetero-interacting abilities.* Biochem Biophys Res Commun, 2002. **292**(4): p. 909-15.
279. Leiva, N., A. Capmany, and M.T. Damiani, *Rab11-family of interacting protein 2 associates with chlamydial inclusions through its Rab-binding domain and promotes bacterial multiplication.* Cell Microbiol, 2013. **15**(1): p. 114-29.
280. Kawasaki, M., K. Nakayama, and S. Wakatsuki, *Membrane recruitment of effector proteins by Arf and Rab GTPases.* Curr Opin Struct Biol, 2005. **15**(6): p. 681-9.
281. Jagoe, W.N., et al., *Purification, crystallization and preliminary X-ray diffraction studies of Rab11 in complex with Rab11-FIP2.* Acta Crystallogr Sect F Struct Biol Cryst Commun, 2006. **62**(Pt 7): p. 692-4.
282. Wei, J., et al., *Molecular dissection of Rab11 binding from coiled-coil formation in the Rab11-FIP2 C-terminal domain.* Biochemistry, 2006. **45**(22): p. 6826-34.
283. Yamamoto, H., et al., *Functional cross-talk between Rab14 and Rab4 through a dual effector, RUFY1/Rabip4.* Mol Biol Cell, 2010. **21**(15): p. 2746-55.
284. Lall, P., et al., *Structure-Function Analyses of the Interactions between Rab11 and Rab14 Small GTPases with Their Shared Effector Rab Coupling Protein (RCP).* J Biol Chem, 2015. **290**(30): p. 18817-32.
285. Lall, P., et al., *Structural and functional analysis of FIP2 binding to the endosome-localised Rab25 GTPase.* Biochim Biophys Acta, 2013. **1834**(12): p. 2679-90.
286. Rodriguez, D.D., et al., *Crystallographic ab initio protein structure solution below atomic resolution.* Nat Methods, 2009. **6**(9): p. 651-3.
287. Wei, J., et al., *Disorder and structure in the Rab11 binding domain of Rab11 family interacting protein 2.* Biochemistry, 2009. **48**(3): p. 549-57.
288. Savitsky, P., et al., *High-throughput production of human proteins for crystallization: the SGC experience.* J Struct Biol, 2010. **172**(1): p. 3-13.